



KATHOLIEKE UNIVERSITEIT
LEUVEN

Arenberg Doctoral School of Science, Engineering & Technology
Faculty of Engineering
Department of Electrical Engineering

ADVANCED SIGNAL PROCESSING FOR MAGNETIC RESONANCE SPECTROSCOPY

Maria Isabel OSORIO GARCIA

Dissertation presented in
partial fulfillment of the
requirements for the degree
of Doctor in Engineering

November 2011

ADVANCED SIGNAL PROCESSING FOR MAGNETIC RESONANCE SPECTROSCOPY

Maria Isabel OSORIO GARCIA

Jury:

Prof. dr. ir. P. Van Houtte, president

Prof. dr. ir. S. Van Huffel, promotor

Prof. dr. U. Himmelreich, copromotor

Dr. D. Sima, copromotor

Prof. dr. M. Hubert

Prof. dr. ir. D. Vandermeulen

Prof. dr. ir. R. Pintelon (VUB)

Prof. dr. ir. D. Graveron-Demilly (INSA Lyon)

Prof. dr. D. van Ormondt (TU Delft)

Dissertation presented in
partial fulfillment of the
requirements for the degree
of Doctor in Engineering

November 2011

© Katholieke Universiteit Leuven – Faculty of Engineering
Kasteelpark Arenberg 1/2200, B-3001 Leuven (Belgium)

Alle rechten voorbehouden. Niets uit deze uitgave mag worden vermenigvuldigd en/of openbaar gemaakt worden door middel van druk, fotocopie, microfilm, elektronisch of op welke andere wijze ook zonder voorafgaande schriftelijke toestemming van de uitgever.

All rights reserved. No part of the publication may be reproduced in any form by print, photoprint, microfilm or any other means without written permission from the publisher.

Legal depot number D/2011/7515/129
ISBN number 978-94-6018-428-4

Foreword

In the first place, I would like to thank my supervisor Prof. Sabine Van Huffel for giving me the opportunity to start a PhD in her research group and for all the scientific and personal support extended during the past four years. Thank you Sabine for the encouragement, help, understanding and for the social meetings, which were important for the integration of the group. I would also like to thank my co-supervisor Prof. Uwe Himmelreich for the *in vivo* data, for the interesting scientific discussions and for all his support during my PhD. I would like to thank especially my co-supervisor Dr. Diana Sima, who from the beginning of my PhD has been an important guide and advisor for almost daily discussions; Diana, I am very grateful for your scientific support and your friendship.

I was very glad to be able to participate as a fellow in the European project 'FAST - Advanced Signal Processing for Ultra Fast Magnetic Resonance - (MRTN-CT-2006-035801)', a Research and Training Network granted by Marie Curie Actions in the 6th Framework Program (2007-2010), <http://fast-mrs.eu>. Thanks to this network I had the opportunity to meet Prof. Danille Graveron-Demilly and Prof. Dirk van Ormondt, with whom I had various inspiring MR physics and error estimation discussions. I sincerely thank them for their openness, encouragement to learn new topics and help in finding responses to challenging queries.

I would like to express my gratitude to Prof. Rik Pintelon, Prof. Mia Hubert and Prof. Dirk Vandermeulen for the valuable and very appreciated suggestions for finalizing this book. A special thanks to Prof. Rik Pintelon for taking your time to illustrate the details and importance of bias estimators.

I also would like to thank all the members and fellows of the FAST project for the interesting discussions inside and outside of the scientific meetings. I am glad that I had the opportunity to share and learn so much from all of you. My sincere gratitude also to the Marie Curie Research Training Network Program (MRTN-CT-2006-035801) for the financial and career development support.

These four years in the BIOMED research group were really a great experience thanks also to all my colleagues who in one or other way contributed to my personal

and scientific development. First, I would like to especially thank Diana, Anca and Mariya with whom I spent most of my research and free time. All these years you were like my European sisters with whom I could share all happy and difficult moments... I am sure that these years would have been very different without you! Second, I sincerely thank my former colleagues Jean-Baptiste and Flemming for their valuable scientific help and MR discussions; I really appreciated it, in particular when starting my PhD. Third, I would like to thank Alexander for sharing his knowledge about signal processing and for creating a nice working atmosphere in the group; thanks also to Katrien for her personal help and friendship and Mauricio and Carlos for their administrative help. Last but not least, I also thank all my BIOMED colleagues and collaborators for their friendship and the lovely time in conferences and social events: Elisa, Vanya, Ben, Maarten, Jan, Steven, Joachim, Sofie V. C., Bori, Bogdan, Ann-Sofie, Kris, Ivan, Rosy, Aileen, Carolina, Milica, Vladimir, Kirsten, Devy, Ninah and Laure. Hartelijke bedankt allemaal! From the very first day I felt welcome in the group.

Finally, I would like to thank my family and my husband for being there for me and supporting me during these years:

Primero quiero agradecerle a mis padres por el soporte moral y por creer en mi. A mis hermanos por darme la oportunidad de finalizar mis estudios y apoyarme economica y moralmente durante todos estos años; especialmente quiero agradecerle a mis hermanos Gloria y Gustavo por la hospitalidad y por darme la posibilidad de realizar mis estudios universitarios; gracias a mis hermanas Ana y Angela por el apoyo y amistad incondicional; mil y mil gracias tambien a mis hermanos Genia, Jose, Tata, Natalia y a todos mis sobrinos! Estoy muy feliz de haber alcanzado este logro y que se sientan orgullosos de mi.

Ich möchte mich auch bei meinen deutschen Familien und Freunden bedanken, weil sie mich so herzlich aufgenommen haben und immer an mich geglaubt haben. Herzlichen Dank an die Lüdemanns, Fischers, Webers, Oma, Müllers, Albrechts, Gerstenkamps, Wömpners, Axmanns und Manfred.

Nicht zuletzt möchte ich Jörg von ganzem Herzen danken. Du hast mich jeden Tag unterstützt, hast mit mir glückliche und traurige Momente erlebt und mir immer Kraft gegeben. Die letzten vier Jahre waren auch wichtig für uns und es war mein großes Glück, dich an meiner Seite zu haben. Ich bin glücklich, dass du jetzt auf mich stolz bist!

Abstract

Assertive diagnosis of cancer, Alzheimer's disease, epilepsy and other metabolic diseases is essential to provide patients with the adequate treatment. Recently, different invasive and non-invasive techniques have been developed for this purpose, nevertheless, due to their harmless properties the non-invasive techniques have gained more value. Magnetic Resonance is a well-known non-invasive technique that provides spectra (metabolite peaks) and images (anatomical structures) of the examined tissue. In Magnetic Resonance Spectroscopy (MRS), molecules containing certain excitable nuclei, such as ^1H , provide the metabolite information. As a consequence, the peaks in the MR spectra correspond to observable metabolites which are the biomarkers of diseases. Finally, metabolite concentrations are computed and compared against normal values in order to establish the diagnosis. The method to obtain such amplitudes is also called quantification and its accuracy is essential for diagnosis assessment.

Quantification of MRS signals is affected by a relatively low signal-to-noise ratio (SNR), a residual water resonance, lineshape distortions, overlapping resonances and underlying macromolecules and lipids affecting their baseline. Our ultimate goal was, therefore, the development of signal processing tools and algorithms to improve the quantification of MRS signals. For this, we first proposed a heuristic method to improve the residual water filtering using Hankel Singular Value Decomposition (HSVD). Additionally, a method for lineshape estimation of distorted MR spectra was developed and evaluated in simulated, *in vitro* and *in vivo* signals. Furthermore, a baseline approach was implemented via a parametric modelling method based on *prior* knowledge acquired from a set of *in vivo* macromolecular signals (measured via inversion recovery), which aims at avoiding long measurements and allowing a flexible set of baseline components. Finally, for the analysis of quantification results we focused on an automatic evaluation of the residual, thereby benefiting MRS spectral analysis in the clinic. This work was developed within the context of the European project 'FAST' (MRTN-CT-2006-035801) - Advanced Signal Processing for Ultra Fast Magnetic Resonance -, which was a Research and Training Network granted by Marie Curie Actions in the 6th Framework Program (2007-2010), <http://fast-mrs.eu>.

Notations

Ala	Alanine
AMARES	Advanced method for accurate, robust and efficient spectral fitting
AQSES	Automated quantification of short echo time MRS spectra
Asp	Aspartate
Cho	Choline
Cr	Creatine
CRLB	Cramér-Rao lower bounds
CSI	Chemical shift imaging
dB	Decibels
DSS	Trimethylsilylpropanesulfonic acid sodium salt
ECC	Eddy current correction
FASTMAP	Fast, automatic shimming technique by mapping along projections
FFT	Fast Fourier transform
FID	Free induction decay
FIR	Finite impulse response
FOV	Field of view
FWHM	Full width at half maximum
GABA	Gamma-aminobutyric acid
GAMMA	General approach to magnetic resonance mathematical analysis
Glc	D-Glucose
Gln	Glutamine
Glu	Glutamate
Glx	Glutamine+Glutamate
Gly	Glycine
GPC	Glycerophosphorylcholine
GSH	Glutathione
GUI	Graphical user interface
HLSVD	Hankel Lanczos singular value decomposition
HLSVD-PRO	HLSVD with partial reorthogonalization
Lac	Lactate
LCModel	Linear combination of model spectra
Lip	Lipids

LOESS	Local regression and smoothing scatter-plots
MDL	Minimum description length
MM	Macromolecule
MOIST	Multiple optimizations insensitive suppression train
MP-FIR	Maximum phase FIR
MRS	Magnetic resonance spectroscopy
MRSI	Magnetic resonance spectroscopic imaging
m-Ins	Myo-inositol
NAA	N-acetyl-aspartate
NAAG	N-acetylaspartylglutamate
NDP	Number of data points
NLLS	Nonlinear least squares
NMR-SCOPE	NMR spectra calculation using operators
OVS	Outer volume suppression
PBS	Phosphate buffer solution
PCh	Phophorylcholine
PCr	Phophocreatine
PE	Phosphorylethanolamine
PRESS	Point-resolved spectroscopy
QUALITY	Quantification improvement by converting lineshapes to the Lorentzian type
QUECC	QU from QUALITY and ECC
QUEST	Quantitation based on quantum estimation
RF	Radio frequency
RMSE	Root mean squared errors
s-Ins	Scyllo-inositol
SAMOS	Subspace-based automatic order selection method
SNR	Signal-to-noise ratio
SPID	Simulation Package based on <i>in vitro</i> databases
SSE	Sum of square errors
STEAM	Stimulated echo acquisition mode
SV	Single voxel
SVD	Singular value decomposition
SW	Spectral width
T	Tesla
Tau	Taurine
TE	Echo time
TI	Inversion time
TR	Repetition time
tCho	Total choline
tCr	Total creatine
VAPOR	Variable power RF pulses and optimized relaxation delays
VARPRO	Variable projection
VOI	Volume of interest

Contents

Foreword	i
Abstract	iii
Notation	v
Contents	vii
1 Introduction	1
1.1 Basics of Magnetic Resonance	1
1.1.1 Magnetic Resonance Spectroscopy (MRS)	5
1.1.2 Magnetic Resonance Spectroscopic Imaging (MRSI) and MRI	11
1.2 Diseases and diagnosis in ^1H MRS	11
1.2.1 Metabolites of interest in ^1H MRS	14
1.3 Goals and overview of the thesis	16
1.4 Conclusions	18
2 Magnetic Resonance Spectroscopy (MRS) signals	19
2.1 Proton MRS signals	19
2.1.1 Time vs Frequency domain signals	20
2.1.2 <i>In vivo</i> signals	20
2.1.3 <i>In vitro</i> signals	22

2.1.4	Simulated signals	24
2.2	Preprocessing MRS signals	25
2.2.1	Time circular shift	26
2.2.2	Frequency alignment	26
2.2.3	Phase correction	28
2.2.4	Truncation vs zero filling	29
2.2.5	Eddy current corrections	30
2.2.6	Lineshape correction/estimation	30
2.2.7	Residual water suppression	35
2.2.8	Baseline correction/estimation	36
2.3	Conclusion	38
3	Quantification	39
3.1	Introduction	39
3.2	Methods	40
3.2.1	Automated Quantification of Short echo time MRS signals (AQSES)	40
3.2.2	Quantitation based on QUantum ESTimation (QUEST)	43
3.2.3	Metabolite profiles	43
3.2.4	Parameters to be considered in quantification of ^1H MRS signals	47
3.2.5	Quantification results	51
3.3	Conclusion	54
4	Filtering of residual water	55
4.1	Introduction	55
4.2	Materials and Methods	56
4.2.1	MRS signals	56
4.2.2	HLSVD method	58

4.2.3	Model order selection	59
4.3	Results	62
4.4	Discussion	67
4.5	Conclusions	71
5	Lineshape estimation in MRS signals	73
5.1	Introduction	73
5.1.1	Assuming a common decay	74
5.1.2	Spectral lineshape determination with self-deconvolution	75
5.1.3	Semi-parametric lineshape estimation without searching in function space	75
5.1.4	Lineshape estimation: self-deconvolution revisited	76
5.2	Materials and Methods	76
5.2.1	MRS signals	76
5.2.2	Quantification with lineshape estimation	78
5.2.3	Smoothing methods	81
5.3	Results with AQSES and AQSES Lineshape	83
5.4	Discussion	86
5.4.1	General considerations about AQSES-Lineshape	86
5.4.2	Residual and other imperfections	90
5.5	Conclusion	91
6	Parametric method for baseline estimation of MRS signals	93
6.1	Introduction	93
6.2	Materials and Methods	94
6.2.1	Animals	94
6.2.2	<i>In vivo</i> ^1H MRS signals	95
6.2.3	Metabolite basis set	97
6.2.4	Baseline estimation	97

6.2.5	Combination of baseline and lineshape estimation	99
6.3	Results	100
6.3.1	Lineshape	100
6.3.2	Baseline	101
6.4	Discussion	106
6.5	Conclusion	107
7	Residual analysis	109
7.1	Introduction	109
7.2	Materials and methods	110
7.2.1	MRS signals.	110
7.2.2	Quantification	111
7.2.3	Statistical residual analysis	112
7.3	Results and discussion	112
7.3.1	Effect of damping factor constraint	112
7.3.2	Lack of metabolites in the basis set	114
7.4	Conclusions	118
8	Summary and further research	119
8.1	Summary	119
8.2	Future work and open problems	120
	Bibliography	123
	Publication list	141
	Curriculum vitae	145

Chapter 1

Introduction

This chapter aims at introducing the reader to Magnetic Resonance (MR), its basic principles and phenomena followed by some applications. In Section 1.1 the basics of MR Spectroscopy (MRS) and MR Spectroscopic Imaging (MRSI) are described together with the parameters involved in the acquisition and interpretation of MR spectra. Section 1.2 refers to the diagnosis of diseases using ^1H MRS(I) data considering the most relevant metabolites. Finally, the goals of the thesis and the outline of each chapter are presented in section 1.3.

1.1 Basics of Magnetic Resonance

One of the non-invasive diagnostic techniques used for detection of cancer and metabolic diseases is Nuclear Magnetic Resonance (NMR) or often referred to as simply Magnetic Resonance (MR). NMR, as its name indicates, is based on the magnetic properties that certain **nuclei** experiment when exposed to an external **magnetic** field. These nuclei have a unique **resonance** frequency related to the radio waves emitted. Compared with other diagnostic techniques such as Computed Tomography (CT), Radionuclide imaging (*e.g.*, Positron Emission Tomography (PET), Gamma camera) and Optical Imaging (Fluorescence), MR emits no ionizing radiation to the patient, making it harmless and feasible for follow up studies in children and adults. The information obtained with MR includes Imaging (MRI), Spectroscopy (MRS) and Spectroscopic Imaging (MRSI). Spectroscopic signals help in the visualization of metabolic information and images provide details of the anatomic structures. Only certain atomic nuclei have a nuclear magnetic moment (also called spin), giving them the properties of a sort of small magnet and a non-zero quantum number. Such nuclei are, for instance,

Proton (^1H) (used in this thesis), Phosphorus (^{31}P), Carbon (^{13}C), Fluor (^{19}F), Nitrogen (^{14}N), Sodium (^{23}Na), etc. Due to its abundance in the human body, the most common nucleus used in MR is ^1H .

An ^1H MR signal is obtained by placing the sample under investigation into a static external magnetic field B_0 to which the angular momentum of the nuclei is aligned (see Fig. 1.1). The magnetic moments align parallel or antiparallel to the direction of B_0 with a spin number of $+\frac{1}{2}$ (low energy state) or $-\frac{1}{2}$ (high energy state), respectively (see Fig. 1.2). Spins rotate about the Z axis (or precess) with a specific frequency called the Larmor frequency (f_0) proportional to the magnetic field B_0 . At the Larmor frequency the nuclei absorb energy causing the proton to change its alignment and to be detected in a magnetic field. This Larmor frequency is defined by:

$$f_0 = \frac{\gamma B_0}{2\pi} \quad (1.1)$$

where γ represents the gyromagnetic ratio specific for each isotope (e.g., $\frac{\gamma}{2\pi}=42.58$, 17.25, 10.71, 40.08, 3.08 and 11.26 MHz/T, for ^1H , ^{31}P , ^{13}C , ^{19}F , ^{14}N and ^{23}Na , respectively). Thus, for the data used in this thesis, with $B_0=1.5$ Tesla (T), 3.0 T, and 9.4 T, the resulting Larmor frequencies for ^1H are $f_0=63.87$, 127.74, and 400.252 MHz, respectively.

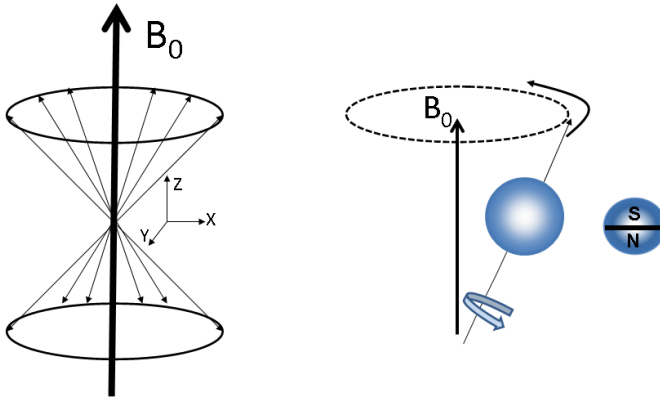


Figure 1.1: *Left: Spins are precessing along two opposite orientations to the external magnetic field B_0 . Right: Spin rotation around its own axis and around the magnetic field axis. Partially adapted from [188].*

The MR signal intensity is reflected in the amount of energy emitted, which depends on the difference between the two energy states given by:

$$\Delta E = \gamma \hbar B_0, \hbar = \frac{h}{2\pi} \quad (1.2)$$

where h is the Planck constant ($6.626 \times 10^{-34} \text{ J sec}$).

In thermal equilibrium the distribution between spin $+\frac{1}{2}$ and spin $-\frac{1}{2}$ is defined by:

$$\frac{n_-}{n_+} = e^{-\Delta E/kT} \quad (1.3)$$

where k is Boltzmann's constant ($1.381 \times 10^{-23} \text{ J/K}$) and T is the temperature in Kelvin. This ratio in Eq. (1.3) is close to unity in normal circumstances producing a low absorption of energy and causing the low signal-to-noise ratio (SNR) of the signal emitted.

In order to excite all the nuclei within the required frequency range a radio frequency (RF) pulse with a selected bandwidth is applied. When the RF field matches the Larmor frequency at which the nuclear magnets naturally precess in the magnetic field B_0 , some of the n_- nuclei are promoted from the low energy state to the high energy state, and n_+ increases. The RF signal is applied as a single powerful pulse, which effectively covers the whole frequency range and lasts a time (t_p) typically of a few microseconds. This oscillating magnetic field (B_1) was applied along the x axis, perpendicular to the applied magnetic field (B_0) which is defined as being along the z axis (see Fig. 1.1, left). The effect of the pulse is to tip the magnetization through an angle given by:

$$\Theta = \gamma B_1 t_p \quad (1.4)$$

Commonly, t_p is chosen so that Θ is 90° , and such pulses are called 90 degree pulses. The magnetization, disturbed from its orientation along the z axis, precesses in the xy plane, generating an oscillating signal, which is to be picked up by a receiver coil. This signal is called the free induction decay (FID) and has a complicated wave pattern decaying away to zero. The decay takes place because the individual nuclei relax, as they get back to their equilibrium states. The MR signal intensity is proportional to the number of nuclei contributing to it, so in case of low SNR, more acquisitions are necessary and their average will represent the final acquired MR signal. Moreover, the signal intensity can be higher by increasing the magnetic

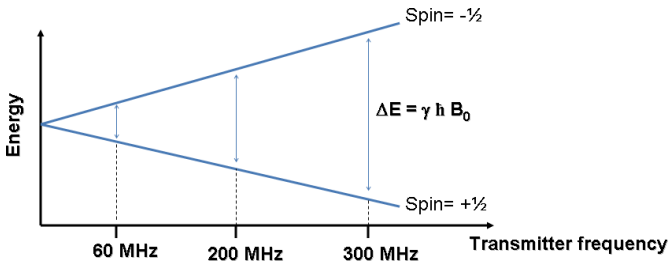


Figure 1.2: Energy level of ^1H spins when an external field B_0 is applied. The spins parallel to B_0 ($+\frac{1}{2}$) correspond to a lower energy level, while spins aligned antiparallel to B_0 ($-\frac{1}{2}$) correspond to higher energy levels.

field B_0 and decreasing the temperature T . However, in *in vivo* studies large temperature variations in patients' bodies are not possible.

Thanks to the difference between the magnetic field at the nucleus and the magnetic field applied, electrons around the nucleus shield it from the applied field and produce the nuclear shielding which allows the differentiation between molecules. On the other hand, the RF pulse is able to excite all nuclei of an isotope and the amount of shielding experienced by a nucleus determines the net magnetic field given by:

$$B = B_0(1 - \sigma') \quad (1.5)$$

where σ' is the dimensionless shielding constant that depends on the electrical environment of a nucleus.

The electron density in a molecule varies according to the type of nuclei and bonds in the molecule, therefore the opposing field and also the net magnetic field vary at each nucleus. This phenomenon is also known as chemical shift and is the reason why different molecules are distinguishable in the MR spectrum as different peaks. However, when nuclei are close to each other and influence each other's magnetic fields, cause something called spin-spin coupling or J-coupling. Thus, coupling arises when multiple spins are within a molecule, producing alterations in the local magnetic field surrounding each nucleus. This is reflected in the MR spectra as the splitting of peaks into multiplet structures.

There are different parameters affecting the detection and measurement of an MR signal: field strength, natural abundance, concentration and mobility in the tissue and spin state. For instance, macromolecules with a molecular weight greater than 20 Kilodaltons are not detected, while those in the millimolar range can be adequately detected. MRS signals can be measured *in vivo* where no intervention

is required, or *ex vivo* on a biopsy of the tissue of interest using High Resolution NMR or Magic Angle Spinning (HR-MAS). Additionally, this extracted biopsy can be used for complementary histopathology studies.

1.1.1 Magnetic Resonance Spectroscopy (MRS)

MRS is the MR technique used to obtain the metabolic information in the form of signals. These signals are the emitted signals and correspond to a sum of complex-damped exponentials in the time domain, also called free induction decay (FID). The transformation in the frequency domain using the Fast Fourier Transform (FFT) is useful to observe the individual molecules in the form of peaks corresponding to the excited nuclei. See Fig. 1.3. Estimating the area under each peak allows the computation of the metabolite concentrations (also known as quantification or quantitation), where the peak area is proportional to the number of spins giving rise to it. In the spectrum, the variation in magnetic field strengths experienced by each molecule is related to their chemical shift, also called resonance frequency, denoted in parts per million (ppm). The representation in the frequency axis is commonly given in ppm in order to be independent from the spectrometer frequency, so that metabolites resonate at fixed ppm-values for all spectrometer frequencies. The transformation from Hz to ppm is:

$$ppm = \frac{f_{Hz} \times 10^6}{f_s} + ppm_{Ref} \quad (1.6)$$

where f_{Hz} is the resonance frequency in Hz (specific frequency for a certain metabolite), f_s the spectrometer frequency in Hz (also called transmitter frequency, specific for the type of scanner) and ppm_{Ref} the ppm value of the carrier frequency (center frequency of the spectrum) which is commonly selected at the water resonance (4.7 ppm) in ^1H MRS. The carrier frequency is the sum of the spectrometer frequency (in MHz) and the spectrum offset (in Hz) about which the pulse is applied. Incorrect setting of the spectrum offset may lead to folded peaks outside the spectral window.

For instance, if we consider a ^1H signal from mouse brain measured at 9.4 T (400.310 KHz), creatine would have a peak located at -671 Hz and the computation of the ppm ratio following Eq.(1.6) is:

$$ppm = \frac{-671 \times 10^6}{400.310 \times 10^3} + 4.7 = 3.025 \text{ ppm} \quad (1.7)$$

If we have a ^1H signal from human brain measured at 3.0 T (127.74 KHz), the same peak of creatine will be located at -209 Hz, leading to 3.07 ppm (Eq.(1.6)).

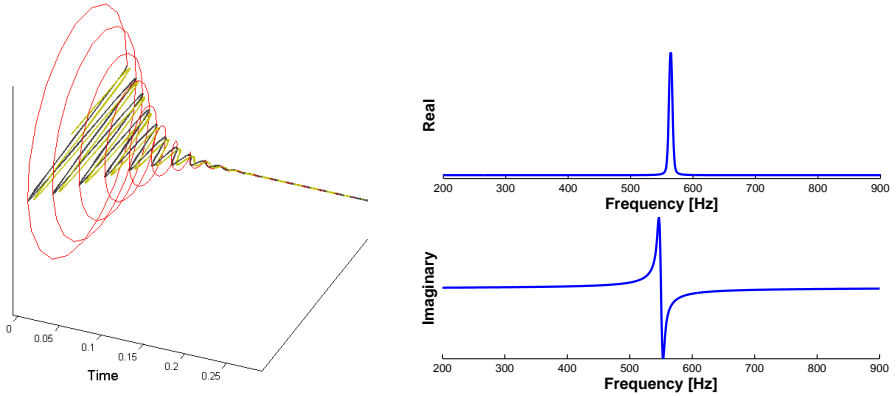


Figure 1.3: Left: Time domain signal representation (i.e., Free induction decay - FID) in two planes corresponding to the real and imaginary parts. Right: Real and imaginary parts of the Fourier Transformed signal. Adapted from [35].

The acquisition parameters of an FID include:

- Pulse sequence: a set of RF pulses are required to select a voxel. The orientation of the selected slice can also be chosen freely by an appropriate weighted combination of the three available field gradients within the MR scanner. For a selection of a volume instead of a slice, three slice selections with different orientations are necessary. The selected volume of interest (VOI) is built by the intersection of the three selected slices. In ^1H MRS the most common pulse sequences are Point-RESolved Spectroscopy (PRESS) [12] and STimulated Echo Acquisition Mode (STEAM) [48]. In the PRESS sequence, a 90° excitation and two 180° refocusing pulses are used and in the STEAM-sequence all three pulses are 90° excitation pulses. See Fig. 1.4.

An additional acquisition sequence used for measuring the contribution of macromolecules and lipids is called inversion recovery. In this sequence, a 180° RF pulse that inverts the magnetization is first applied followed by a 90° RF pulse that brings the residual longitudinal magnetization into the xy plane where it can be detected by an RF coil. This technique is time inefficient due to the large recovery delay needed to allow the complete recovery of the signal. The time between the initial 180° degree pulse and the 90° degree pulse is the inversion time (TI) [35]. Alternatively, a short TI inversion recovery sequence (STIR) has been proposed by Dwyer *et al.* [43] for fat suppression, where a relatively short inversion time is used to null the fat signal while maintaining water and soft tissue signal. In practice, several

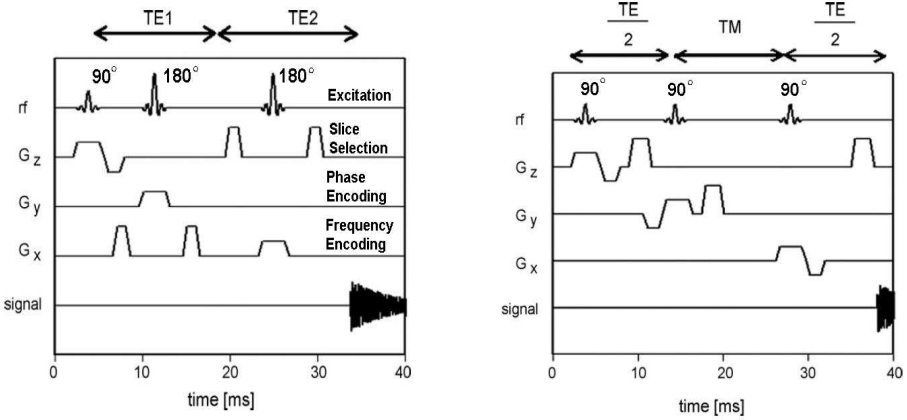


Figure 1.4: Left: PRESS sequence with three RF pulses applied simultaneously with field gradients along the main axes of the magnet. Right: STEAM sequence with the refocusing gradients positioned before the second RF pulse and after the third RF pulse. Only the first part of the data acquisition time is shown as the first part of the FID. Figures from [80].

inversion times are measured and finally the one with maximum metabolite suppression is selected.

- Echo Time (TE): represents the time in milliseconds (ms) between the application of the first pulse and the beginning of the data acquisition. MRS signals can be acquired at long and short TE, where long TE signals provide a good observation of slowly decaying components (*e.g.*, N-acetyl-L-aspartate (NAA), Choline (Cho) and Creatine (Cr)), while short TE signals provide more metabolic information. Typical long TE signals are in the range between 60 and 300 ms and short TE signals are in the range between 1 and 50 ms. An illustration of the difference between short and long TE is shown in Fig. 1.5.
- Repetition time (TR): is the time between successive pulse sequences applied to the same slice.
- T_1 : is also called the spin-lattice relaxation time and refers to the time to reduce the difference between the longitudinal magnetization after the RF pulse and its equilibrium value by a factor of e^1 , where e is Euler's number $e = 2.71828$. Thus, we have

$$M_z(t) = M_0(1 - e^{-\frac{t}{T_1}}) \quad (1.8)$$

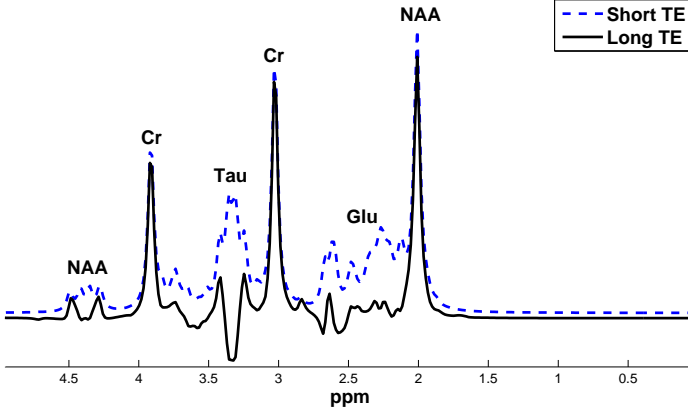


Figure 1.5: Simulated signal composed of Cr, Glu, NAA and Tau obtained using a PRESS sequence with short TE (5 ms) and long TE (272 ms). These simulations were performed using NMR-SCOPE [164].

where $M_z(t)$ is the longitudinal net magnetization at time t and M_0 the initial net magnetization aligned with B_0 . See Fig. 1.6.

- T_2 : is also called the spin-spin relaxation time and refers to the time constant which describes the return to equilibrium of the transverse magnetization M_{xy} as:

$$M_{xy}(t) = M_{xy_0} e^{-\frac{t}{T_2}} \quad (1.9)$$

where M_{xy_0} is the net transversal magnetization at time 0. T_2 is always $\leq T_1$. The net magnetization in the xy -plane goes to zero and then the longitudinal magnetization still grows until the net magnetization is reached along the z -axis.

- T_2^* : is also known as the effective transverse relaxation time, thus, the time constant for the observed decay of the FID. It is a combination of transverse relaxation and magnetic field inhomogeneity effects. In the presence of a homogeneous magnetic field $T_2^* = T_2$, however, in an inhomogeneous field $T_2^* < T_2$. We have the following relation between time and frequency domain parameters:

$$T_2^* = \frac{1}{\pi \nu_{\frac{1}{2}}} \quad (1.10)$$

where $v_{\frac{1}{2}}$ corresponds to the linewidth¹ of the Fourier transformed signal (*i.e.*, the Full Width at Half Maximum (FWHM)). See Fig. 1.6.

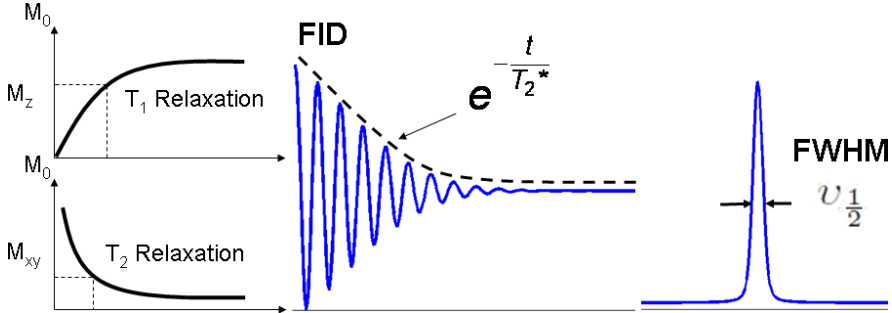


Figure 1.6: Left: Graphical representation of the T_1 and T_2 relaxation times along the magnetization M_0 . The time constants T_1 and T_2 are measured in seconds (or ms) and refer to the exponential nature of the two relaxation processes. Middle: real part of the FID during relaxation and its envelope, which is related to the T_2^* relaxation time. Right: Real part of FFT of the FID showing the linewidth of the spectrum, which corresponds to the Full Width at Half Maximum (FWHM). Adapted from [35].

- Single or multi-voxel: Single-voxel (SV) MRS measures a signal from a single volume, while multi-voxel MRS measures signals from a grid of multiple volumes. See Fig. 1.8.
- Number of averages: number of acquisitions performed in order to increase the SNR.
- Number of points (NDP): number of time samples used in the acquisition.

When the homogeneity of the magnetic field is inappropriate, a technique called shimming (referring to adjustment) is normally performed. By shimming a magnet, the magnetic field becomes more homogeneous and a better spectral resolution can be obtained. Broad lines, asymmetric lines, and a loss of resolution are indications that a magnet needs to be shimmed. The shape of an NMR line is a good indication of which shim is mis-adjusted.

Shimming can be performed by tuning the Z , X or Y gradient coils. Z indicates that the field produced by these shims are symmetric about the z axis of the magnetic field. Fig. 1.7 shows graphically how the profiles of the magnetic fields produced by Z^1 , Z^2 and Z^3 appear. The shape of fields is described by their names: Z^1 is a linear gradient across the sample, Z^2 is parabolic, Z^3 is cubic, etc.

¹In the time domain we refer to the damping or the decay of the FID MRS signal, while in the frequency domain we refer to the linewidth or lineshape of the spectral peaks.

The higher the power of the Z inhomogeneity, the further away the asymmetry is from the center of the line. Room temperature shims are metal coils able to generate small variable magnetic fields, which compensate for imperfections [68].

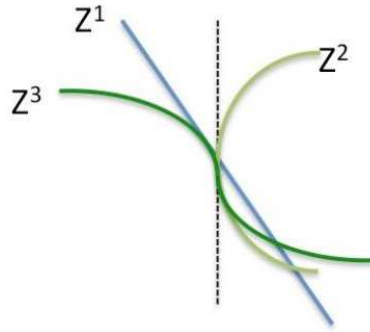


Figure 1.7: This plot shows graphically the profiles of the magnetic fields produced by Z^1 , Z^2 and Z^3 . Obtained from [68]

Proton (^1H) MRS is the most common spectroscopy technique used in brain studies, where up to 15-20 metabolites can be distinguished and quantified [128, 170, 111, 169, 38]. The metabolites commonly observed in ^1H MRS are: N-acetyl-L-aspartate (NAA), Creatine (Cr), Choline (Cho), Myo-inositol (m-Ins), Lactate (Lac), Glutamate (Glu) and Glutamine (Gln). However, depending on the magnetic field, TE, SNR and the overlap between metabolites, some of these metabolites are barely observed. For instance, due to their short relaxation times, the resonances of Glu, Gln and m-Ins are not well visualized at long TEs, while short TEs allow a better resolution of metabolites resonating with short relaxation time. Another effect of TE happens in metabolites like Lac: at echo times around even multiples of $1/J$ -coupling (144 ms or 136 ms), the Lac doublet at 1.3 ppm appears positive (pointing upwards), while at odd multiples of $1/J$ -coupling the resonance appears negative (pointing downwards).

In vivo ^1H MRS signals contain a water resonance several orders of magnitude larger than those of metabolites. In order to visualize the metabolites, a suppression of the water peak is required. For this purpose, several water suppression techniques included in the acquisition protocol, such as presaturation, watergate, water flip-back and suppression by coherence pathway rejection, are typically used to provide a residual water signal at the level of most observable metabolites [47, 170, 21, 117, 112]. Moreover, when ^1H *in vivo* MRS signals are measured, an unsuppressed water signal is also acquired. This water signal contains a prominent water resonance together with barely visible metabolites of interest and is commonly used as reference for phase correction and quantification, as will be explained in chapter 2 and 3.

1.1.2 Magnetic Resonance Spectroscopic Imaging (MRSI) and MRI

MRSI is also known as Chemical Shift Imaging (CSI) or multi-voxel spectroscopy, where the visualization of spectral intensities from multiple voxels is achieved. It provides a set of signals (FIDs) containing the metabolic information in a two- or three dimensional grid of volume elements called voxels, allowing the identification of different neighboring regions in the tissue under investigation. In contrast to MRSI, MRI provides the anatomical image of the scanned region giving the morphology (*i.e.*, tissue structure). The spatial distribution of protons in the form of images in the chosen slice is localized by using different gradients. These images can be obtained in the same measurement session and used as complementary diagnostic information. A great advantage of MRI is the difference in contrast between tissues. Moreover, in order to enhance the specific characteristics of a certain region, contrast agents are injected intravenously. For some diseases, it is advantageous to evaluate both, the anatomical image and the individual spectra because with the anatomical image only certain structures and diseases can be clearly identified, whereas individual spectra can complementary be used to extract metabolic information per voxel. See Fig. 1.8.

MRSI resolution is limited by the low SNR, which can be improved by measuring large voxels or increasing the number of averages. Processing and quantification of MRSI data can be performed similarly to single voxel MRS, however, some studies have shown that by including spatial information in the quantification of MRSI data, improvements in the metabolite estimates and metabolite maps can be achieved [28, 78].

1.2 Diseases and diagnosis in ^1H MRS

MRS and MRSI play an important role in the non-invasive diagnosis of cancer and metabolic diseases such as: pediatric diseases [39], brain diseases (*e.g.*, Alzheimer's disease, multiple sclerosis, ischemia, inflammation) [100, 49], epilepsy [64], brain tumors [15], cardiovascular diseases, breast and prostate cancer [116], liver and muscle diseases [99]. In particular, ^1H is highly used due to its natural abundance in the body and its capability of detection in different tissues.

In MRS/MRSI, increases or decreases in metabolite concentrations are used to address the type and gravity of diseases by comparing to normal ranges. These concentrations can be obtained by quantifying MRS signals and different methods have been developed for this purpose [129, 176, 158, 66, 180]. Basically, the area under the peaks (obtained by the so-called peak integration method) in the MR spectrum corresponds to the metabolite concentration, however, more

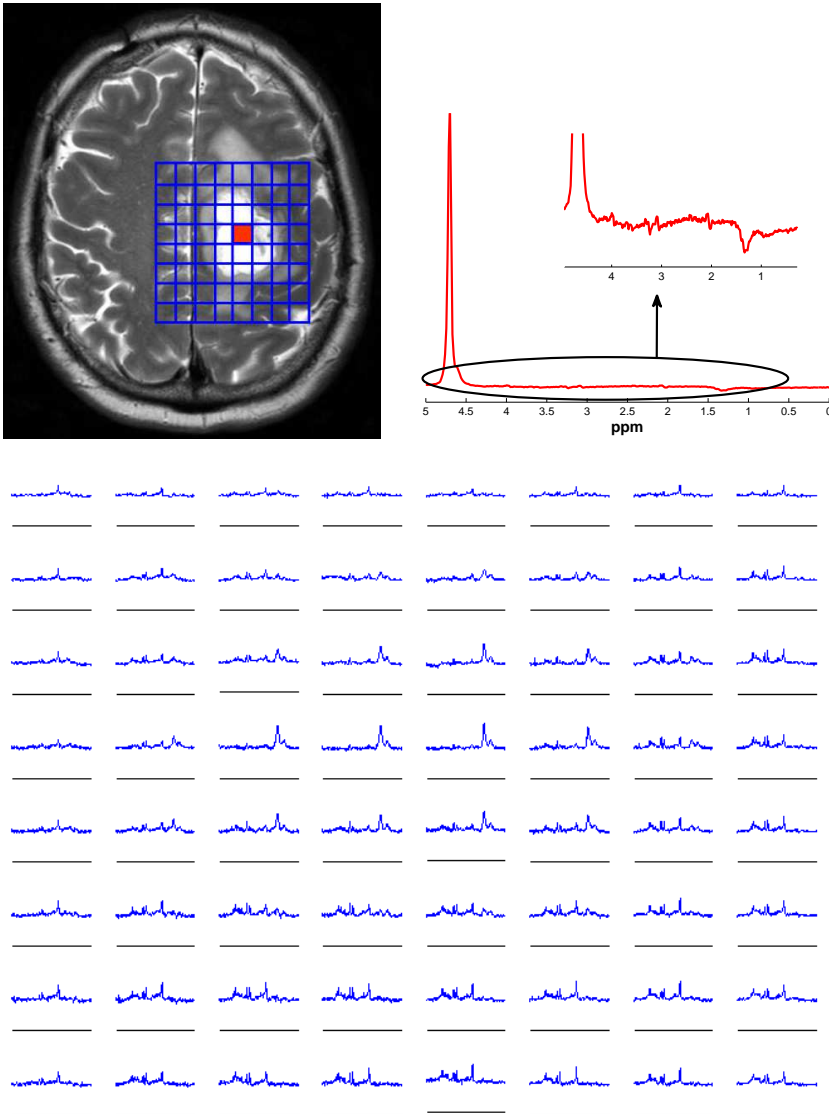


Figure 1.8: Brain MRI and MRSI data of a patient acquired at 3.0 T in a Philips MR scanner (Achieva, Philips, Best, The Netherlands). MRSI parameters were: PRESS pulse sequence with the water suppression method MOIST (Multiple Optimizations Insensitive Suppression Train), repetition time (TR)=2 s, echo time (TE)=35 ms, spectral width (SW)=2 KHz and number of data points (NDP)=2048 points. Measurements were done at the University Hospital of the Katholieke Universiteit Leuven, Belgium. Top left: T₂-weighted image. Top right: Spectrum of the selected voxel without water filtering; the region between 0.5 ppm and 4.5 ppm corresponds to the region of interest. Bottom: Set of spectra from the voxels of interest preprocessed by water filtering.

advanced methods based on the fitting of metabolite profiles to the *in vivo* FIDs or corresponding spectra have been successfully applied [140, 143, 137, 182, 28]. A further step, which is not addressed in this thesis, corresponds to the classification and automatic diagnosis, based on the obtained metabolite estimates (or the “feature extraction” step) from quantification [98].

A list of metabolites known to be important biomarkers of diseases in ^1H MRS are listed in section 1.2.1 and Fig. 1.9 shows three MR spectra measured at different magnetic fields and indicating the main biomarkers of diseases. In this thesis, ^1H MRS in the brain has been essentially used for studying lineshape, baseline and residual analysis issues. Spectra from normal brain, Alzheimer’s disease and epilepsy [123, 122, 121, 120] have been used for validating the proposed methods.

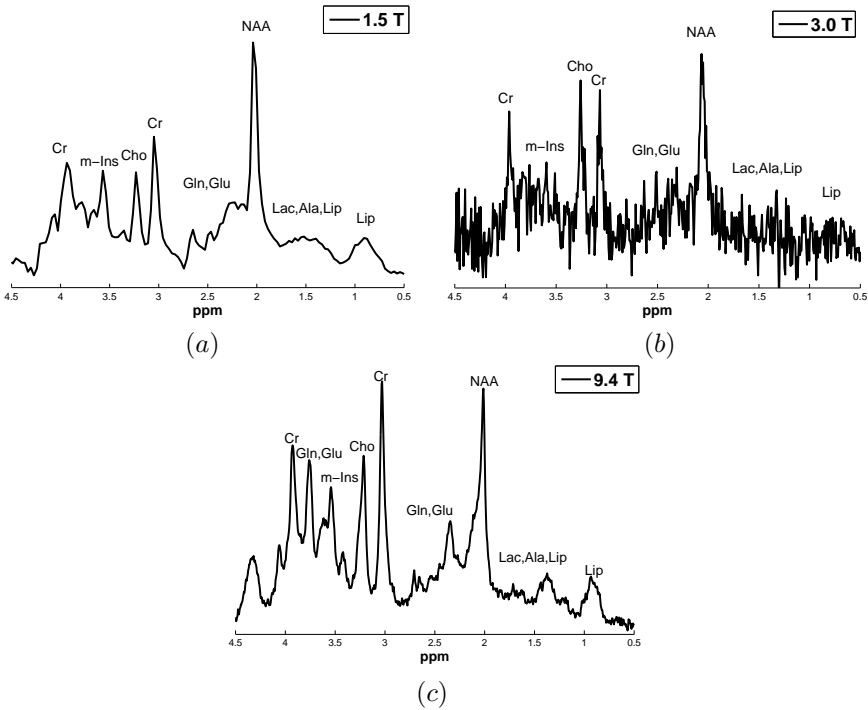


Figure 1.9: Real part of the spectra of three *in vivo* signals acquired at: (a) 1.5 T with acquisition parameters: PRESS pulse sequence, $TR=6$ s, $TE=23$ ms, $SW=1$ KHz, $NDP=512$ points, 64 averages. (b) 3.0 T with acquisition parameters: PRESS pulse sequence, $TR=2$ s, $TE=35$ ms, $SW=2$ KHz, $NDP=2048$ points, 1 average. (c) 9.4 T with acquisition parameters: PRESS pulse sequence, $TR=4$ s, $TE=12$ ms, $SW=4$ KHz, $NDP=2048$ points and 256 averages.

1.2.1 Metabolites of interest in ^1H MRS

- **Alanine (Ala):** This amino acid is present in the human brain at a concentration of about 0.5 mM, presenting higher values in the case of tumors such as meningioma and glioma. It has two main resonances: a doublet located at 1.47 ppm, which highly overlaps with the resonances from lipids and macromolecules, and a quartet located at 3.77 ppm [56].
- **Aspartate (Asp):** This is an excitatory amino acid with multiple resonances at 3.89 ppm, 2.65 ppm and 2.80 ppm. Its concentration in the brain is about 1-2 mM [56].
- **Choline (Cho) - Phosphorylcholine (PCh) - Glycerophosphocholine (GPC):** Choline components consist of brain myelin and fluid-cell membranes. The main peak is observed as a singlet at 3.2 ppm which contains a mixture between Cho, PCh and GPC, also denoted as total Choline (tCho). The concentration in human brain is approximately 1-2 mmol/Kg wet weight, with approximately 0.6 mM of PCh, 1 mM of GPC and only a small concentration of free Cho of about 0.03 mM. Changes in tCho are associated to changes in membrane composition, such as membrane turnover and demyelination [56]. An increase may indicate cancer, ischemia, head trauma, Alzheimer's disease or multiple sclerosis, while a decrease may indicate a liver disease and stroke. Cho compounds are known to be larger in tumor than in normal tissues.
- **Creatine (Cr) - Phosphocreatine (PCr):** These metabolites reflect the energetic status of the tissue and, due to their stability, they are often used as an internal reference for computing relative concentrations. Total Creatine (tCr) is characterized by two singlets, one at 3.03 ppm and the other one at 3.9 ppm. In the human brain, Cr and PCr have been found to be in concentrations between 4.8-5.6 mM and 4-5.5 mM, respectively; however, small differences have been observed in gray and white matter. Due to their short T_2 and overlapping with other resonances, the separation of the Cr and PCr resonances is difficult in *in vivo* MRS [56].
- **γ -Aminobutyric acid (GABA):** It is a primary inhibitory neurotransmitter with low concentrations in the brain of approximately 1 mM. Increased levels have been used for treatment of epileptic seizures and muscle spasms. GABA resonances contain multiplets centered at 1.89 ppm, 2.28 ppm and 3.01 ppm, which unfortunately overlap with other metabolite resonances and hinders their estimation [56].
- **D-Glucose (Glc):** It is essential in the brain as a source of energy and as a precursor for other compounds. Its concentration is about 1 mM, but can increase to 9 mM due to the plasma Glc. It contains two anomers (α and

β) which coexist in aqueous solutions, with an equilibrium concentration of 36% and 64%, respectively. The signal corresponding to the β -Glc anomer is eliminated when water suppression is performed. For both anomers, the resonance groups are located in the range between 3.2 ppm and 3.88 ppm [56].

- **Glutamate (Glu):** It is the most abundant amino acid in the brain at a concentration of about 12 mM. It is known to be an excitatory neurotransmitter presenting changes in different diseases. It has resonances at 3.74 ppm, 2.04 ppm and 2.35 ppm, therefore, the overlapping with resonances of GABA, NAA and Gln complicates its estimation [56].
- **Glutamine (Gln):** It is a precursor and storage form of Glutamate. It has a concentration of about 2-4 mM and presents multiple resonances between 2 to 3.8 ppm. At low magnetic field, the separation between Gln and Glu is difficult, so their contributions are usually combined and called Glx [148].
- **Glutathione (GSH):** This metabolite is a tripeptide made up of glycine, cysteine and glutamate, which is present as reduced (GSH) and oxidated (GSHH) in living systems. GSH is an important antioxidant for maintaining the normal red-cell structure and keeping hemoglobin in the ferrous state. Its concentration is about 2-3 mM and is mostly located in astrocytes. Differences in the GSH levels have been reported in neurodegenerative diseases. GSH resonates at 2.15 ppm, 2.55 ppm 2.93 ppm, 2.98 ppm, 3.77 ppm and 4.56 ppm. These resonances, however, overlap with those of Glu, Gln, GABA, Cr, Asp and NAA, making their estimation complicated [56].
- **Glycine (Gly):** It is a simple amino acid acting as inhibitory neurotransmitter and antioxidant. Its concentration is about 1 mM in human brain with a singlet at 3.55 ppm overlapping with that of m-Ins. Gly differences have been observed in diverse types of tumors [56].
- **Lactate (Lac):** This is the end product of the anaerobic glycolysis, and due to its low concentrations in normal brain, it is difficult to observe in *in vivo* MRS. High concentrations are observed in diseases such as stroke, trauma, tumors and hyperventilation. Its characteristic resonance is a doublet located at 1.31 ppm but it highly overlaps with the resonances from lipids and macromolecules. Moreover, a quartet resonating at 4.09 ppm may overlap with the water resonance [56].
- **Myo-inositol (m-Ins):** The concentration of m-Ins in neonates is initially high and can be detected at short TE. It is a precursor for inositol lipid synthesis and is a constituent of membrane lipids. It is characterized by a multiplet around 3.56 ppm with a normal concentration between 4-8 mM [56]. m-Ins is considered to be essential for cell growth, acting as an osmolyte,

and a storage form for glucose [149]. Changes in the m-Ins levels have been associated with Alzheimer's disease [70, 149, 191], hepatic encephalopathy [101], and brain injury [150].

- **N-Acetyl aspartate (NAA) - N-Acetylaspartylglutamate (NAAG):** This amino acid is a marker of the neural function present in the central and peripheral nervous systems (mainly localized in neuron, axons, and dendrites) of several species, and it is present at high concentrations heterogeneously distributed within the brain [110, 139]. Its concentration changes in the presence of neurological disorders. NAA has seven protons giving signals between 2 and 8 ppm, where its main resonance shows a singlet around 2.01 ppm. The typical concentration of NAA in *in vivo* human brain has been reported to be between 7-16 mmol/Kg of wet weight, while the concentration of NAAG in normal brain has been reported in the range of 0.6-3 mmol/Kg wet weight [56]. Because NAAG is structurally similar to NAA and Glutamate, many of their resonances overlap and can only be distinguished at high magnetic fields. NAAG has the main resonance at 2.04 ppm, appearing as a shoulder of the main resonance of NAA. This metabolite has been one of the markers for neuronal integrity, but altered levels may not always represent neuron loss [105].
- **Phosphorylethanolamine (PE):** It contains multiple resonances at 3.22 ppm and 3.98 ppm. Its concentration in human brain is about 1.4 mM [56].
- **Scyllo-inositol (s-Ins):** It is the second most abundant isomer of inositol that is found in mammals. It has a singlet resonance at 3.34 ppm, and in humans its concentration is reported to be closely coupled with that of myo-inositol, with a ratio of 12:1 [56].
- **Taurine (Tau):** Tau is an amino acid with several biological functions, such as osmoregulation and modulation of the action of neurotransmitters. It is high in neonates and decreases to 1.5 mM in adults. Its spectrum contains two triplets at 3.25 and 3.42 ppm. In *in vivo* studies at low magnetic field, these resonances overlap with the resonances of m-Ins and Cho [56].

1.3 Goals and overview of the thesis

This thesis aims at improving the preprocessing and quantification of MRS signals acquired *in vivo* at low and high magnetic fields in humans and animals. By improving quantification, diagnosis of cancer and metabolic diseases can be better assessed and becomes more reliable. Therefore, advanced signal processing of MRS data is approached after acquisition to improve quantification results thereby

enhancing the diagnosis. Specifically, improvements on the water filtering [119], lineshape [123] and baseline estimation [121] using advanced statistics and signal processing methods are proposed in this thesis, making use of simulated, *in vitro* and *in vivo* data measured mainly at the University Hospital of the Katholieke Universiteit Leuven. Furthermore, additional studies have been addressed to highlight the importance of residual analysis after quantification [122].

The research described here has been developed within the FAST project (*Advanced Signal-Processing for Ultra-Fast Magnetic Resonance*, MRTN-CT-2006-035801, a Research and Training Network (RTN) granted by Marie Curie Actions in the 6th Framework Program (2007-2010), <http://fast-mrs.eu>). This project aimed to pave the way to real-time MRSI, including cutting-edge MRSI signal processing algorithms for quantification and imaging of metabolites (a virtual scanner based on quantum mechanics, advanced semiparametric estimation and innovative graphical user-interfacing), ultra-fast data acquisition at the forefront of MR-methodology and innovative e-Training/transfer of knowledge for young researchers and experts. Additionally, it aimed to establish MRSI as a non-invasive routine tool in the clinic for combating major diseases (*e.g.*, MRSI during surgery) and an innovative graphical user-interface with web-collaboration to enable interactive communication sessions, with data- and action-sharing, between multiple users. The partners' expertise ranged from medicine to theoretical physics, including biochemistry, chemistry, physics, signal processing, informatics, numerical algebra, together with four industrial partners. Thus, FAST aimed to make MRSI a reliable, ultra-fast, non-invasive, metabolite monitor for the clinic. As a fellow of this project, my work was focused on the improvement and development of statistical and signal processing techniques for metabolite quantification.

The thesis is organized as follows:

Chapter 1 illustrates the basic principles of MR and the type of data used in the thesis. In this chapter, general information about the characteristics of MRS signals, measurement parameters, data studied and the most relevant metabolites in ^1H MRS is included. Finally, it presents the goals and structure of the thesis.

Chapter 2 introduces the details of MRS signals and the preprocessing steps required before quantification. Here, different methods studied and applied to the considered MRS data are also outlined. Additionally, some of the most common signal preprocessing problems are discussed in detail.

Chapter 3 describes some existing quantification methods developed for MRS and MRSI signals. In particular, the Automated Quantification of Short Echo time MRS Spectra (AQSES) and the quantitation based on QUantum ESTimation (QUEST) are introduced in more detail, as they are the methods used and modified in this thesis for obtaining metabolite concentrations.

Chapter 4 investigates the causes of incomplete water suppression in MRS and MRSI signals. Initially, the water filtering method HLSVD-PRO was used for accurate peak removal, however, choosing the adequate number of sinusoids was found to play an important role. Therefore, this chapter presents a heuristic approach to automatically determine an overestimated number of sinusoids that can be set in HLSVD in order to improve the peak removal not only for *in vivo*, but also for *in vitro* signals.

Chapter 5 describes the lineshape distortion problem and presents a lineshape estimation method that allows the quantification of lineshape-distorted MRS signals. This method has been validated in simulated, *in vitro* and *in vivo* ^1H MRS signals.

Chapter 6 is related to the background estimation of MRS data, more specifically, the macromolecular baseline. Making use of already acquired macromolecular signals, an advanced method for accurate, robust and efficient spectral fitting (AMARES), is used for estimating specific macromolecular and lipid resonances. These resonances are further used for creating a basis set of estimated individual baseline peaks which facilitates the quantification of baseline distorted signals.

Chapter 7 investigates the accuracy of quantification via residual analysis. Using different statistical tools, the presence of residual peaks and overfitting is evaluated.

Chapter 8 summarizes the main achievements of the thesis and outlines ideas for future research.

1.4 Conclusions

In this chapter, MRS and MRSI have been introduced and their applications in the diagnosis of tumor and metabolic diseases have been addressed. This thesis focuses on the preprocessing and intermediate steps for improving quantification of MRS(I) signals.

Chapter 2

Magnetic Resonance Spectroscopy (MRS) signals

In this chapter, the characteristics of MRS signals are described in detail considering their acquisition protocol and complexity. Section 2.1 presents the properties and types of ^1H MRS used in this thesis, namely simulated, in vitro and in vivo signals. In Section 2.2 some preprocessing and correction methods for analyzing MRS signals are presented.

2.1 Proton MRS signals

Thanks to its high sensitivity, ^1H MR has been successfully employed for studying *in vivo* tissues. ^1H MRS signals are measured in the time domain and often represented in the frequency domain for a better visualization of the metabolite resonances. When proton MR is used, all molecules containing ^1H are excited and can be observed in the MR spectrum, *e.g.*, water, metabolites and possibly macromolecules/lipid components. For diagnosis purposes, only metabolite and macromolecules/lipid information are of interest, therefore, the water resonance is usually filtered out to increase the reliability of metabolite estimation [167, 2, 62, 21, 112].

When quantifying metabolites, the biochemical information in the studied tissues can be obtained, helping clinicians in the understanding of metabolites in normal and pathological conditions. Recently, the clinical implementation of ^1H MRS has increased due to the technical improvements and performance of available MR scanners.

2.1.1 Time vs Frequency domain signals

Time domain MRS signals have ideally a decaying shape, also called FID, corresponding to a sum of complex-damped exponentials. However, in order to be able to visually observe the contribution of individual metabolites, MRS signals are transformed to the frequency domain using the FFT. This technique produces a spectrum that allows the visualization of peaks, which correspond to resonances of the detected metabolites reflecting the metabolic information of the tissue under investigation.

Noise standard deviation.

The noise standard deviation (σ) of an MRS signal can be computed in the time and in the frequency domain. In the time domain, it is usually computed from the last points of the FID (typically around 100) while in the frequency domain it is computed from the metabolite-free region (*i.e.*, from 6 to 10 ppm in ^1H MRS). In order to be able to numerically compare both computations, it is necessary to divide the σ computed in the frequency domain by \sqrt{NDP} . This issue arises from the fact that some implementations of FFT (such as the one in Matlab) do not use a normalization factor. In practice, it is important to consider that the time domain signal could be influenced by 'ghost' echoes and the frequency domain signal could be influenced by baseline contamination [83]. Therefore, a moving window along each signal is used and σ is set to the smallest standard deviation among all the windows.

2.1.2 In vivo signals

In vivo ^1H MRS signals are obtained without surgical intervention and allow in a non-invasive and non-ionizing way the diagnosis of cancer and metabolic diseases. The method employed to compute metabolite concentrations (amplitudes) is called quantification. This can be done by computing the area under each peak or by using a linear combination of individual peaks or metabolite profiles.

The set of metabolite profiles considered in some quantification methods contain complex-valued time domain signals that can be measured *in vitro* or simulated with information from quantum mechanics. Govindaraju *et al.* [56] present a list of ^1H NMR chemical shift and J-coupling values for 35 metabolites that can be detected by *in vivo* or *in vitro* NMR studies of mammalian brain. This information is also suitable for computer simulation of metabolite spectra.

The model describing a short TE *in vivo* time-domain MRS signal $y(t)$ as a combination of several metabolite profiles is:

$$y(t) = \sum_{k=1}^K a_k e^{(j\phi_k)} e^{(-d_k t + 2\pi j f_k t)} v_k(t) + B(t) + w(t) + \epsilon(t) \quad (2.1)$$

where K is the number of metabolites, $v_k(t)$ the metabolite profile in the basis set ($k = 1, \dots, K$), a_k the amplitudes, ϕ_k the phase shifts, d_k the damping corrections, f_k the frequency shifts due to B_0 inhomogeneity, $B(t)$ is the baseline due to macromolecules/lipid contamination, $w(t)$ the water resonance and $\epsilon(t)$ denotes white noise with standard deviation σ .

The *in vivo* signals used in this thesis were measured with the following acquisition parameters:

- **1.5 T signals.** These are single voxel MRS signals from a volunteer's brain acquired on a 1.5 T Philips NT Gyroscan (Philips Medical Systems, Best, The Netherlands) MR scanner. The acquisition parameters were: PRESS pulse sequence [12], TR=6 s, TE=23 ms, SW=1 KHz, NDP=512 points, 64 averages and a volume PRESS box of $4 \times 3 \times 3$ cm³. A spectrum with these acquisition parameters is shown in chapter 1 section 1.2 Fig. 1.9 (a).
- **3.0 T signals.** These are MRSI signals from a patient acquired on a 3.0 T Philips MR scanner (Achieva, Philips, Best, The Netherlands). The MRSI acquisition parameters were: PRESS pulse sequence with the water suppression method MOIST, TR=2 s, TE=35 ms, SW=2 KHz, NDP=2048 points, 1 average, FOV= 16×16 cm², VOI= 8×8 cm², slice thickness=1 cm, acquisition voxel size= 1×1 cm², reconstruction voxel size= 0.5×0.5 cm², shimming=pencil beam (first and second order), parallel imaging with SENSE factor: left-right=2, anterior-posterior=1.8, outer volume saturation bands with circular shape with gap 30 mm, power 10, in order to avoid lipid contamination from the skull. A spectrum with these acquisition parameters is shown in chapter 1 section 1.2 Fig. 1.9 (b).
- **9.4 T signals.** These are single voxel signals from mice acquired on a 9.4 T Bruker Biospec small animal MR scanner (Bruker BioSpin MRI, Ettlingen, Germany) with a magnet bore of 20 cm using a 7 cm linear body resonator as transmitter combined with a circularly polarized ¹H mouse brain surface coil for signal reception. The MR acquisition parameters were: PRESS pulse sequence with implemented pre-delay outer volume suppression as well as the water suppression method, VAPOR [170], TR=4 s, TE=12 ms, SW=4 KHz, NDP=2048 points and 256 averages. Spectra were corrected for B_0 instability due to eddy currents as well as B_0 drift using the Bruker

built-in routines. Remaining shimming problems, line broadening and non-Lorentzian character of the peaks may still be present after correcting for eddy currents. Shimming was performed using FASTMAP [59]. A spectrum with these acquisition parameters is shown in chapter 1 section 1.2 Fig. 1.9 (c).

2.1.3 In vitro signals

In vitro MRS signals refer to signals measured from phantom solutions containing either individual metabolites or a solution containing metabolic mixtures. Individual metabolite profiles can be used as basis set for the quantification of *in vivo* signals. These phantom solutions are produced with known concentrations that are taken into consideration for absolute quantification.

Three *in vitro* basis sets of metabolites used in this thesis were measured with the following acquisition parameters:

- **1.5 T.** A set of metabolites was measured on a 1.5 T Philips NT Gyroscan (Philips Medical Systems, Best, The Netherlands) MR scanner containing solutions of: Ala, Asp, Cr, GABA, Glc, Gln, Glu, GPC, Gly, Lac, m-Ins, NAA, PCh and Tau. Metabolites phantom solutions had concentrations from 50 to 200 mM and were dissolved in Phosphate Buffer Solution (PBS). 5 mM 3-trimethylsilyl-1-propane-sulfonic acid (DSS) was added as a chemical shift reference. Due to their chemical reaction in PBS, the metabolites GPC and PCh were dissolved in 100 mM NaCl instead of PBS. pH control was also required to assure reliability and avoid shifting of peaks such as NAA, Lac and Glu; thus, the pH for every phantom was adjusted to 7.20 ± 0.10 . The VOI was positioned almost in the middle of the phantom containing the metabolites.

Two reference compounds not overlapping with other metabolite resonances were added to the phantoms. The concentration of these compounds is unknown but they are assumed to be equal in all phantoms. One of these resonances is located at 0.0 ppm and the second one is located at 8.44 ppm (normally used for alignment and scaling purposes, respectively).

The MR acquisition parameters were: PRESS pulse sequence, TR=6 s, TE=23 ms, SW=1 KHz, NDP=2048 points and 64 averages with a volume PRESS box of $2 \times 2 \times 2$ cm³. B_0 eddy current correction [79] was performed using the water reference signal. Fig. 2.1 shows the real part of the spectra for the measured metabolites.

- **3.0 T.** The basis set of metabolites contained the same metabolites measured at 1.5 T. The MRS acquisition parameters were: 3.0 T Philips MR scanner

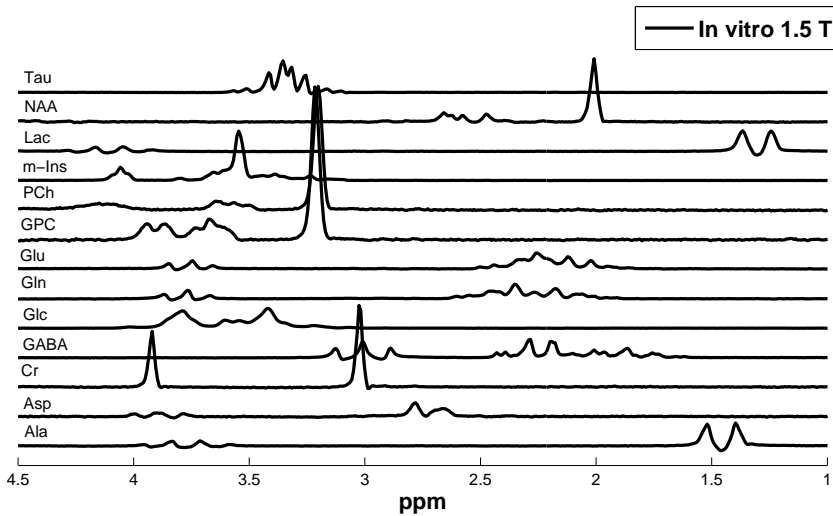


Figure 2.1: Real part of the spectra of the *in vitro* basis set of metabolites acquired at 1.5 T and used for quantification of MRS signals. Metabolites used for quantification are: Ala, Asp, Cr, GABA, Glc, Gln, Glu, GPC, Lac, m-Ins, NAA and Tau. Acquisition parameters: PRESS pulse sequence, TR=6 s, TE=23 ms, SW=1 KHz, NDP=2048 points and 64 averages.

(Achieva, Philips, Best, The Netherlands), PRESS pulse sequence with the water suppression method MOIST (Multiple Optimizations Insensitive Suppression Train), TR=2 s, TE=35 ms, SW=2 KHz, NDP=2048 points, a 8 channel head coil, 128 averages, iterative shimming, saturation bands with circular shape with gap 19 mm and power 3. Fig. 2.2 shows the real part of the spectra for the measured metabolites.

- 9.4 T.** The basis set of metabolites contained the same metabolites measured at 1.5 T plus the metabolite profiles of GSH and PE. In cases where s-Ins was required, its profile was generated from the model solution Gly by shifting the Gly resonance to the appropriate location. In the same way the profiles of NAAG and PCr were created from the NAA and Cr, respectively. The MR acquisition parameters were: 9.4 T Bruker Biospec small animal MR scanner (Bruker BioSpin MRI, Ettlingen, Germany), with a magnet bore of 20 cm using a 7 cm linear body resonator as transmitter combined with a circular polarized ^1H rat brain surface coil for signal reception, PRESS pulse sequence with implemented pre-delay outer volume suppression and water suppression VAPOR, TR=8 s, TE=20 ms, SW=4 KHz, NDP=6144 points and 64 averages. No B_0 drift correction was used. The basis set of reference metabolites is shown in Fig. 2.3.

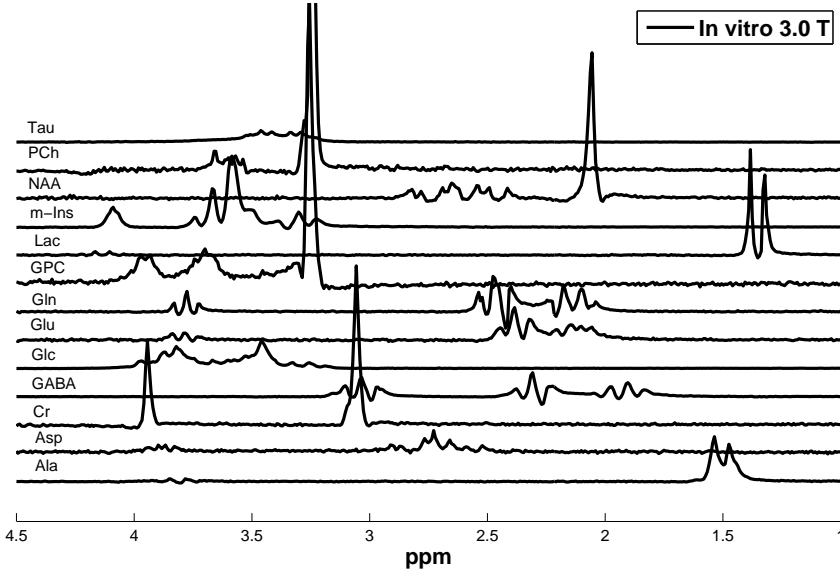


Figure 2.2: Real part of the spectra of the *in vitro* basis set of metabolites acquired at 3.0 T and used for quantification of MRS signals. Metabolites used for quantification are: Ala, Asp, Cr, GABA, Glc, Gln, Glu, GPC, Lac, m-Ins, NAA and Tau. Acquisition parameters: PRESS pulse sequence, $TR=2$ s, $TE=35$ ms, $SW=2$ KHz, $NDP=2048$ points and 128 averages.

2.1.4 Simulated signals

Making use of *prior* knowledge from measured metabolites, MRS signals and individual metabolites can also be simulated by providing the acquisition and quantum mechanical information: number of spins and spin parameters (J-coupling, chemical shift, etc.) and acquisition parameters (echo time, sequence, number of points and sampling frequency). Simulation of MRS signals becomes interesting because multiple individual measurements can be avoided. Several software packages have been developed for this purpose [160, 56, 165]. Fig. 2.4 shows two sets of metabolites obtained with similar parameters, namely (a) a set of *in vitro* measured metabolites and (b) a set of simulated metabolites. As can be seen here, only small differences are noticeable and therefore, both sets of metabolites can be used for quantification. Moreover, Cudalbu *et al.* [31] also proved that the quantification results obtained with both basis sets are similar. Further details about simulated metabolite signals and how to model them are given in chapter 3.

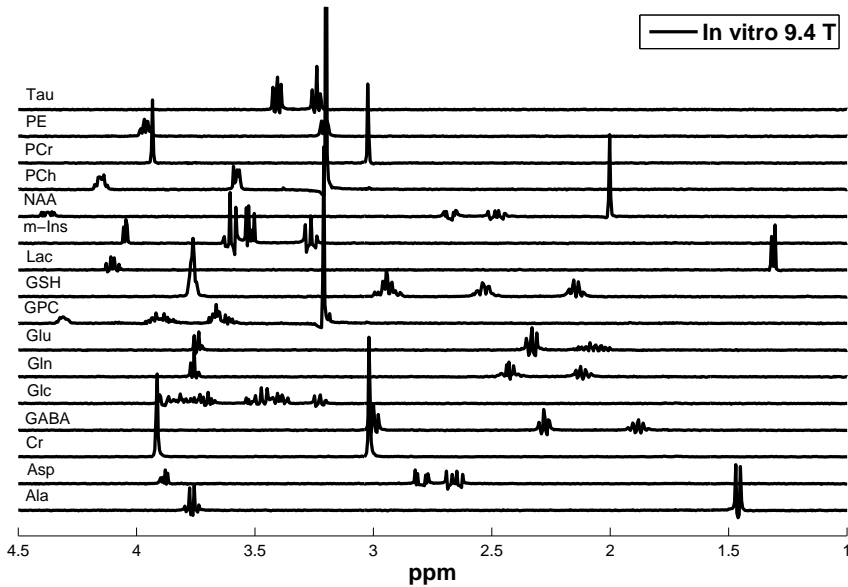


Figure 2.3: Real part of the spectra of the *in vitro* basis set of metabolites acquired at 9.4 T and used for quantification of MRS signals. Metabolites used for quantification are: Ala, Asp, Cr, GABA, Glc, Gln, Glu, GPC, Lac, m-Ins, NAA, PCh, PCr, PE and Tau. Acquisition parameters: PRESS pulse sequence, TR=8 s, TE=20 ms, SW=4 KHz, NDP=6144 points and 64 averages.

2.2 Preprocessing MRS signals

MR signal processing is required in order to extract relevant information about the metabolites. In the case of ^1H MRS, an essential procedure is related to the removal of the water resonance and other unwanted components [167, 2, 27, 62, 21, 112]. Moreover, the correction of signal artifacts originating at the acquisition level is also necessary [168, 46, 83, 183, 77]. In [138], Pouillet *et al.* suggest that all preprocessing techniques should be applied in the adequate order because some steps may affect the subsequent procedures.

The preprocessing methods below are only a fragment of the extensive procedures' list that can be applied to *in vivo* ^1H MRS:

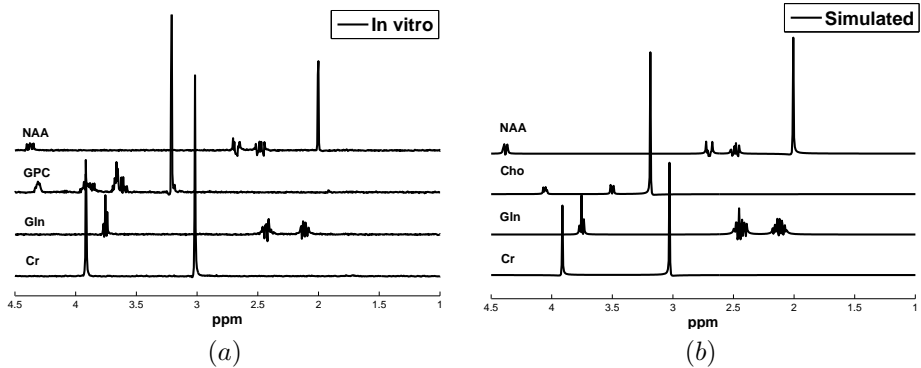


Figure 2.4: Comparison of an *in vitro* and simulated basis set of metabolites. (a) Set of *in vitro* spectra illustrating Cr, Gln, GPC and NAA, measured at 9.4 T in a Bruker scanner with acquisition parameters: PRESS sequence, $TR=8$ s, $TE=20$ ms, $SW=4$ KHz and 64 averages. (b) Simulated spectra illustrating Cr, Gln, Cho and NAA, obtained with a protocol similar to that described for the *in vitro* signals in (a); these simulations were performed in NMR-SCOPE [164].

2.2.1 Time circular shift

Due to an analog-digital filter incorporated in the Bruker system, the first data points of the time domain signal (FID) are initially zero and then increase until the actual FID starts [26]. The circular shift consists of removing data points from the beginning and adding them to the end of the signal, thus the data are shifted N points. The time circular shift is performed in the time domain for data which have been digitally filtered and decimated before saving the FID. Fig. 2.5 shows the FID and its respective spectrum before and after applying the time circular shift correction. As can be seen on the top plot, without correcting the time circular shift no resonances can be actually observed in the frequency domain. On the plot below, the initial points are added to the end of the FID and a well resolved spectrum can be observed. In order to avoid difficulties in the time domain quantification, these last points of the FID are simply truncated.

2.2.2 Frequency alignment

Spectral alignment is essential for most of the quantification methods. In this preprocessing step the FID is transformed to the frequency domain and the spectra are shifted such that some recognizable peaks reach the desired frequency locations [93, 184, 52]. In ^1H MRS, the resonance frequency of observable metabolites is known and, therefore, they can be used for shifting the full spectra. For instance,

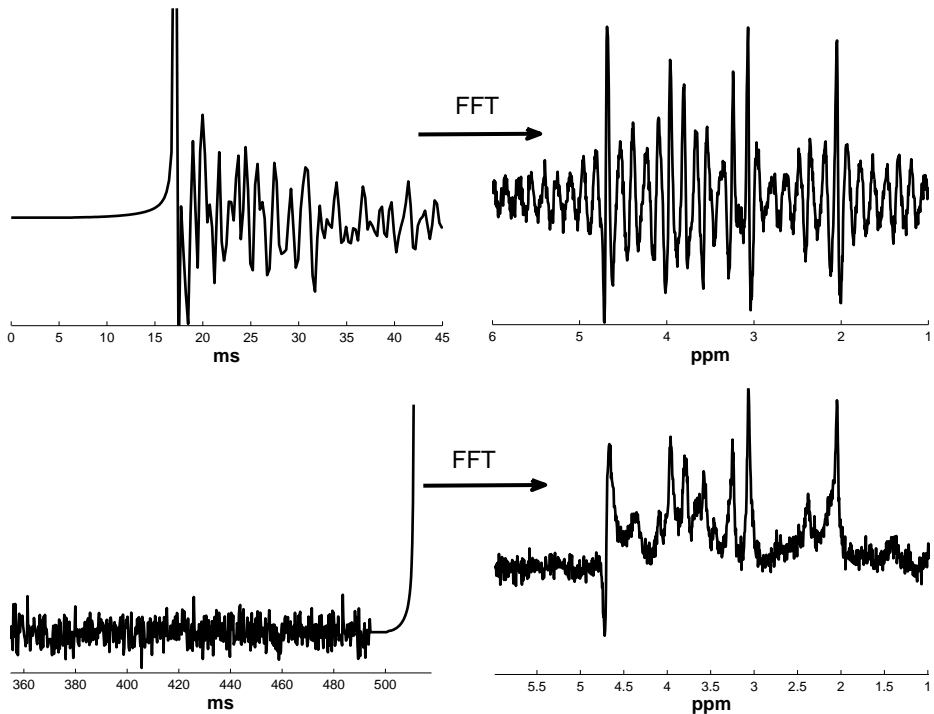


Figure 2.5: Real parts of time and frequency domain representation of an *in vivo* signal from mouse brain measured at 9.4 T in a Bruker scanner using a PRESS sequence and with acquisition parameters of $TR=4$ s, $TE=12$ ms, $SW=4$ KHz and 256 averages in a VOI of size $3 \times 1.75 \times 1.75$ mm³. Top: the first points of the FID are nearly zero, giving rise to a distorted spectrum as shown in the right plot. Bottom: time circular shift corrected signal where the initial points have been added to the end of the FID and produce a sort of increasing tail; the well defined spectrum shown in the right plot indicates the effect of time circular shift correction.

the main resonance of NAA (known to be located at 2.01 ppm) is commonly used as reference and spectra are aligned according to this peak. See Fig. 2.6.

In some particular cases, the chemical shifts of *in vivo* metabolites can vary depending on the tissue, temperature and pH. These variations affect the accurate estimation of metabolite resonances, especially when fitting a set of metabolite profiles to the *in vivo* signal. Therefore, advanced alignment using for instance quantum mechanics, may be necessary if displacement of individual spectral peaks in a metabolite are detected [92].

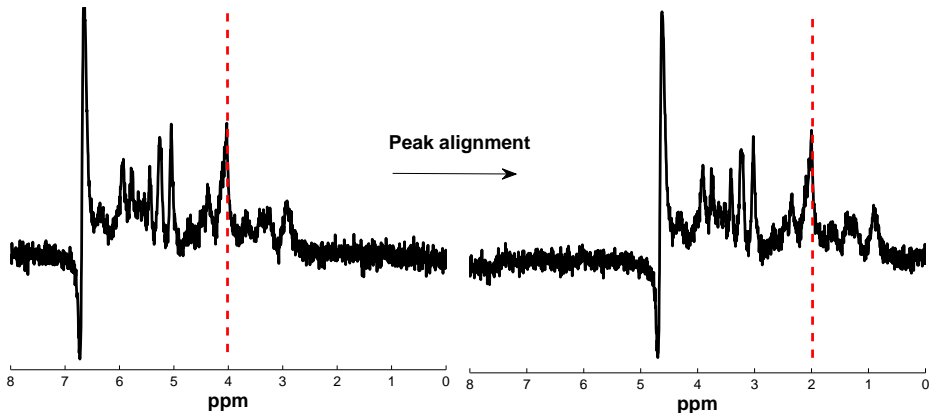


Figure 2.6: Real part of spectrum of an *in vivo* signal from mouse brain measured at 9.4 T in a Bruker scanner using a PRESS sequence and with acquisition parameters of $TR=4$ s, $TE=12$ ms, $SW=4$ KHz and 256 averages in a VOI of size $3 \times 1.75 \times 1.75$ mm³. Normally, the carrier frequency is located at the water peak (i.e., 4.7 ppm), however, when this position is changed the metabolites of interest resonate at different locations. Nevertheless, the resonance frequency of other peaks in ¹H MRS is known (e.g., NAA at 2.01 ppm) and can be used for peak alignment.

2.2.3 Phase correction

When MRS spectra are not zero-phased (also called absorption mode, thus peaks of interest pointing upwards), a correction is required in order to improve visualization and spectral analysis [22, 53, 126]. This correction consists of the multiplication of the complex spectrum by a complex phase factor equal to the initial phase of the FID [73]. In particular, for frequency domain methods (e.g. peak integration) zero-phased spectra are required before quantification in order to obtain reliable metabolite estimates. On the other hand, for the time domain methods presented in this manuscript, the phase correction is not necessary because all processing and analysis is done considering the real and imaginary parts of the time domain signal.

The usual phase correction term consists of two components, one frequency-dependent (first order phase) and the other one frequency-independent (zero order phase). The component which is frequency dependent is different for each peak in the spectrum. In order to phase-correct the spectrum, both the zero and the first order phases must be adjusted. This adjustment is, however, performed separately for the two phase correction components. To adjust the zero order phase manually, it is sufficient to tune the phase until all peaks in the real part of the spectrum are

positive. Adjusting the first order phase corresponds to the modification of the begin time of the MR signal, *i.e.*, the FID would no longer be supposed to start at time 0, but at a time $t_0 \neq 0$. See Fig. 2.7.

jMRUI [164] allows manual and automatic phase corrections, alternatively, other methods such as ACME [22] can be used to perform automatic phase correction. Moreover, quantification in the time domain can fit zero and first order phase factors.

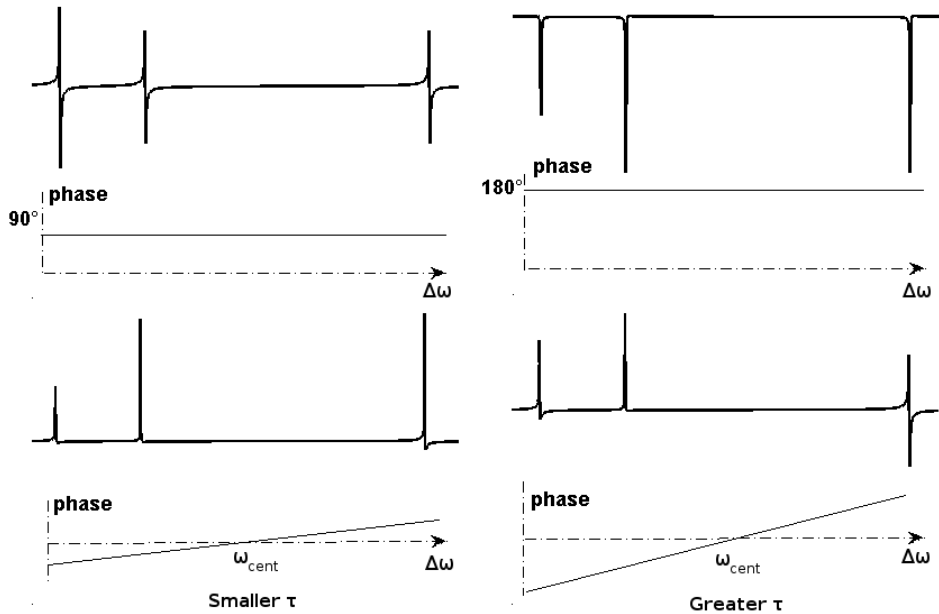


Figure 2.7: Top: zero order phase distortion influencing all peaks in the spectrum in the same way. Bottom: first order phase distortion influencing the peaks depending on the central frequency ω_{cent} and the parameter τ which determines how steeply the first order phase changes with the frequency. Figure reproduced from [73].

2.2.4 Truncation vs zero filling

In the acquisition of an FID, the time between successive data points is called dwell time and determines the spectral window. Hence, the total number of points multiplied by this dwell time represents the total time that the FID is sampled, which is also called the acquisition time. In order to adequately truncate the signal, it is necessary to consider that the minimum sampling frequency is twice the Nyquist frequency. The Nyquist Theorem states that the minimal sampling

frequency f_s of the time domain data (FID) should be at least twice the largest frequency difference, denoted here by ν , *i.e.*, $f_s \geq 2 \times \nu$; thus, the digital resolution of a signal is given by $\frac{f_s}{NDP}$. Therefore, a large NDP is essential for obtaining high resolution peaks in the spectrum.

- **Truncation:** This is the operation used to reduce the number of points in the acquired signal (FID). Truncation of an MRS signal consists of removing the last data points of the FID, as shown in Fig. 2.8. As a result, the spectral resolution is reduced, however, a severe truncation produces typical oscillatory ripples that can be observed in the spectrum [73]. This operation is computationally favorable for time domain quantification methods, though disadvantageous for frequency domain quantification methods.
- **Zero filling:** By adding zeros after the last data point of the FID it is possible to increase the digital resolution in the frequency domain (see Fig. 2.9). However, adding zeros to the acquired FID brings no new information to the signal, therefore, no improvement of the true resolution is obtained. Still, it improves the digital resolution and, thus, helps with the characterization of the peak shapes in the spectrum when frequency domain quantification methods are used. Zero filling is useful when a longer acquisition time would only result in the acquisition of noise [73].

Finally, it is important to consider that avoiding ripples in the baseline can be achieved by multiplying the FID with an exponential function (also called apodization), which ought to be performed *prior* to zero filling if the FID has not decayed to the noise level at the end of the acquisition window [73].

2.2.5 Eddy current corrections

Eddy currents are caused by the scanner and can not always be avoided. They are induced by the rapid switching in the magnet of the gradient coils and surrounding metal structures. These currents are a manifestation of Faraday's law of induction caused by the switching of the magnetic field gradients [35]. Klose [79] has developed a method to correct eddy currents (called ECC) by point-wise dividing the water suppressed signal by the phase term of the water unsuppressed signal.

2.2.6 Lineshape correction/estimation

Common lineshape models used in MRS [131, 127]:

Lorentzian: The spectrum of ^1H NMR signals contain symmetrical lines about the central peak depending on the size and shape of the molecular

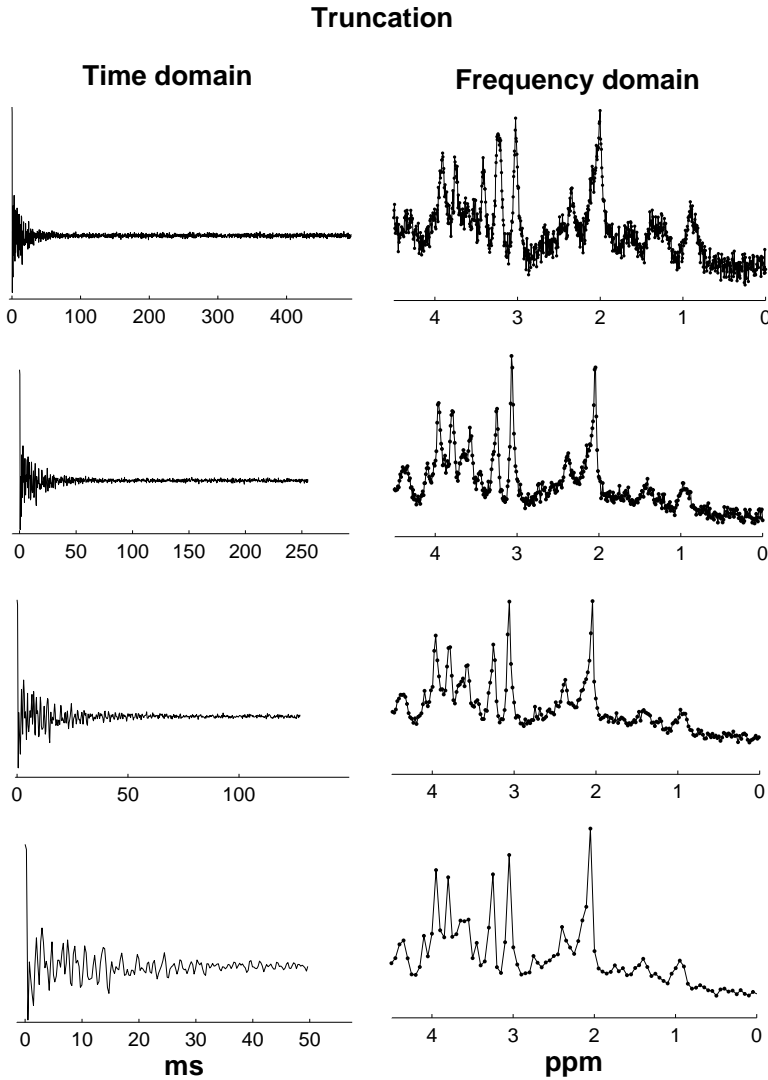


Figure 2.8: Real parts of time and frequency domain representations of an *in vivo* MRS signal from mouse brain measured at 9.4 T in a Bruker scanner using a PRESS sequence and with acquisition parameters of $TR=4$ s, $TE=12$ ms, $SW=4$ KHz and 256 averages in a VOI of size $3 \times 1.75 \times 1.75$ mm³. These plots show the original and the truncated signal with increasing number of truncation points, where the decrease in frequency resolution can be observed (points in the spectra).

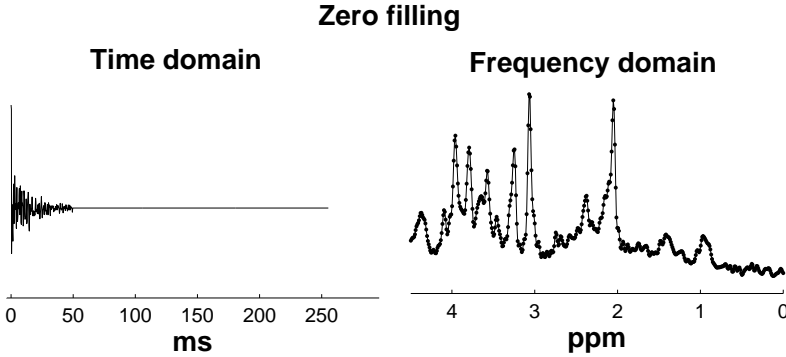


Figure 2.9: Real parts of time and frequency domain representations of an *in vivo* MRS signal from mouse brain measured at 9.4 T in a Bruker scanner using a PRESS sequence and with acquisition parameters of $TR=4$ s, $TE=12$ ms, $SW=4$ KHz and 256 averages in a VOI of size $3 \times 1.75 \times 1.75$ mm³. Zero-filled signal corresponding to the lower truncated signal from Fig. 2.8.

subgroup. Moreover, the interaction between the nuclear spins of the neighboring molecular groups causes broadening in these lines. Under ideal circumstances, MR spectra are expected to have a Lorentzian lineshape, thus the corresponding decay in the time domain has the formula:

$$D_L(t) = e^{-\alpha t} \quad (2.2)$$

Gaussian: When the relative orientations and positions of randomly distributed and interacting species do not change with time, a Gaussian lineshape is obtained. This lineshape is a consequence of the Central Limit Theorem, which states that if a large number of statistical distributions are summed, the result will tend to be a Gaussian (Normal) distribution. A Gaussian lineshape can thus be considered as the result of the influence of many unknown/unparameterizable factors. The decay in the time domain has then the formula:

$$D_G(t) = e^{-\beta t^2} \quad (2.3)$$

Voigt: The Voigt lineshape is the product of Gaussian and Lorentzian lineshapes. The Lorentz part expresses the ideal T_2 decay mechanism, while the Gaussian part the influence of unknown/unparameterizable factors. The time domain formula is:

$$D_V(t) = e^{-\alpha t - \beta t^2} \quad (2.4)$$

The time and frequency domain representation of these functions are shown in Fig. 2.10.

MRS quantification methods commonly assume that the spectral resonances have lineshapes of the Lorentzian type, which is acceptable under ideal experimental circumstances. Nevertheless, due to magnetic field inhomogeneities, imperfect shimming, residual eddy current effects, and macro-/micro- susceptibility effects caused by tissue heterogeneities, this Lorentzian shape is inadequate. Alternatively, other shapes such as Gaussian [127] and Voigt [104] have been used to compensate this problem [35].

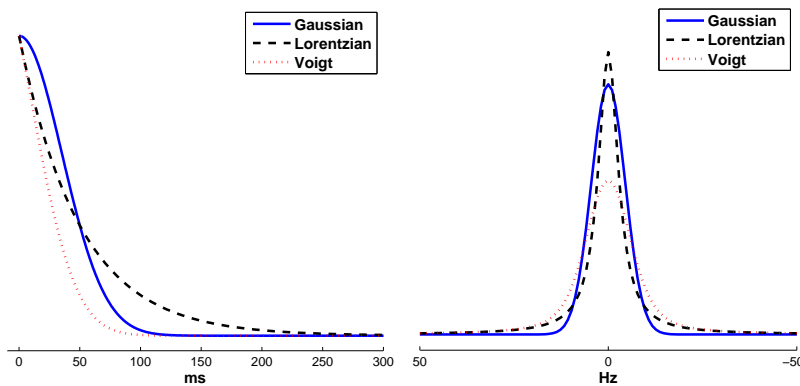


Figure 2.10: Real part of the time (left) and frequency (right) domain of ideal lineshapes: Lorentzian, Gaussian and Voigt.

Furthermore, Abragam [1] suggested that in solid state (including tissue), NMR can yield many different shapes. Thus, the lineshape may have any arbitrary form different from the basic Lorentzian, Gaussian or Voigt type (see Fig. 2.11). From the results presented by Deelchad [38], the microscopic susceptibility effects are the main factor contributing to the line broadening as the field strength increases since the contribution of the relaxation pathways via dipolar mechanisms to T_2 are relatively small compared to the relaxations induced by local magnetic susceptibility relaxation effects. Therefore, several lineshape estimation methods have been developed as part of the pre-processing steps to deal with different lineshapes and correct the distortions.

Some of the methods related to hardware setup are called shimming techniques, and are applied during the MR scanning session in order to correct field inhomogeneities and thus improve spectral quality [59, 11, 74, 75]. MRS acquisitions at high magnetic fields exhibit lineshape distortions that may only be corrected using higher-order shimming techniques, which are not always available

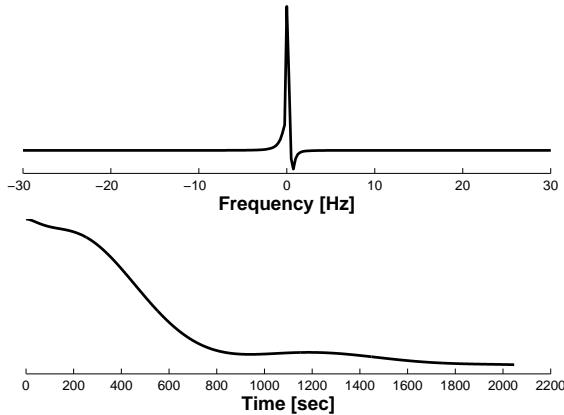


Figure 2.11: Real parts of the frequency and time domain representations of a simulated eddy current and lineshape distortion function.

[59, 60, 83]. Moreover, in measurements near an air cavity such as sinuses, shimming can not always compensate for local field inhomogeneities, and the lack of spectral quality leads to lineshape distortions.

Methods aiming at enhancing the spectral resolution of ^1H MRS signals based on the deconvolution of spectra using the lineshape derived from a reference signal have been successfully applied to *in vivo* MRS signals [115, 34, 178, 6, 107]. De Graaf *et al.* [34] proposed the time domain deconvolution method called **QUALITY**, in which the FID is point-wise divided by a reference signal obtained separately or via inverse Fourier transform of an isolated single resonance from the original spectrum. As a consequence, Lorentzian lineshapes can be approximated. Some years later, Bartha *et al.* [6] proposed the spectroscopic lineshape correction called **QUECC** by integrating the lineshape correction methods **QUALITY** and **ECC**. Similarly, Metz *et al.* [107] proposed a simple and effective reference deconvolution method for resolution enhancement in MRS which uses the shape of a single resonance line to measure the actual frequency distribution produced by the local B_0 inhomogeneity and then deconvolves that distribution from the whole spectrum. This is a simple linear process which requires no *prior* knowledge of the number of lines, their intensities, or their relaxation characteristics, and no fitting procedures are used.

Apart from these methods used as a preprocessing step, there are other lineshape estimation methods included in the quantification of MR signals, which will be described in detail in chapter 3.

2.2.7 Residual water suppression

In vivo ^1H MRS signals contain a water resonance usually 10^3 to 10^4 larger than those of metabolites. Thus, to be able to identify metabolites and obtain a high SNR, an efficient suppression of the water peak is required. Water suppression techniques during acquisition provide a residual water signal at the level of most observable metabolites [47, 170, 21, 117, 112]. Although these methods have a good performance, there is usually an incomplete water suppression and residual water remains in the signal (see Fig. 2.12, left). As a consequence, the metabolite peaks near the water resonance are altered and the tail of the residual water may affect the baseline of the signal. Furthermore, complete and accurate suppression of unwanted peaks in *in vitro* metabolite measurements is essential for reliable quantification. Therefore, numerical methods are required to suppress the unwanted peaks after acquisition.

Hankel Singular value decomposition (HSVD) -based methods have been successfully used for water removal [129, 190, 90]. Similarly, time domain [102], filtering [167, 175, 136], wavelets [2] and indirect covariance [23] methods have shown to provide good results.

In chapter 4 we propose to combine HLSVD with a heuristic method to overestimate the model order in HLSVD. Results obtained for *in vitro* and *in vivo* signals show a complete elimination of water and reference peaks.

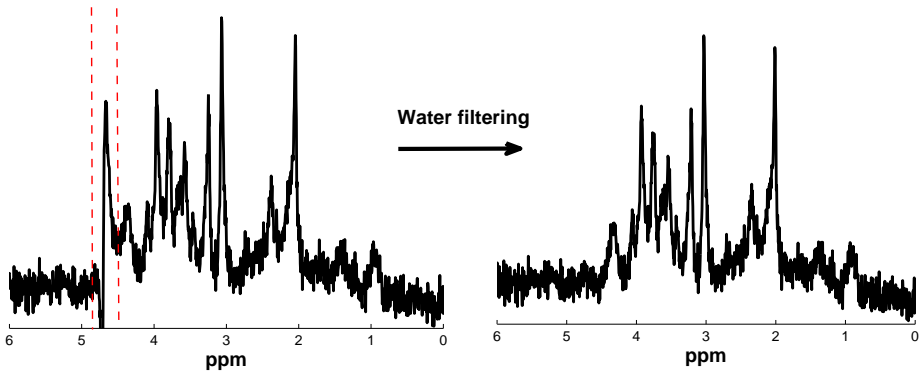


Figure 2.12: Real part of an *in vivo* spectrum from mouse brain measured at 9.4 T in a Bruker scanner using a PRESS sequence and with acquisition parameters of $TR=4$ s, $TE=12$ ms, $SW=4$ KHz and 256 averages in a VOI of size $3 \times 1.75 \times 1.75$ mm³. Left: unfiltered signal. Right: water suppressed signal using the method HLSVD-PRO [90].

2.2.8 Baseline correction/estimation

Baseline estimation is very important in the quantification of *in vivo* MRS signals and can be the source of many systematic errors, therefore, an adequate correction/estimation method is necessary. Successful baseline correction approaches have been presented for *in vitro* [7] and *in vivo* measurements [71, 118, 153].

The baseline of *in vivo* MRS signals is characterized by a broad and non-flat unknown spectrum overlapping with the peaks of interest. This baseline has very short T_2^* values corresponding to lipids and macromolecules. Therefore, it can be identified with a fast decaying FID. In *in vivo* ^1H MRS signals with long TE the baseline is not present, while short TE signals exhibit a significant baseline distortion.

The major issue with the baseline is that it complicates quantification and affects accurate metabolite estimation. An additional reason for obtaining a baseline distortion in *in vivo* ^1H MRS signals is the incorrect or incomplete water suppression/filtering, since the tail of the water peak may also affect the baseline of the neighboring resonances [73].

Several acquisition and numerical methods have been proposed to correct the baseline before or during quantification. On the one hand, despite the time consuming required for the acquisition-based methods such as inversion recovery, they are widely used. In this group of baseline methods, Knight [81] proposed the application of multiple inversion recoveries for suppression of macromolecule resonances in short TE ^1H MRS of human brain. Moreover, Hofmann *et al.* [67] proposed the characterization of the macromolecule baseline in localized ^1H MR spectra of human brain based on a series of saturation recovery scans allowing the simultaneous recording of the macromolecular baseline and the fully relaxed metabolite spectrum. Compared to inversion recovery, the saturation recovery method is less susceptible to T_1 differences inherent in signals from different metabolites or introduced by pathology. Seeger *et al.* [155] presented a reliable detection of macromolecules in single volume ^1H NMR spectra of the human brain, indicating that the spatial presaturation of fat-containing regions leads to a sufficient suppression of the lipid contamination and enables the detection of highly reproducible macromolecular resonances. Thus, in single voxel as well as in multiple voxel MR acquisitions, the combination of volume selection and outer volume presaturation is highly recommended to ensure accurate detection and reliable evaluation of even small pathological alterations in macromolecules. More recently, Kunz *et al.* [88] proposed a novel diffusion-weighted spectroscopy method to determine the macromolecular resonances.

Alternatively, when no baseline measurement has been performed in the acquisition step, numerical methods based on, *e.g.*, polynomials and splines to fit a smooth function below the actual spectrum have been widely used [162, 61, 25, 185, 37].

For instance, Cobas *et al.* [25] presented an automatic baseline correction of NMR data by modelling the baseline based on the Whittaker smoother algorithm using basically spline curves. Chang *et al.* [19] proposed a fully automated method for baseline correction which is able to accurately determine baseline points in very dense spectra without destroying the lineshapes of prominent peaks; to this end, signal points are differentiated from baseline points. Golotvin and Williams [54] create a smooth spectrum and use it for baseline area recognition and modeling; moreover, to complete the model, an interpolation technique is employed over the signal regions and the model is subtracted from the measured spectrum giving a flat baseline. See Fig. 3.3.

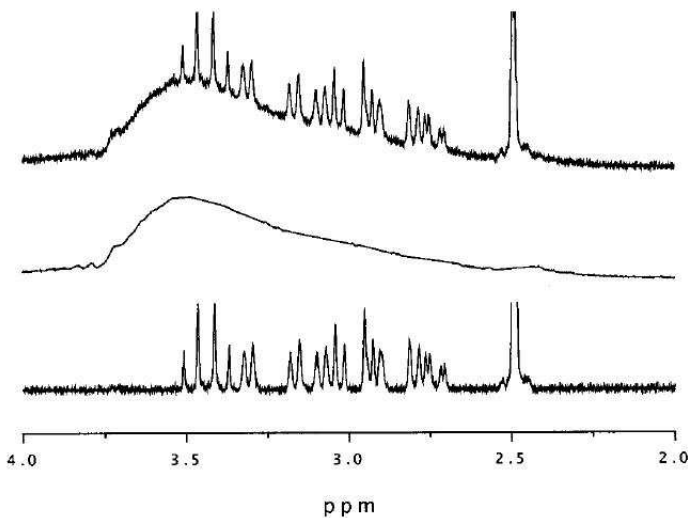


Figure 2.13: ^1H MR spectrum illustrating the baseline estimation method proposed by Golotvin and Williams [54]. Top: Original 400 MHz spectrum with a water hump. Middle: the baseline model consisting of fragments of the smoothed spectrum and regions interpolated by straight lines. Bottom: the spectrum after baseline subtraction. Figure from [54].

Diverse baseline estimation methods applied during quantification have been proposed using either inversion recovery measurements or semi-parametric modeling methods. Such methods have been proposed by Provencher [140], Soher *et al.* [161], Ratiney *et al.* [143], Elster *et al.* [45], Pouillet *et al.* [137] and the method presented in this thesis in chapter 6 [121]. Additionally, Gottschalk *et al.* [55] and Cudalbu *et al.* [33] have compared the baseline estimation using both, inversion recovery and semi-parametric estimation. Further details on the estimation of the baseline during the quantification are described in chapters 3 and 6.

2.3 Conclusion

This chapter describes the MRS signals used in this thesis and the preprocessing steps used before analysis. Particular interest is focused on the water filtering, the lineshape and the baseline estimation. Concerning the water filtering of *in vivo* signals and reference peaks from *in vitro* signals, a detailed description of the proposed methods with overestimation is given in chapter 4. Moreover, a lineshape estimation method used for correcting *in vivo* signals is described in detail in chapter 5. Finally, the baseline estimation approaches using AQSES, QUEST and parametric methods based on individual peaks, are further discussed in chapter 6.

Chapter 3

Quantification

Chapter 3 presents the quantification methods used in this thesis and the main issues to consider when quantifying in vivo ^1H MRS signals. Particularly, the quantification methods AQSES and QUEST are introduced and some hints about handling simulated and in vitro metabolite basis sets are given. Finally, section 3.2.5 deals with the interpretation and understanding of quantification results.

3.1 Introduction

In vivo MRS signals contain the metabolite information of the tissue under investigation. Nowadays, MRS(I) can be non-invasively performed in the most important organs of the body and serves as a complementary tool for diagnosis. This technique avoids unnecessary surgeries and facilitates the early detection of cancer and metabolic diseases. However, limitations concerning the quality and direct interpretation of MRS(I) data need to be solved. Therefore, continuous improvements of acquisition techniques, hardware and protocols are being developed in order to overcome these problems. All these achievements increase the potential of integrating MR techniques in the clinical diagnosis routine [64].

Although numerous MRS studies have shown to successfully serve in the non-invasive and complementary diagnosis of multiple diseases [98, 64, 100, 179], reliable quantification is still an issue and further improvements are necessary.

Several quantification methods have been developed in the time and the frequency domain allowing the quantification of MR signals from different nuclei measured at different TEs, such as LCModel [140, 141], AMARES [176], QUEST [143], AQSES

[137]. Other quantification methods are based on time-domain non-iterative fitting (HLSVD) [4, 129, 171, 20, 40, 90, 91], iterative time- and frequency domain fitting [158], semi-parametric fitting [45], variable projection (VARPRO) [16, 172], time domain fitting of one peak at a time and wavelet modelling for the baseline [147, 41], constrained least squares (TARQUIN) [145, 182], genetic algorithms [108], fast Padé transform [9, 8], artificial neural networks [10, 66], sparse representation [63], circular fitting [51] and principal component analysis [13, 166]. An extended review of time- and frequency domain methods has been given in [174, 109] and more recently in [138]. Pouillet *et al.* [138] present the advantages and drawbacks of each method, together with an overview of preprocessing methods including lineshape correction and removal of unwanted components. Moreover, advice about processing and data handling depending on the data under investigation is also given. Finally, other studies have compared the performance between quantification methods [76, 32], where inclusion of *prior* knowledge appeared to be important for the robustness and accuracy of metabolite estimates.

3.2 Methods

In this section, two time-domain metabolite quantification methods for short TE MRS signals are presented. Both methods are based on fitting the model presented in chapter 2 section 2.1.2 Eq.(2.1), using a basis set of metabolites. The baseline distortions are taken into account in different ways using semi-parametric estimation. Both methods have been developed by partners of the FAST project (*Advanced Signal-Processing for Ultra-Fast Magnetic Resonance*, MRTN-CT-2006-035801, a Research and Training Network granted by Marie Curie Actions in the 6th Framework Program (2007-2010), <http://fast-mrs.eu>).

3.2.1 Automated Quantification of Short echo time MRS signals (AQSES)

The method mostly used and improved in this thesis is AQSES [137]. This method provides the metabolite amplitudes of short MRS data and these amplitudes are the weighting coefficients of a linear combination of corrected *in vitro* metabolite profiles used for quantification. A major issue in short TE data is the presence of a smooth lipid/macromolecular baseline underneath the spectra. In AQSES, this baseline ($B(t)$ from Eq.(2.1)) is fitted via nonparametric modeling using a basis of splines [44]. This baseline is computed to be smooth in the frequency-domain, but fitting is done in the time domain [134, 157].

To be able to fit the model and the smooth baseline together, a regularized nonlinear least squares (NLLS) criterion is considered:

$$\min \frac{1}{N} \sum_{t=t_0}^{t_{N-1}} |y(t) - \sum_{k=1}^K a_k e^{(j\phi_k)} e^{(-d_k t + 2\pi j f_k t)} v_k(t) + B(t)|^2 + \lambda^2 \|Dc\|^2 \quad (3.1)$$

where the estimated signal includes the baseline computed using splines, ($B(t) = \mathcal{B} \cdot c$, where \mathcal{B} is a spline basis matrix and c the linear coefficients multiplying the splines matrix), $\lambda^2 \|Dc\|^2$ gives the degree of smoothness to the splines in the frequency domain. In particular, the regularization matrix D is needed to measure the smoothness of the baseline in the frequency domain, taken as a (combination of) discrete derivative operator(s) and λ is a fixed regularization (penalty) parameter that can be automatically selected using a generalized cross validation criterion [157]. Concerning the residual water ($w(t)$ in Eq.(2.1)), it could be filtered out using a maximum-phase pass-band FIR filter [136]. Alternatively, HLSVD methods can also be used for filtering out the water resonance before performing quantification [90]. AQSES fits the model to the experimental data using constrained optimization based on the Levenberg-Marquardt [114] algorithm. Improvements in quantification performance can be obtained by including *prior* knowledge [16] between metabolites.

In order to assess quantification results, the approximate Cramér-Rao lower bounds (CRLB) [17, 18] are computed. They provide an indication about the uncertainty and reliability of the estimated amplitudes (concentrations). Exact CRLBs provide, for any choice of noise level, the lowest possible estimation errors for the model parameters for any estimation procedure, but they can only be computed if we have an exact model function depending on a finite number of model parameters and if we know the true values of those model parameters. Then, CRLBs are computed from the diagonal elements of the inverse of the Fisher information matrix (\mathcal{F}^{-1}) evaluated at the true values of the model parameters. Since the nonlinear least squares estimator (maximum likelihood estimator) is asymptotically normally distributed (by application of the central limit theorem), \mathcal{F}^{-1} acts as an asymptotic covariance matrix for the model parameters and ellipsoidal confidence bounds with a given confidence level can be constructed with this covariance matrix. The individual CRLBs for each model parameter are the diagonal elements of \mathcal{F}^{-1} . In maximum likelihood estimation, the estimated parameter values are substituted for the unknown true parameter values, thus giving an “observed” Fisher information matrix and leading to approximate CRLBs. Moreover, when part of the model is unknown (semi-parametric estimation), as it is the case for MRS signals with baseline contributions or with unknown decay function, the estimated parameters are necessarily biased. In general, the CRLB theory does not hold for this situation. Only under some

additional assumptions, Ljung [97, chapter 9, p. 283] and later Pintelon and Schoukens [130, chapter 15, p. 502] provided an extensive explanation of the validity of CRLB for biased, but consistent estimators.

Small CRLB values may (but not necessarily) indicate good parameter estimates, however, they can be affected by low SNR, incomplete basis set of metabolites or metabolites with similar spectral characteristics. These CRLB are proportional to the variance of the residue obtained from subtracting the fitted signal and the baseline from the original signal. Additionally, the results can be evaluated performing residual analysis.

AQSES has been implemented in the Java open source available software AQSES GUI [36, 137] and as a quantification method inside the Matlab[®] graphical user interface SPID [135]. See Fig. 3.1 for an illustration. More recently, AQSES has been included in the jMRUI software package [165] and is available as a plug in.

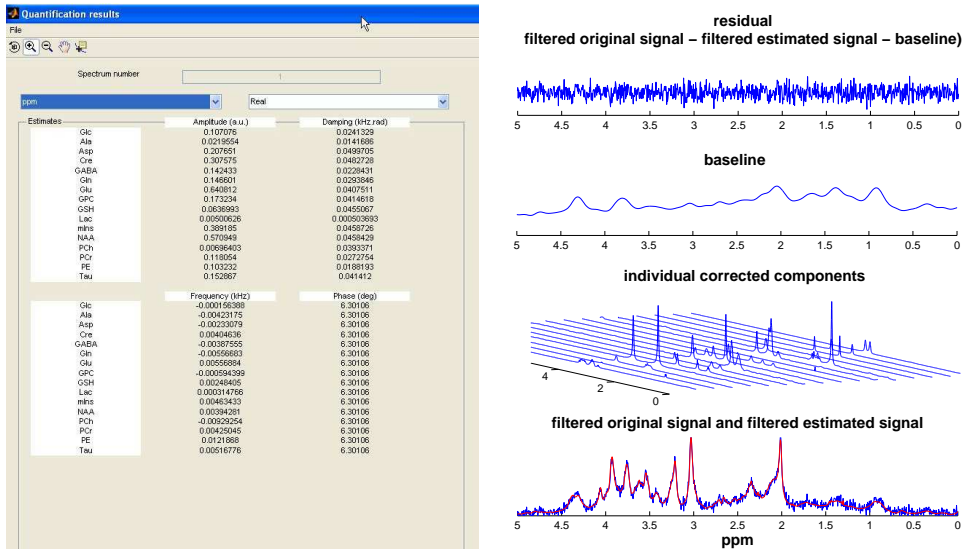


Figure 3.1: Quantification results window for AQSES in SPID (left side) of an *in vivo* ^1H MRS signal from mouse brain measured at 9.4 T in a Bruker scanner using a PRESS sequence and with acquisition parameters of $TR=4$ s, $TE=12$ ms, $SW=4$ KHz, $NDP=2048$ and 256 averages in a VOI of size $3 \times 1.75 \times 1.75$ mm³. The basis set of 16 metabolites used in the quantification were measured *in vitro*. The plots on the right side from top to bottom correspond to: residue, baseline (computed with splines using a small regularization parameter $\lambda=0.1$), estimated metabolites and original with estimated signal.

3.2.2 Quantitation based on QUantum ESTimation (QUEST)

Similar to AQSES, QUEST [143, 144] is a time domain quantification method that can accommodate any basis set lineshape to the experimental signal with Lorentzian corrections via NLLS. Here, the inclusion of *prior* knowledge between metabolites and the computation of the CRLB are similar to AQSES. Additionally, it requires the water removal as a preprocessing step (*e.g.*, HLSVD [129, 186, 90]). The baseline estimation is integrated in the quantification and estimated via a non-parametric procedure based on the short T_2^* of macromolecules and lipids. QUEST assumes the baseline to be present only in the first data points of the time domain signal (FID).

The baseline estimation approaches in QUEST are called ‘Subtract’ and ‘InBase’ [143] and consists of the following steps [134]:

- (i) Truncate the initial data points of the original FID which are expected to contain the macromolecules and lipids contribution.
- (ii) Estimate the metabolite parameters from the truncated signal using NLLS fitting with a metabolite-only basis set.
- (iii) Using the estimated metabolite parameters, reconstruct the non-truncated metabolite signal and subtract it from the original FID to obtain a noisy version of the macromolecular signal.
- (iv) Model the macromolecular signal by a sum of K exponentially damped sinusoids using HSVD. Thereafter, the baseline in QUEST can be handled in two ways:
 - (a) Obtain a metabolite-free signal by **subtracting** the modeled macromolecular signal from the original FID and quantify the resulting signal. This algorithm is called Subtract-QUEST.
 - (b) The modeled macromolecular signal is **added to the basis set of metabolites** and the original FID is quantified using this new basis set. This algorithm is called InBase-QUEST.

QUEST has been implemented as a quantification method in the software package jMRUI¹ [165]. See Fig. 3.2 for an illustration.

3.2.3 Metabolite profiles

Quantification methods using a basis set of metabolite profiles rely on the quality and number of metabolites included in the basis set and facilitate the quantification

¹<http://www.mrui.uab.es/mrui/> (Accessed: June 1, 2011)

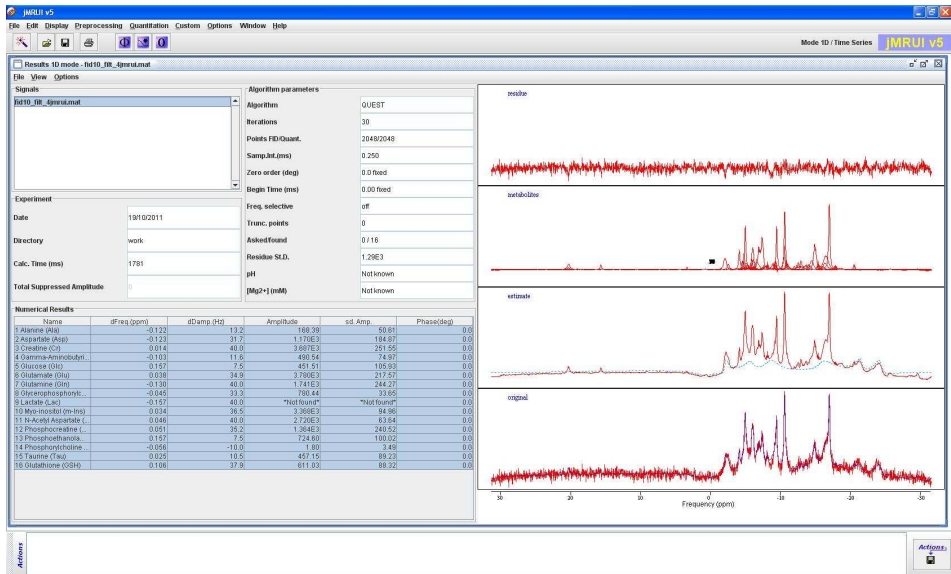


Figure 3.2: Quantification results window for QUEST in jMRUI (left side) of an *in vivo* ^1H MRS signal from mouse brain measured at 9.4 T in a Bruker scanner using a PRESS sequence and with acquisition parameters of $TR=4$ s, $TE=12$ ms, $SW=4$ KHz, $NDP=2048$ points and 256 averages in a VOI of size $3 \times 1.75 \times 1.75$ mm³. The basis set of 16 metabolites used in the quantification were measured *in vitro*. The plots on the right side from top to bottom correspond to: residue, estimated metabolites, estimated signal with baseline (computed by truncating the first 20 points of the FID) and original with estimated signal.

of overlapping peaks. These signals can be created via simulations based on quantum mechanics (e.g., NMR-SCOPE [58] and GAMMA [160]), or from *in vitro* spectra measured using phantom solutions of individual metabolites. In both cases, the basis set should satisfy the same acquisition scheme as that of the signals under investigation.

Simulated basis set

In this thesis, we use NMR-SCOPE [58] for simulating metabolite profiles. The sequence and spin parameters can be defined as follows:

- Acquisition sequence: PRESS was the pulse sequence used in this thesis. Moreover, NMR-SCOPE allows the setting of additional sequences and their corresponding phases.

- Echo Time (TE) in ms: This parameter is important and should be equal to that of the *in vivo* measured signals.
- Number of data points (NDP): This number is set equal to the number of acquisition points in the measured signal, which is normally a power of 2 and is also related to the sampling frequency. Usually, an NDP from 512 to 2048 is good enough to acquire an *in vivo* signal.
- Sampling step in ms: This parameter is also called dwell time and is equal to the time between data points.
- Damping factor in Hz: This damping allows the simulation of spectra with a linewidth similar to that of *in vivo* signals (a value of 10 Hz is normally used).
- Number of spins: jMRUI [165] provides a set of metabolite files with their spin characteristics *i.e.*, the chemical shifts and coupling constants for ^1H NMR based on the work presented by Govindaraju *et al.* [56].
- Transmitter frequency in Hz: It is absolutely necessary to indicate the magnetic field at which the signals need to be simulated (*e.g.*, 63.861 Hz for 1.5 T).
- Carrier frequency: In case of ^1H MRS, the carrier frequency is usually located at the water peak, thus, at 4.7 ppm.

Until now, the effects of temperature, pH, B_0 inhomogeneities and RF pulses were not included in the NMR-SCOPE simulation package. However, Starcuk *et al.* [163] have recently presented an updated NMR-SCOPE tool. This package gives the MR spectroscopist the possibility to simulate MR signals with the real shaped pulses used in the experiment. Moreover, it is possible to obtain proper spectral patterns including line phases influenced by frequency selective excitation, and to study the effects of various parameters with minimum programming.

In vitro basis set

For several studies described in this thesis, a set of *in vitro* metabolite profiles measured at 1.5 T, 3 T and 9.4 T were acquired. A full description of the acquisition protocol and a figure illustrating all three basis sets is presented in chapter 2 section 2.1.3. Concerning temperature of the phantoms, it is acceptable to measure metabolites at room temperature up to 3 T. However, at higher fields it is necessary to increase the temperature to 37°C, especially for Cr and PCr [142]. Basically, the basis set should have a higher SNR and resolution than the *in vivo* MRS signals. Moreover, it is important to measure all metabolites at the same location in the scanner in order to keep the same voxel size positioned in the middle

of each phantom and to shim before each acquisition is done. The acquisition time should be taken long enough to allow the FID to decay into the noise.

Using *in vitro* profiles yield the following advantages and drawbacks:

Advantages

- The characteristics of *in vitro* profiles are usually closer to the *in vivo* measured signals due to similar field conditions.
- Once a basis set is correctly acquired, it can be used to quantify all *in vivo* signals measured under similar conditions. Moreover, variations in the TR, the spectral bandwidth and the acquisition time per scan are allowed.

Drawbacks

- In contrast to simulated basis sets, the acquisition of individual signals require a lot of effort and expertise (scanner and personnel). Since all *in vivo* MRS signals will be further quantified using the measured basis set, this measurements must be carefully performed. Thus, reliability of quantification results also depends on the quality of those measured *in vitro* profiles [142].
- Phantom solutions of individual metabolites degrade with time, which means that some phantoms may only be used immediately after preparation (*e.g.*, Gln, GSH). This issue makes the measurements more expensive and inflexible for posterior measurements. Therefore, for consistency it is better to acquire them all with different protocols in one session [142].
- Metabolite spectra must have higher accuracy and resolution than the *in vivo* spectra. This can be achieved by measuring highly concentrated phantom solutions, which are rather expensive [142].
- Acquisition of *in vitro* signals is done at the TE of the *in vivo* signal, however, if the acquisition protocols are updated or changed, new measurements are required to fit the new protocol.

Simulated or *in vitro* basis set?

Differences in both sets of metabolites are sometimes observed. However, some studies encountered insignificant differences in metabolite estimates when using both approaches in quantification [31, 181]. Regardless of the way of obtaining the basis set, spectral quality has a large influence on metabolite quantification, therefore, it is essential to carefully simulate and measure these metabolite profiles.

When realistic signals can not be achieved with simulations, a well measured *in vitro* basis set is more appropriate. Nevertheless, a very important issue to consider is the number and selection of metabolites used for quantification.

- A list of the main metabolites to be included in quantification of ^1H MRS signals are: Ala, Asp, Cr, Cho compounds (GPC, PCh), GABA, Glc, Gln, Glu, m-Ins, Lac, NAA, NAAG, PCr, s-Ins and Tau. This list can be decreased or extended depending on the data quality (metabolites present) and the magnetic field.
- The metabolite profile of Gly is a singlet that can not be resolved from m-Ins (~ 3.56 ppm), and therefore, it should not be included in the basis set [142].

3.2.4 Parameters to be considered in quantification of ^1H MRS signals

Before performing quantification, it is essential to consider different quantification parameters important for increasing the reliability and accuracy of metabolite estimates. When using a basis set of metabolites the following parameters need to be set:

Damping constraint

In order to allow the individual metabolite profiles to vary in damping, such that they can adequately fit the experimental signal, it is necessary to set a damping constraint. This parameter is measured in Hz in AQSES [137] and QUEST [143] and can take positive or negative values, meaning that the damping in the basis set can be bigger or smaller than that of the experimental signal. In AQSES there is a unique input number to be considered positive and negative while in QUEST it consists of two input parameters - one positive and one negative. This parameter is set manually in both quantification methods. It is important to consider that a small damping constraint will not allow the metabolites (which usually have a smaller damping) to correctly fit the *in vivo* signal. On the contrary, a very large damping constraint will be disadvantageous for small metabolites, as they will rather fit the baseline. We propose a way to compute an approximate damping constraint (see [122] or chapter 7), by computing the upper bound for the damping factor constraint as the difference between the FWHM of the reference water signal and a reference peak selected from the *in vitro* metabolites (*e.g.*, NAA). Further influence on quantification and experimental results about this issue are described in chapter 7.

Frequency constraint

Similar to the damping constraint, the setting of the frequency constraint allows the metabolite profiles to be shifted, such that they are aligned and can adequately fit the corresponding metabolites in the experimental signal. Setting of this parameter in AQSES and QUEST is similar to the setting of the damping constraint. Usually, simulated and *in vitro* signals have a frequency location similar to that of the experimental signals, however, small shifts may be required in order to correct for temperature and pH changes. On the other hand, shifting of relative resonances in one metabolite may occur and advanced frequency alignment is required [92].

Baseline estimation

The baseline methods used before quantifying *in vivo* signals have been described in chapter 2. Thus, the baseline estimation methods described in this section are focused on: (a) inversion recovery (acquisition technique described in chapter 1), (b) modeling with splines in AQSES [137], (c) truncation of the initial points of the FID implemented in QUEST [143] and (d) a proposed parametric method with individual peaks based on measured macromolecular baselines [121] described in detail in chapter 6.

- (a) Inversion recovery. The Baseline from inversion recovery allows the suppression of metabolite resonances and visualization of macromolecules and lipids. The obtained signal can be included in the basis set of metabolites for fitting short TE signals contaminated with short T_2^* components. Results in *in vivo* signals using this method have been reported in [128, 30, 33, 121, 88, 55].

Kreis *et al.* [85] proposed the integrated data acquisition and processing (IPAD) method based on a combined 2-dimensional experimental and fitting strategy to determine metabolite contents, relaxation times, and macromolecular baseline in single examinations of individual subjects. With this approach, a series of localized saturation recovery spectra are recorded and combined with 2-dimensional *prior* knowledge fitting to simultaneously determine metabolite T_1 , T_2 , concentrations and macromolecular baseline. Seeger *et al.* [154] proposed an extension of the basis set of brain metabolites by including several parameterized components for macromolecules and lipids derived from metabolite-nulled *in vivo* spectra of normal brain and high-grade gliomas. Further studies using the measured baseline in quantification methods such as LCModel [141, 111] have been presented in [128]. Other approaches using QUEST [30, 29, 55] and AQSES [120] have been more recently presented.

- (b) Modeling with splines in AQSES. The baseline is characterized by a smooth function modeled with a basis of splines as described in Section 3.2.1. This set of splines is fitted together with the model functions (metabolites) following a regularized NLLS criterion and the degree of smoothness can be tuned via a regularization parameter. In [120] (see also chapter 6) a comparison of baseline approaches using inversion recovery and the modeled splines in AQSES suggests that a combination of both methods provides a better approximation of the macromolecular baseline.
- (c) Truncation of the initial points of the FID. The components having a short T_2^* correspond to macromolecules and lipids. Their contribution is, therefore, present in the first points of the FID and this property is used by the QUEST algorithm. Further details about the baseline estimation approach in QUEST are described in Section 3.2.2 on Page 43. This technique has been demonstrated to be a reliable method to estimate the macromolecular baseline in short TE *in vivo* signals [30, 33, 55].
- (d) Parametric method with individual peaks based on measured macromolecular baselines. A basis set of resonances corresponding to macromolecules and lipids is obtained by extracting the information from measured inversion recovery signals. Then, extracted resonances are used together with the basis set of metabolites to fit the baseline allowing frequency and damping corrections to fit different experimental signals [154, 67, 121]. This baseline method with parametric peaks is further explained in chapter 6.

Lineshape

The ideal lineshape of MR spectra is considered to be Lorentzian, however, due to field inhomogeneities and tissue heterogeneities this Lorentzian lineshape may change and take any arbitrary form. The model in Eq.(2.1) includes Lorentzian lineshape corrections for all spectra. However, a lineshape correction method or a lineshape estimation may be required in order to obtain reliable quantification results. Additionally, in quantification methods such as peak integration, a phase correction, ECC [79] and lineshape estimation are essential for reliable metabolite estimation. In the quantification based on a basis set of metabolites, each profile has normally a lineshape of Lorentzian type as a result of a well-shaped simulated signal or a homogeneous phantom.

Some preprocessing methods such as ECC [79], QUALITY [34] and QUECC [6] described in Section 2.2.6 are not always able to correct lineshape distortions. There exist also several reference-free methods that extract a common lineshape by modelling the signal itself [140, 106, 107, 132, 158, 156, 123] or by magnetic field mapping [42]. Therefore, in order to adequately fit the metabolite profiles to

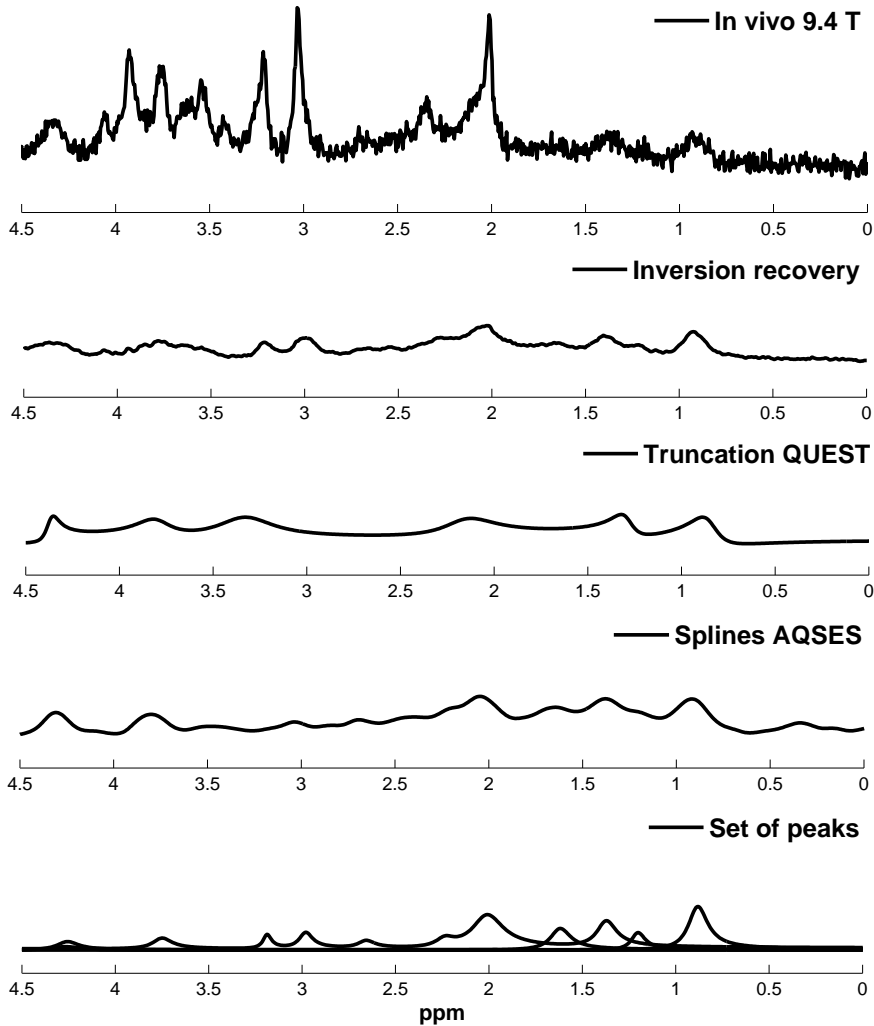


Figure 3.3: Real part of a ^1H in vivo spectrum from mouse brain measured at 9.4 T in a Bruker scanner using a PRESS sequence and with acquisition parameters of $TR=4$ s, $TE=12$ ms, $SW=4$ KHz, $NDP=2048$ points and 256 averages in a VOI of size $3 \times 1.75 \times 1.75$ mm 3 . The three plots below the in vivo signal correspond to different baseline estimation methods: inversion recovery, QUEST (truncating 20 points), AQSES (splines with small $\lambda=0.1$) and parametric method with 11 identified peaks selected according to the method presented in chapter 6.

the lineshape distorted spectra, it is recommended to modify the lineshape of the metabolite profiles.

Maudsley [106] proposed a method to determine spectral lineshapes using deconvolution of the data with an initial estimate of the same spectrum, referred to as self-deconvolution. It determines amplitude and phase lineshape distortions which may be caused by field inhomogeneity and gradient eddy current effects. This lineshape is incorporated into a parametric spectral analysis procedure, resulting into a reduction of the number of parameters to be determined and an accuracy improvement of the fit. In a similar approach, Sima *et al.* [156] study the self-deconvolution method for automatic estimation of the unknown lineshape distortion and show that using adequate hyper-parameters for denoising the estimated lineshape, the overall quantification results are improved. Later, Osorio *et al.* [123] presented an improvement of the method described in [156] by reducing the number of hyper-parameters in the denoising step and showed results in simulated, *in vitro* and *in vivo* signals. Further details about this last method are described in chapter 5.

Popa *et al.* [132] proposed a lineshape estimation method inferred from the data at hand. Because the estimation of metabolite concentrations is usually done by NLLS fitting of a physical model function based on minimizing the residue, the semi-parametric task is handled by two criteria: (a) obtaining a minimal residue and (b) limiting the width of the spectral line.

Prior knowledge

Due to the difficulty of disentangling the contributions from overlapping resonances, underlying baseline (macromolecule and lipid components), water resonance and random noise, previous studies suggest that the inclusion of *prior* knowledge increase the accuracy and reliability of the metabolite estimates. In the past, *prior* knowledge referred to imposing relations between individual peaks (*e.g.*, known frequency location, equal damping and phase, constant amplitude ratios) [20, 158, 40, 41, 16, 17, 172, 176]. More recently, *prior* knowledge involves the use of appropriate metabolite basis sets [140, 143, 137, 182] and, in the case of MRSI data, even imposing spatial constraints such as smoothness in the spectral parameter maps [78, 28].

3.2.5 Quantification results

Metabolite estimates provided by quantification are used to determine their concentration in either an absolute or relative way. When absolute molar concentrations are considered, a direct comparison between, for instance, a healthy

and a diseased tissue is possible. On the other hand, relative concentrations are computed using ratios between peak areas of other metabolites and therefore, a direct comparison is not possible. Here, the assumption that the denominator remains constant and is not a part of the disease process studied is essential. For instance, the peak of Creatine at 3.03 ppm is widely used as the denominator and its concentration is relatively stable with age but reflects variations with tumors and diseases [151]. Finally, obtaining reliable absolute concentrations is a challenge due to the numerous factors affecting the final results. In practice, the differences in the T_1 and T_2 relaxation times, diffusion, susceptibility and location of VOI need to be considered between the calibration compound and the acquired MR signal.

Absolute vs relative concentrations

Absolute concentrations are obtained taking into account a calibration signal and measurement parameters between the reference signal and the measured MR signal (*e.g.*, T_1 and T_2 relaxation times which are tissue dependent, localization, etc.). Absolute concentrations are normally given in millimoles [mM=mmol/L] (number of moles of metabolite per liter of tissue water), or molality [mm=mmol/Kg] (number of moles of metabolite per kilogram of tissue water). A way to calculate the absolute concentrations is:

$$[C_{met}] = \left(\frac{S_{met}}{S_{ref}} \right) [Ref] C_n C_{av} \quad (3.2)$$

where C_{met} is the concentration of a particular metabolite, S_{met} is the amplitude of the metabolite signal with the applied correction factors (*e.g.*, T_1 , T_2 , hardware, localization, etc.), S_{ref} is the amplitude of a reference signal with the applied correction factors, $[Ref]$ is the concentration of the reference compound, C_n is the correction for the number of equivalent nuclei for each resonance and C_{av} the correction for the number of averages [35].

In absolute quantification the following computations can be considered:

- Using an internal concentration reference. The peak areas in the acquired spectrum are compared with the areas of a ‘stable’ reference compound. In ^1H MRS, the water, tCr and NAA are normally used as references, however, their concentrations may change during the development of diseases. For instance, NAA has been found to change in neurodegenerative diseases and when discriminating between water and cerebrospinal fluid (CSF) a difference of about 30-40% has been observed [84].

When the water is used as reference, the term $[Ref]$ in Eq.(3.2) becomes the concentration of water which is equal to 110 M. This concentration is obtained as:

$$C_{H_2O} = \frac{n_{H_2O}}{V} \quad (3.3)$$

where n_{H_2O} is the molecular mass of the water molecule and V the volume of the VOI. Because the molecular mass of water molecule is 18 g/mol, the density of water is 1000 g/L and the water molecules contains 2 protons, we have that $C_{H_2O} = \frac{1000g/L}{18g/mol} \times 2 = 111$ M, but it is normally set as 110 M.

Additionally, a correction factor corresponding to the water content in the VOI is necessary. This correction factor is ~ 0.82 for gray matter, ~ 0.73 for white matter, >0.95 for CSF and ~ 0.78 for skeletal muscle [35].

- Using an external concentration reference. For this approach, a reference signal from a calibration sample can be obtained and the concentration is computed using Eq.(3.2). With this technique, problems caused by the B_1 field distribution can be solved by symmetric placement of the sample with respect to the coil [35].
- Using an external simulated phantom concentration reference. This can be obtained by simulating human tissue using a spherical phantom of known composition. In this method, systematic errors such as B_1 inhomogeneity and localization affect the phantom and the tissue in similar ways. Usually, a reference sample with resonances outside the region of interest is selected (*e.g.*, TMS, DSS) [35].

Relative concentrations can be obtained by dividing the estimated amplitudes by a reference peak or reference signal. For instance, the Creatine peak at 3.03 ppm and the water reference signal are commonly used for this purpose. These concentrations are given in arbitrary units [65, 72].

Considering both strategies one may conclude that [134]:

- Relative concentrations are less sensitive to abnormalities than absolute concentrations.
- When using a reference peak for obtaining relative concentrations, it is essential to consider a peak that does not change (which may be difficult to assure depending on the variability of the tumor or metabolic disease).
- Errors coming from relative concentrations may be higher compared to absolute concentrations [72, 95].
- Absolute concentrations require the correct assessment of calibration signals and measurement conditions.

3.3 Conclusion

In this chapter the main issues involved in the quantification of ^1H MR signals have been presented. Special focus was given to the quantification methods AQSES and QUEST (mostly used in this thesis) and the parameters involved in the improvement of quantification reliability. Additional studies considering these methods and further improvements concerning the removal of the unsuppressed water, lineshape and baseline will be discussed in chapters 4, 5 and 6.

Chapter 4

Filtering of residual water

In this chapter several model order selection methods using HLSVD for peak removal are presented. The aim is to introduce the water filtering in ^1H MRS signals using HLSVD and describe a way to automate the selection of the number of sinusoids to be used in HLSVD.

4.1 Introduction

In vivo ^1H MRS signals contain a water resonance usually 10^3 to 10^4 larger than those of metabolites. Several acquisition techniques are able to suppress this resonance, however, a residual peak remains and may affect the metabolites in the neighborhood or the baseline of the signal. Furthermore, complete and accurate filtering of unwanted peaks¹ in *in vitro* metabolite solutions is essential for building up a basis set used in quantification.

Numerical methods have been developed to suppress the remaining peaks in the MR signals, such as singular value decomposition (SVD) [129, 190, 90], filtering [102, 167, 175, 136], wavelets [2] and indirect covariance methods [23], which require the setting of specific parameters.

Hankel Singular Value Decomposition (HSVD) methods [87, 4, 186, 129] have been successfully used for modeling and quantifying an MRS signal as a sum of exponentially damped complex-valued sinusoids of Lorentzian type. Moreover, the computation time of the SVD can be reduced significantly by using the Lanczos algorithm (HLSVD) [129]. When HLSVD is used for filtering, the modeled

¹By unwanted peaks we mean not only the residual water, but also the peaks corresponding to the buffer solution and additional reference peaks (see chapter 2 section 2.1.3).

components in the desired region (corresponding to the water and unwanted peaks) can be subtracted from the original signal. Then, HLSVD filters out these resonances without affecting the resonances of the metabolites of interest. On the other hand, when HLSVD is used for quantification, the amplitudes of the individual components provide the metabolite concentrations. In both cases, the expected number of sinusoids (*i.e.*, the model order K) and cutoff frequencies where peaks should be suppressed are defined by the user and therefore, performance depends on these user defined parameters.

Several approaches have been focused on the automatic determination of an optimal model order K and reliable water peak removal [86, 173, 96, 14, 125, 89, 69, 187]. Their validation in simulated, noiseless or non-overlapping peaks shows promising results. However, a validation study in real *in vivo* signals will provide more insight of the power of each method.

Cabanes *et al.* [14] presented a method to estimate the model order for HLSVD based on a large series of simulated signals coming from *in vivo* short echo time signals with distorted water lineshapes and low SNR. After validating the method using HLSVD with different model orders, an optimal model order of 25 ($K = 25$) appeared to be a good choice for short TE *in vivo* ^1H MRS signals of human brain.

Other studies have suggested model orders of 10 [50] and 25 [31] for *in vivo* and *in vitro* signals obtained at 1.5 T and 7.0 T, respectively, corresponding to the visible peaks in the spectra. Due to the fact that MRS resonances may have a non-ideal Lorentzian shape, an overestimation of the model order used in HLSVD may be beneficial. In this case, multiple complex-damped sinusoids can better describe a non-Lorentzian lineshape-distorted resonance.

4.2 Materials and Methods

4.2.1 MRS signals

In vitro and *in vivo* data were acquired at different magnetic fields:

1.5 T signals.

These signals were acquired on a 1.5 T Philips NT Gyroscan (Philips Medical Systems, Best, The Netherlands) MR scanner.

- *In vitro* signals. The following metabolites were measured *in vitro* to be used as basis set for quantification: Ala, Asp, Cr, GABA, Glc, Gln, Glu, GPC, Lac, m-Ins, NAA, PCh, and Tau. A complete description of the acquisition

protocol and a figure illustrating the basis set is presented in chapter 2 section 2.1.3.

- *In vivo* signals. Single voxel MRS data from a volunteer's brain were acquired on a 1.5 T scanner. A complete description of the acquisition protocol and a figure illustrating an *in vivo* signal is presented in chapter 2 section 2.1.2.

3.0 T signals.

These signals were acquired on a 3.0 T Philips MR scanner (Achieva, Philips, Best, The Netherlands).

- *In vitro* signals. The basis set of metabolites measured at 3.0 T contained the same metabolites used at 1.5 T. A complete description of the acquisition protocol and a figure illustrating the basis set is presented in chapter 2 section 2.1.3.
- *In vivo* signals. MRSI data from a patient were acquired with a 3.0 T scanner. A full description of the acquisition protocol and a figure illustrating an *in vivo* signal is presented in chapter 2 section 2.1.2.

9.4 T signals.

These signals were acquired on a 9.4 T Bruker Biospec small animal MR scanner (Bruker BioSpin MRI, Ettlingen, Germany).

- *In vitro* signals. The basis set of metabolites at 9.4 T contained the same metabolites used at 1.5 T plus two additional metabolites: GSH and PE. A complete description of the acquisition protocol and a figure illustrating the basis set is presented in chapter 2 section 2.1.3.
- *In vivo* signals. These single voxel signals were acquired from wild-type mice and a model mice for Alzheimer's disease (APP.V717I transgenic mice²). A full description of the acquisition protocol and a figure illustrating an *in vivo* signal is presented in chapter 2 section 2.1.2. Mice were anesthetized by using 1.25% isoflurane and their heads were immobilized during the experiments.

All experiments were performed conform with regional, national and European regulations.

²These mice serve as valuable preclinical models for the amyloid pathology in Alzheimer's disease and are exploited for biotechnological and pharmaceutical drug development

MRS signals were preprocessed before quantification following the steps described in chapter 2 section 2.2 according to the acquired signals, (*i.e.*, *in vitro* and *in vivo* at different magnetic fields):

- a) *Time circular shift.* A time circular shift of 68 points (provided with the scan files) was applied to all *in vitro* and *in vivo* Bruker signals. Consequently, a truncation of those last points from the tail is necessary to ensure that the FID decays into the noise.
- b) *Eddy current corrections.* All *in vitro* 1.5 T signals were eddy current corrected using Klose's method [79]. For the 3.0 T and 9.4 T signals, this procedure is performed in the scanner software directly.
- c) *Phase correction.* Zero order phase corrections were applied to 1.5 T and 9.4 T signals.
- d) *Water and reference peak filtering.* This step is evaluated in detail in the next sections. Basically, we need to filter out the residual water in all *in vivo* and *in vitro* ^1H MRS(I) signals, as well as the reference peaks in the *in vitro* signals.

4.2.2 HLSVD method

HLSVD [129] is a reliable method for peak filtering with application in different fields, which decomposes a signal into a sum of exponentially damped complex-valued sinusoids [90, 89, 69]. HLSVD is non-iterative and requires minimal user interaction (black box method). Therefore, very limited *prior* knowledge about the resonances can be imposed on the fitting procedure and the model function is limited to exponentially decaying sinusoids (*e.g.*, Lorentzian).

The signal of length N is arranged in a matrix as follows:

$$\mathbf{H}_{L \times M} = \begin{pmatrix} x_1 & x_2 & \dots & x_M \\ x_2 & x_3 & \dots & x_{M+1} \\ \vdots & \vdots & \ddots & \vdots \\ x_L & x_{L+1} & \dots & x_N \end{pmatrix}$$

where $L > K$, $M > K$ and $L + M - 1 = N$, K being the (unknown) number of exponentially decaying sinusoids. Then, the matrix will be decomposed in: $\mathbf{H}_{L \times M} = U_{L \times L} S_{L \times M} V^H_{M \times M}$, where U , V are unitary, H stands for conjugate transpose of a matrix, S is the diagonal matrix which contains the singular values. The rank of the matrix, *i.e.*, the number of non-zero singular values, is equal to the model order in a noiseless signal, *i.e.*, K , but \mathbf{H} will be full rank in the presence of noise in the signal.

Concerning the size of the Hankel matrix, it has been demonstrated [14] that it is convenient not to use the last points of the signals which contain only noise. Above a certain SNR, the singular values of \mathbf{H} , arranged in decaying order, can be split into signal-related and noise-related singular values. Then, the noise-related singular values are smaller than the K singular values describing the signal, *i.e.*, they are closer to zero [129].

For well-resolved spectra with reasonable SNR, the value of K can be determined from the sharp cutoff in magnitude of the singular values, or the number of resolved peaks in the spectrum above a predefined threshold region. However, for low SNR spectra, the determination of an appropriate threshold region is more difficult.

HLSVD applied to MRS signals provides K exponentially damped complex-valued sinusoids with specific amplitudes A_k , frequencies f_k , dampings d_k and phases ϕ_k , corresponding to every peak in the signal. Thus, for water and unwanted peak suppression, the exponentially damped sinusoids located at specified frequency regions are selected and subtracted from the original signal. In this study, we use HLSVD-PRO [90] to filter all MRS signals; this is an implementation of HLSVD, where the singular value decomposition is computed using the Lanczos method with Partial ReOrthogonalization.

4.2.3 Model order selection

Several studies have focused on the optimal model order selection and different approaches have been developed for that purpose [96, 14, 125, 189, 69, 187]. However, determining whether K should be equal to or larger than the number of visible peaks in the spectrum remains an issue. On one hand, underestimating K leads to a poor signal decomposition where not all peaks are modeled and therefore a frequency selective region suppression may lead to a significant residual. On the other hand, a too large overestimation of K results in a signal decomposition including noise components and generates unwanted spectral features. Therefore, Lin *et al.* [96] suggest that the choice of K is related to the SNR, the overlapping frequencies and the length of the signal.

Here, we consider 5 different methods to estimate the model order used in HLSVD: (a) rank determination [173], (b) Minimum Description Length (MDL) [96], (c) Subspace-based Automatic Order Selection (Samos) [125], (d) Fixed model order of 25 [14, 31] and (e) a simple heuristic approach based on overestimation. The methods in (a), (b) and (c) estimate the model order automatically using the SVD and the method in (e) is a fast peak-counting based approach.

a) Rank determination method

This method is described in [173, p. 89] and presents the rank determination of a noisy matrix. If the elements in a low-rank matrix are affected by

independently and identically distributed zero mean errors with variance σ^2 , an appropriate rank (*i.e.*, the number of singular values that can be numerically considered nonzero) is selected from counting how many singular values of the diagonal matrix S are larger than

$$\sqrt{2 \max\{L, M\}}\sigma \quad (4.1)$$

where $L \times M$ are the dimensions of the data matrix (in our case the Hankel matrix \mathbf{H}). σ^2 is computed in MRS signals from the last sample points (*e.g.*, the last 100) of the time domain signal, which are assumed to contain only noise (see chapter 2 section 2.1.1).

b) **Minimum description length (MDL)**

This method was initially described independently by Schwarz [152] and Rissanen [146], see also [177]. Schwarz used Bayesian arguments assuming that each competing model can be assigned a *prior* probability, and the model that yields the maximum posterior probability is selected. In parallel, Rissanen considered information theoretic arguments, where each model is used to encode the observed data and the model that yields the minimum code length is selected. Later, Lin *et al.* [96] applied MDL to MRS signals and determined the optimal value of K by minimizing a discrete function of the singular values already computed:

$$MDL(k) = -\log \left[\frac{(\prod_{i=k+1}^L \sigma_i)^N}{(\frac{1}{L-k} \prod_{i=k+1}^L \sigma_i)^{(L-k)N}} \right] + \frac{1}{2}k(2L - k) \quad (4.2)$$

where σ_i are the singular values of \mathbf{H} , *i.e.*, the diagonal elements of the matrix S .

c) **Subspace-based Automatic Order Selection method (Samos)**

Papy *et al.* [125] proposed a model order estimator based on the matrix $U_k^{tb} = [U_k^\uparrow | U_{k\downarrow}]$ by varying k from 1 to $L-2$ with unit step. U_k contains the first k left singular vectors of the Hankel matrix \mathbf{H} . The matrices U_k^\uparrow and $U_{k\downarrow}$ are derived from U_k by omitting its first and last row respectively. Then, the SVD of U_k^{tb} is computed as $U_k^{tb} = Y\Gamma W^H$ where the matrix Γ is a diagonal matrix which contains the singular values γ_i . Using Γ , it is possible to estimate the model order K as

$$\tilde{K} = \arg \max_k \frac{1}{E(k)}, 1 \leq k < (L - 1)/2 \quad (4.3)$$

where

$$E(k) = \frac{1}{k} \sum_{i=k+1}^{2k} \gamma_i \quad (4.4)$$

d) **Fixed model order of 25**

A fixed model order of 25 has been widely used in HLSVD methods to filter out resonances from *in vivo* and *in vitro* spectra. As described in [14, 31], a fixed model order of 25 can be used to sufficiently suppress the residual water of *in vivo* and *in vitro* signals.

e) **Heuristic approach based on overestimation**

We propose an alternative approach to estimate the model order by overestimating the number of sinusoids describing one single resonance. First, the time domain signal is truncated in order to obtain a spectrum with lower, but still adequate, spectral resolution. Then, considering the spectral resolution of the truncated signal, an estimated number for the model order is obtained by counting spectral points significantly above the noise level.

(A) **Truncation.** Because the metabolite information is contained in the decaying part at the beginning of the FID, we aim to decrease the spectral resolution of long signals by truncating the completely decayed part containing only noise. This truncation point is computed based on the point at which the FID starts decaying into the noise.

To find this truncation point, all points of the original signal smaller in absolute value than the standard deviation σ computed as explained in chapter 2 section 2.1.1 are selected. Due to signal oscillation, the first selected points might not necessarily belong to the noise and therefore they should not be considered as part of the tail. In order to select the truncation point, these points are binned (as in a histogram) and K-means clustering function from Matlab[®] is used to separate the bins into two classes according to their height. The class with higher average height represents truly noise points, since they reflect high density of selected points lower than σ . Finally, the first point of this class is selected as the truncation point. This whole procedure is fully automated.

(B) **Model order overestimation.** An approach considering the frequency resolution of the truncated signal is proposed to determine an overestimated model order K . First, the Fourier transform of the truncated FID, which is a lower resolution but less noisy spectrum than the one obtained from the full-length FID, is computed. Then, we consider that the number of frequency points describing the resonances of the truncated spectrum is a good approximation of an overestimated

number of sinusoids. Finally, the model order K is computed as the number of spectral points outside a noise-related threshold region defined by $[-5\sigma, 5\sigma]$, as shown in Fig. 4.1 (b).

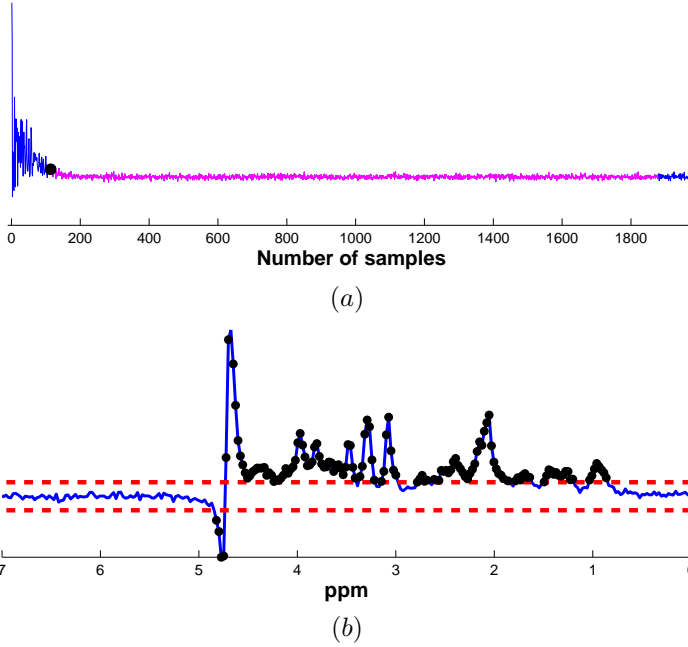


Figure 4.1: (a) Real part of the time domain signal showing the sample point determined for truncation. (b) Real part of the truncated spectrum showing the selection of the model order K equal to the number of spectral points outside the threshold region $[-5\sigma, 5\sigma]$.

4.3 Results

In order to evaluate the performance of the methods described in section 4.2.3, we consider *in vivo* and *in vitro* ^1H MRS signals and filtered them using HLSVD-PRO. Results of the obtained model orders using all methods are listed in Table 4.1.

Table 4.2 shows the relative standard deviations after suppressing the water resonance computed as $\frac{\sigma_{\text{filteredWater}}}{\sigma_{\text{originalFID}}}$, where $\sigma_{\text{filteredWater}}$ is the standard deviation of the spectral region from 4.5 ppm to 5.5 ppm and $\sigma_{\text{originalFID}}$ is the noise standard deviation of the time domain signal. In Table 4.2 a value below 1 indicates that some noise components might have been eliminated, a value above 1 indicates that the filtering of the desired peaks was incomplete and a value close

to 1 indicates that the noise level is similar to the original noise and the filtering was done appropriately.

In contrast to the heuristic overestimation approach, the selection of the model order for long signals (length NDP) is computationally expensive for the other methods due to the computation of the SVD of the corresponding $L \times (NDP - L + 1)$ matrix. Moreover, using the truncated signal to compute the model order for the method presented in a) to d), lower a less adequate model orders are obtained (results not shown).

In the presence of low SNR, the performance of all methods is similar (*e.g.*, for *in vivo* MRSI signals measured at 3.0 T, with SNR values between 4 dB and 10 dB) independently of the model order. In this case, a low model order (*e.g.*, 25) performs as good as a high model order because only the resonances corresponding to the main metabolites are perceived, while the small ones are embedded in the noise. Results shown in Fig. 4.2 to 4.9 illustrate the filtering using all methods.

Table 4.1: HLSVD model order estimated for ^1H MRS signals acquired at 1.5 T, 3.0 T and 9.4 T (column 1) considering different *in vitro* and *in vivo* measurements (column 2) and using several model order estimation methods (columns 3 to 7): rank determination method [173], MDL method [96], Samos method [125], a fixed model order of 25 as described in [14, 31] and the proposed heuristic approach based on overestimation.

Signal		Method					SNR (dB)
		Rank det.	MDL	Samos	Fixed K	Overest.	
1.5 T	In vivo	39	16	1	25	44	23
	NAA	137	21	458	25	309	23
	PCh	139	18	3	25	219	24
3.0 T	In vivo (1)	241	2	1	25	87	4
	In vivo (2)	205	2	2	25	78	9
	Lac	81	16	4	25	239	21
	Glu	103	24	1	25	231	10
9.4 T	In vivo	163	5	488	25	134	12
	Glc	206	36	34	25	126	10

- **Filtering signals at 1.5 T.**

Filtering of residual water and reference peaks for the NAA and PCh signals was done by suppressing all peaks in the frequency region outside the interval [1 ppm, 4.44 ppm]. As can be seen in Table 4.1 the rank determination, Samos and the overestimation methods provide a high model order for the NAA signal, whereas a low model order was obtained for the PCh signal. Results shown in Fig. 4.2 and Fig. 4.3 illustrate the incomplete filtering of

Table 4.2: Standard deviation of the ppm region near the water resonance (i.e., 4.5 ppm to 5.5 ppm) for all investigated signals using the model order illustrated in Table 4.1. Each standard deviation was normalized to the noise standard deviation in the original signal. We have highlighted the standard deviations closer to 1 to indicate that the residual water was filtered sufficiently, but without filtering noise components.

Signal		Method				
		Rank det.	MDL	Samos	Fix K	Overest.
1.5 T	In vivo	2.25	5.15	33.41	3.78	1.35
	NAA*	2.06	3.71	1.65	2.66	1.39
	PCh	1.49	2.11	20.39	1.76	0.89
3.0 T	In vivo (1)	1.12	3.30	9.06	1.55	1.16
	In vivo (2)	1.08	2.76	2.76	1.41	0.96
	Lac*	1.50	3.63	27.68	1.89	1.41
	Glu	0.83	1.82	25.80	1.81	1.03
9.4 T	In vivo	1.19	2.24	0.55	1.23	1.29
	Glc	0.89	0.99	0.99	0.99	0.99

*The FID of this metabolite is not fully decayed, therefore we computed the standard deviation from a metabolite-free region in the frequency domain

the reference peaks at 0 ppm and 8.4 ppm. The *in vivo* signal presented in Fig. 4.4 is a short MRS signal with high SNR, here the peak suppression was done by removing all resonances in the frequency region outside the interval [0 ppm, 4.3 ppm]. Results show that a good water suppression is obtained when using all methods, except Samos, which resulted in almost no suppression of the water resonance.

• Filtering signals at 3.0 T.

The *in vitro* Lac signal contained an extra peak at 3.7 ppm (due to phantom contamination) which was successfully suppressed using the overestimation method (see bottom of Fig. 4.5). Filtering was done by suppressing all peaks in the frequency region outside the interval [1 ppm, 4.44 ppm] and the peaks in the interval between [3.35 ppm, 3.88 ppm]. The *in vitro* Glu signal also contained an extra unwanted peak at 3.26 ppm which was well suppressed using the rank determination and the overestimation method. Filtering was done by suppressing all peaks in the frequency region outside the interval [1 ppm, 4.44 ppm] and the peaks in the interval [3.03 ppm, 3.44 ppm]. In this case, a high model order was beneficial to eliminate all unwanted resonances. The plot in Fig. 4.6 shows a residual resonance at 3.26 ppm for most of the methods. The *in vivo* MRSI signal shown in Fig. 4.7 has a low SNR. Filtering was done by suppressing all peaks in the frequency region outside the interval [0 ppm, 4.3 ppm]. Results in Table 4.2 show that at low SNR

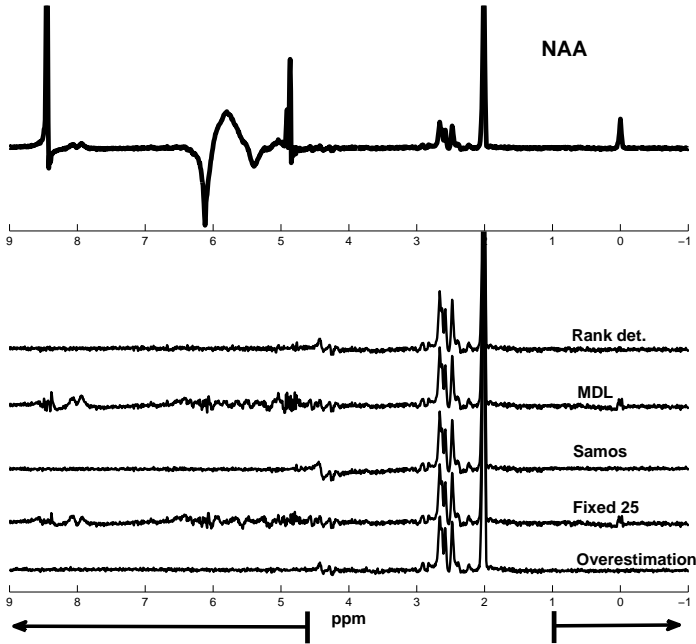


Figure 4.2: *Top: Real part of the spectrum of in vitro NAA measured at 1.5 T with acquisition parameters: Philips scanner, PRESS sequence, TR=6 s, TE=23 ms, SW=1 KHz, NDP=2048 points and 128 averages. Bottom: filtered signal with HLSVD-PRO with the model orders computed from all methods. All modelled peaks in the frequency region outside the interval [1 ppm, 4.44 ppm] were suppressed. Residual resonances are visible in the water and reference peak regions, i.e., 4.7 ppm, 0 ppm and 8.44 ppm.*

the model order plays a less important role and comparable results can be obtained regardless of the method.

- **Filtering signals at 9.4 T.**

The *in vitro* Glc is a long MRS signal with 6144 points and a good frequency resolution. It contained an extra unwanted peak at 2.8 ppm which was only suppressed when using a large model order. Filtering was done by suppressing all peaks in the frequency region outside the interval [2.95 ppm, 4.44 ppm]. From the results shown in Table 4.1, model orders between 25 and 206 were obtained, however, results in Table 4.2 show that similar filtering results at the water region were obtained for all methods. Fig. 4.8 illustrates the filtering results where a clear water suppression is observed, however, at the region between the dashed lines (2.8 ppm) as well as at 0 ppm, a good suppression is only achieved with the rank

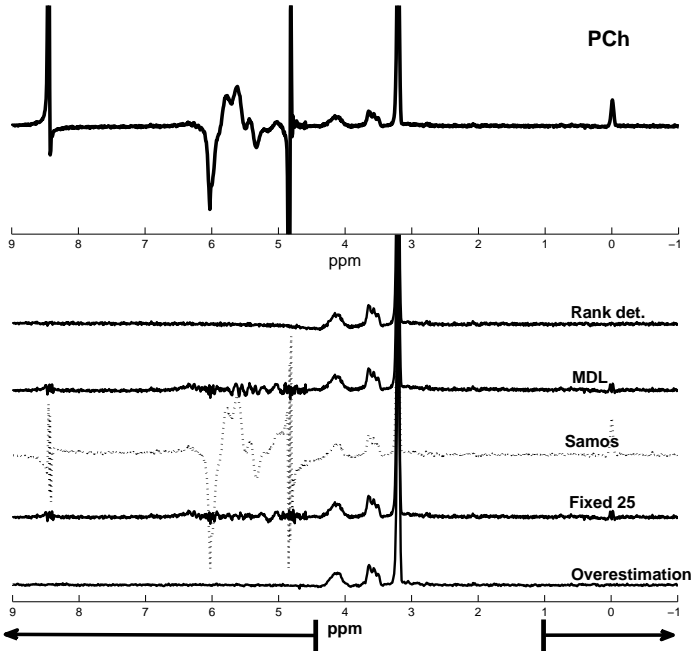


Figure 4.3: Top: Real part of the spectrum of *in vitro* PCh measured at 1.5 T with acquisition parameters: Philips scanner, PRESS sequence, $TR=6$ s, $TE=23$ ms, $SW=1$ KHz, $NDP=2048$ points and 128 averages. Bottom: filtered signal with HLSVD-PRO with the model orders computed from all methods. All modelled peaks in the frequency region outside the interval [1 ppm, 4.44 ppm] were suppressed. Residual resonances are visible in the water and reference peak regions, i.e., 4.7 ppm, 0 ppm and 8.44 ppm; the dotted line in the middle correspond to the incomplete filtering using Samos.

determination and the overestimation methods (high model orders). The *in vivo* signal in Fig. 4.9 shows a good water resonance suppression when using the fixed model order and the overestimation methods. Filtering was done by suppressing all peaks in the frequency region outside the interval [0 ppm, 4.3 ppm]. Moreover, Table 4.2 shows that the rank determination method provides a slightly better standard deviation. On the contrary, the Samos method provided a too large model order suppressing the water and the noise resonances in the water region.

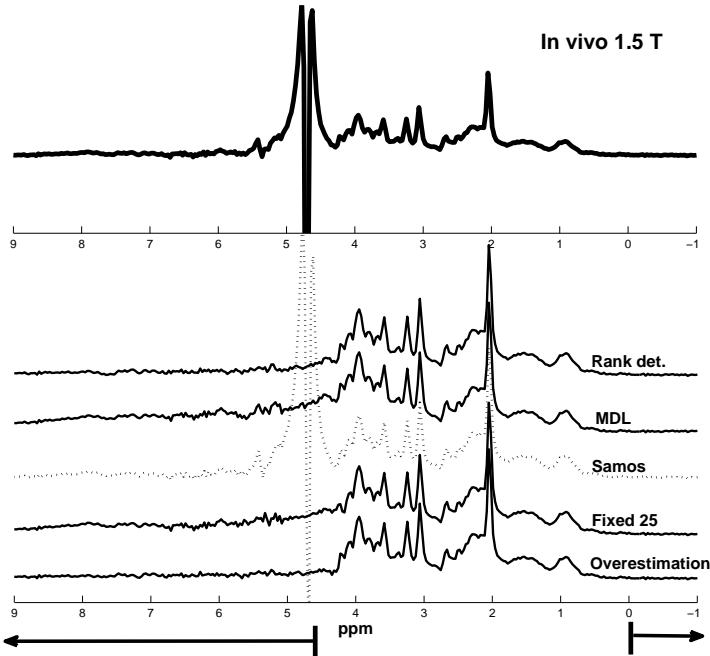


Figure 4.4: Top: Real part of the spectrum of an *in vivo* MRS signal measured at 1.5 T with acquisition parameters: Philips scanner, PRESS sequence, TR=6 s, TE=23 ms, SW=1 KHz, NDP=512 points and 64 averages. Bottom: filtered signal using HLSVD-PRO with the model orders computed from all methods. All modelled peaks in the frequency region outside the interval [0 ppm, 4.3 ppm] were suppressed; the dotted line in the middle correspond to the incomplete filtering using Samos.

4.4 Discussion

HLSVD can be used for reliable filtering of water and unwanted resonances in *in vitro* and *in vivo* signals. However, we have shown that the model order plays an important role. We presented the results obtained when filtering resonances using HLSVD-PRO, in particular, including a model order estimation method for peak suppression when MR signals have different residual water shapes, low and high SNR, long and short MRS signals and well-resolved peaks. To this end, we compared four model order estimation approaches from the literature and proposed a heuristic approach that overestimates the model order. For some of the signals illustrated here, the performance of the existing methods is limited.

The rank determination method has been used to reliably obtain the numerical rank of a noisy matrix, however, in the presence of high SNR signals, noise

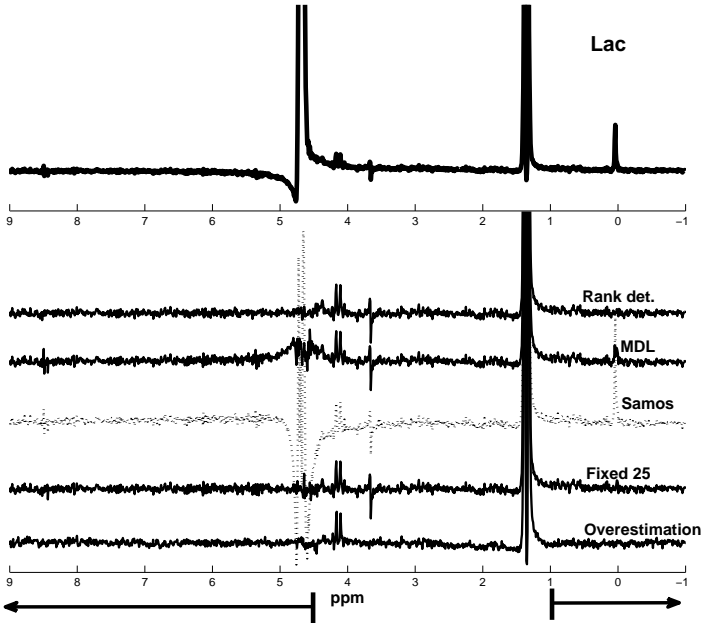


Figure 4.5: Top: Real part of the spectrum of *in vitro* Lac measured at 3.0 T with acquisition parameters: Philips scanner, PRESS sequence, $TR=2$ s, $TE=35$ ms, $SW=2$ KHz, $NDP=2048$ points and 128 averages. Bottom: filtered signal with HLSVD-PRO with the model orders computed from all methods. All modelled peaks in the frequency region outside the interval [1 ppm, 4.44 ppm] were suppressed; additional peaks in the interval between [3.35 ppm, 3.88 ppm] were also suppressed. Residual resonances are visible in the water and reference peak regions, i.e., 4.7 ppm, 0 ppm, 3.3 ppm and 8.44 ppm; the dotted line in the middle corresponds to the incomplete filtering using Samos.

components may be also modeled. Concerning the MDL method, it has been successfully used to model noisy MRS signals having relatively good computational efficiency, high precision and accuracy of the estimated spectral parameters and less tendency for spurious estimates at low SNR. The Samos method assumes a good separation of the signal and noise subspace, is based on the shift invariance property of the dominant subspace of the Hankel data matrix and has been successfully compared to the ESTimation ERror method (ESTER) [3] (which is also based on the shift invariance property). However, a possible reason for its inaccuracy is the predominance of the water peak which will have priority in the modeling. Samos method has not been used for ^1H MRS signals before, though. Finally, a fixed model order of 25 sinusoids has been successfully used to decompose *in vitro* and *in vivo* signals [14, 31]. Nevertheless, good results depend

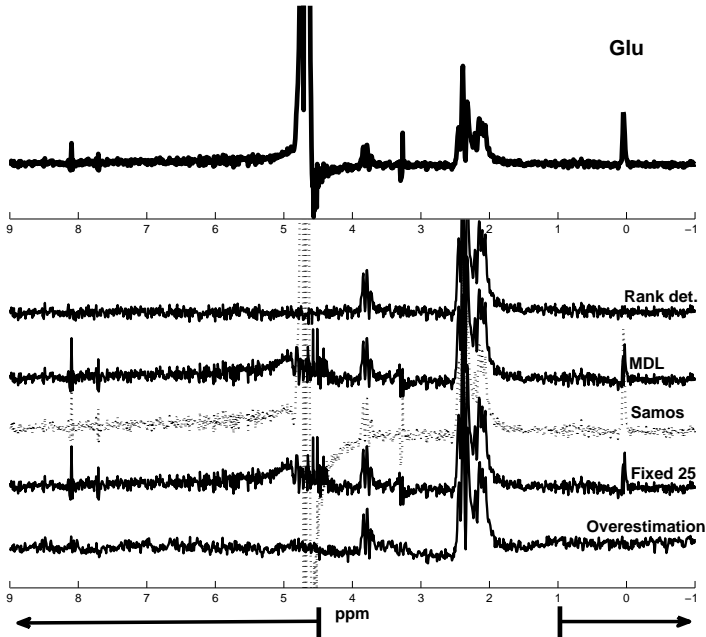


Figure 4.6: *Top: Real part of the spectrum of in vitro Glu measured at 3.0 T with acquisition parameters: Philips scanner, PRESS sequence, TR=2 s, TE=35 ms, SW=2 KHz, NDP=2048 points and 128 averages. Bottom: filtered signal with HLSVD-PRO with the model orders computed from all methods. All modelled peaks in the frequency region outside the interval [1 ppm, 4.44 ppm] were suppressed; additional peaks in the interval between [3.03 ppm, 3.44 ppm] were also suppressed. Residual resonances are visible in the water and reference peak regions, i.e., 4.7 ppm, 0 ppm, 3.3 ppm and 8.44 ppm; the dotted line in the middle corresponds to the incomplete filtering using Samos.*

on the particular signal characteristics and therefore this fixed model order of 25 may also be inaccurate.

Compared to other methods, the overestimation approach is able to suppress distorted lineshapes and multiple resonances in the presence of low or high SNR. A major advantage of the proposed overestimation method is that long signals can be reliably truncated to a sample point where no metabolite information is contained and acceleration of the HLSVD computations can be achieved. The proposed overestimation method is able to identify a large number of resonances and therefore, suppression of the selected unwanted peaks can be accurately achieved. In this study, we focused on ^1H MRS signals, but potential implementation in other applications is also feasible.

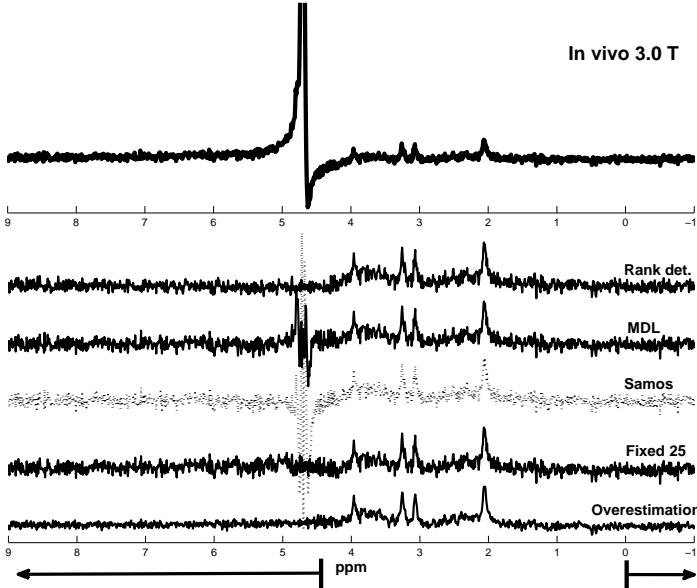


Figure 4.7: Top: Real part of the spectrum of an *in vivo* MRSI signal measured at 3.0 T with acquisition parameters: Philips scanner, PRESS sequence, $TR=2$ s, $TE=35$ ms, $SW=2$ KHz, $NDP=2048$ points and 1 average. Bottom: filtered signal with HLSVD-PRO with the model orders computed from all methods. All modelled peaks in the frequency region outside the interval $[0$ ppm, 4.44 ppm] were suppressed; the dotted line in the middle corresponds to the incomplete filtering using Samos.

Results in Table 4.2 are related to the frequency region around the water resonance *i.e.*, between 4.5 ppm and 5.5 ppm. However, when analyzing *in vitro* MRS signals, we must consider additional resonances present in the region between 0 ppm and 8.44 ppm, which correspond to reference peaks that must be suppressed. These peaks may be tiny compared to the residual water or the metabolite peaks, thus an overestimated model order may be beneficial.

An important aspect to consider when filtering MRS signals is the fact that both *in vitro* metabolites and *in vivo* signals will be used to assess metabolite concentrations via quantification.

HLSVD-PRO has been broadly used for suppression of unwanted resonances, however, other methods of filtering such as MP-FIR [167] have also proven to provide successful results. In [136] MP-FIR was compared with HLSVD-PRO in the context of quantification accuracy. However, preprocessing with MP-FIR is not advisable due to a nonlinear phase distortion occurring in the filtered signals.

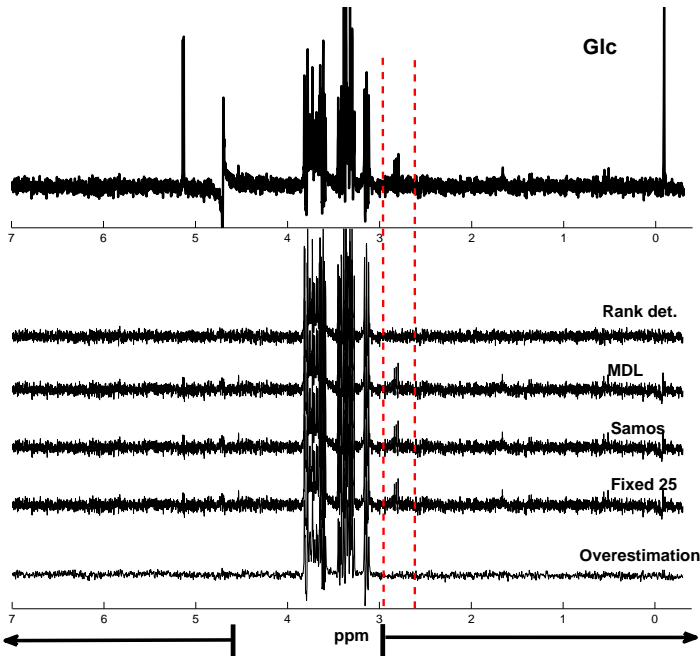


Figure 4.8: Top: Real part of the spectrum of *in vitro* Glc measured at 9.4 T with acquisition parameters: PRESS pulse sequence with implemented pre-delay OVS as well as the water suppression method VAPOR, FASTMAP shimming correction, $TR=4$ s, $TE=12$ ms, $SW=4$ KHz, 64 averages and $NDP=6144$ points. Bottom: filtered signal with HLSVD-PRO with the model orders computed from all methods. All modelled peaks in the frequency region outside the interval [2.95 ppm, 4.44 ppm] were suppressed. Residual resonances are visible at the region around 2.8 ppm (between the two vertical dashed lines).

This study is important for the assessment of quantification results via residual analysis (see chapter 7 for further details about residual analysis). For instance, a significant residual may be observed when incorrect peaks suppression is obtained in the preprocessing step, as a result the final assessment of conclusions is affected.

4.5 Conclusions

In this study, we have evaluated the suppression of water and unwanted peaks for different *in vitro* and *in vivo* ^1H MRS signals obtained at 1.5 T, 3.0 T and 9.4 T. These signals were representative for evaluation of different SNRs, water shapes and signal resolutions. Normally, acquisition protocols include a residual

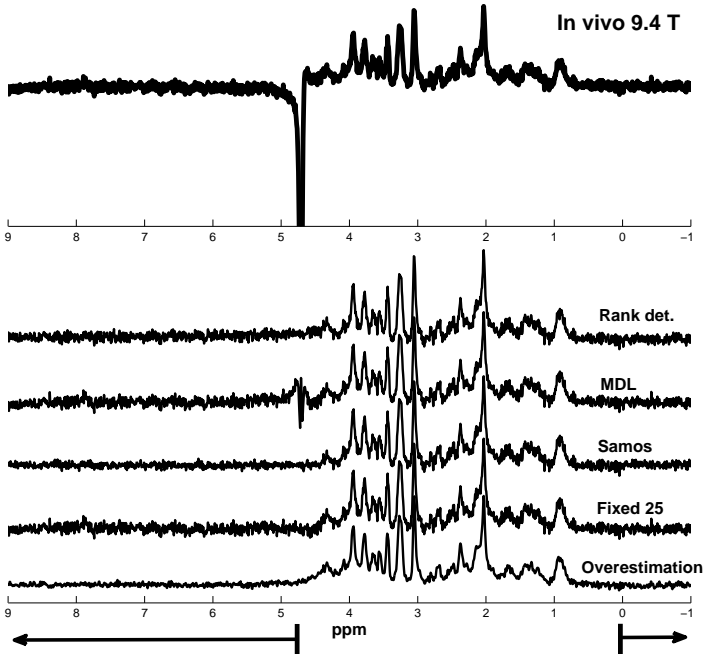


Figure 4.9: Top: Real part of the spectrum of an *in vivo* MRS signal measured at 9.4 T with acquisition parameters: PRESS pulse sequence with implemented pre-delay outer volume suppression (OVS) as well as the water suppression method VAPOR, FASTMAP shimming correction, $TR=4$ s, $TE=12$ ms, $SW=4$ KHz, 256 averages and 2048 points. Bottom: This signals was filtered with HLSVD-PRO with the model orders computed from all methods. All modelled peaks in the frequency region outside the interval [0 ppm, 4.3 ppm] were suppressed.

water suppression method, but incomplete water removal may affect metabolite resonances and the signal's baseline. However, in MRS signals a good peak suppression is essential to achieve accurate quantification results and is therefore important for disease assessment.

The proposed model order determination approach was successfully evaluated and compared to other methods applied to different *in vitro* and *in vivo* signals for filtering of residual water and additional reference peaks. Although the computation of the SVD using a large model order is computationally intensive, automatic truncation of the MRS signal allows us to keep a reasonable computational time while providing a more accurate decomposition of the signal.

Chapter 5

Lineshape estimation in MRS signals

The lineshape estimation of MRS signals is studied in detail and a revised-deconvolution method described in [156, 123] is presented. Results obtained from validation of the methods in simulated, in vitro and in vivo ^1H MRS signals show the potential of this method. Finally, some conclusions concerning applications of the lineshape estimation are presented.

5.1 Introduction

The lineshape is defined in the frequency domain as the shape of a spectral component (or peak). When the broadening is homogeneous, it is ideally represented by a Lorentzian, Gaussian or Voigt function, corresponding in the time domain to an exponentially decaying sinusoid. When magnetic field perturbations, field inhomogeneities or tissue heterogeneities are present, these lineshapes are disturbed (in symmetry and linewidth) making the fitting of the MR signal using an basic lineshape (*e.g.*, Lorentzian) unreliable or tending to mislead the metabolite estimates. In practice, the lineshape of MR signals is determined by the decay function (damping) of the time domain signal.

Popa [131] describes the origin of the most common lineshapes used in MRS: *a)* Lorentzian lineshapes arise from the intrinsic interactions between spins and under perfect acquisition conditions, spectra are expected to have a Lorentzian lineshape. *b)* Gaussian lineshapes can be considered as the result of the influence of many unknown/unparameterizable factors, such as the spatial distribution of the actual

B_0 magnetic field. c) Voigt lineshapes are the product of Gaussian and Lorentzian lineshapes, where the Lorentz part expresses the T_2 decay mechanism while the Gaussian part the influence of unknown/unparameterizable factors.

Some of the lineshape problems are related to faster relaxation (*i.e.*, when the external local magnetic field is not ideally homogeneous, this produces a shorter effective relaxation time T_2^*), inhomogeneities caused by the magnet design, tissue inhomogeneities, variations in the tissue type or paramagnetic material inside the bore, such as dental materials in filling, crowns, metallic dental implants and head holders. Hence, *in vivo* measurements are more susceptible to sample heterogeneities compared to *in vitro* signals.

Different approaches related to the lineshape correction as a preprocessing step have been described in chapter 2 section 2.2.6 and those related to the lineshape estimation during quantification are described in chapter 3 section 3.2.4. Because reference deconvolution methods require the use of a separate reference acquisition signal or a well-separated reference peak, there are limitations related to extra acquisitions, missing water reference (when targeting other nuclei rather than ^1H) and unclear reference peak separation due to overlapping of resonances. On the other hand, self-deconvolution methods using the lineshape estimation during quantification assume a common distortion for all metabolites within a measurement and appeared to be more robust. In both cases, it is possible to correct for lineshape distortions either by convolving a non-decaying metabolite database with the estimated lineshape or by deconvolving the experimental signal by the estimated lineshape function.

Several methods incorporate parametric and non-parametric techniques for modelling the lineshape, such as exponential functions, polynomials, sinusoids, wavelets or splines, which include the adjustment of certain hyper-parameters for those specific functions. For instance, Provencher [140], uses a balance between over-parameterization and over-simplification of the baseline and lineshape parameters. He uses a complex regularization scheme, having a flexible lineshape model in the frequency domain together with a constrained regularization to determine the amplitude coefficients describing the lineshape. In [158], Slotboom *et al.* model the lineshape together with the regular model parameters, thus the lineshape is modelled as a sum of weighted Dirac delta functions in the frequency domain.

5.1.1 Assuming a common decay

Starting in 1995, Maudsley [106] proposed the determination of spectral lineshapes using the deconvolution of the data with an initial estimate of the decay function obtained from the same spectrum. In particular, all resonances are assumed to be distorted in a similar way, thus, the lineshape broadening is dominated by

macroscopic and microscopic magnetic susceptibility effects, *i.e.*, the lineshape is determined by T_2^* and not T_2 . More recently, Deelchad [38] reported that microscopic susceptibility effects are the main factor contributing to the line broadening as the field strength increases. In [133], Popa *et al.* explained that at high B_0 , these susceptibility effects are due to the heterogeneity within the analyzed tissue and, therefore, anatomical structures containing fluid or air have different magnetic susceptibilities, causing inhomogeneity of the applied magnetic field B_0 . Moreover, the frequencies of the sinusoids contained in the signal are proportional to B_0 and the inhomogeneity of B_0 affects the lineshapes in an unknown manner. Finally, if the decay mechanisms other than B_0 inhomogeneity are insignificant, and the spatial distributions of the metabolites are equal, the decays of all individual sinusoids making up the signal should be approximately equal [133].

5.1.2 Spectral lineshape determination with self-deconvolution

There exist some self-deconvolution methods proposed by [106, 132, 156, 123] and obtained by point-wise dividing the spectral time domain signal by an initial estimate of the decay function obtained from the same signal. Unfortunately, the estimated lineshape is affected by noise and therefore, an additional smoothing procedure is required to avoid error propagation. This is explained and illustrated in section 5.2.3.

The self-deconvolution method proposed by Maudsley [106] determines the amplitude and phase of the lineshape caused by inhomogeneity and eddy current effects. Because the obtained lineshape function is affected by noise, the smoothing procedures proposed by Maudsley are based on weighted Gaussian-shaped functions, the fitting to a polynomial function and the parametrization of the time-domain signal with several exponentials. After determination of the lineshape, the obtained function can be incorporated in a parametric spectral analysis method to improve the accuracy of the fit.

5.1.3 Semi-parametric lineshape estimation without searching in function space

Popa *et al.* [132, 133] use the same principle and assumptions proposed by Maudsley [106], considering an incomplete model (*i.e.*, unknown lineshape). In this work, the authors devise a method that substitutes the smoothing of the lineshape function for physical *prior* knowledge about the maximum frequency present in the lineshape function. Thus, the high frequency components in the decay function must be penalized. This is achieved by imposing two optimization criteria in the fitting of the model to the MRS signal: minimal residue and minimal amplitude

of high frequency components in the decay function. Due to the fact that the model function involves both physical and mathematical model parameters, it is called semi-parametric estimation. A plug-in version of this lineshape estimation method is planned to be included in the quantification package jMRUI [164].

5.1.4 Lineshape estimation: self-deconvolution revisited

Sima *et al.* [156] presented a revised study of the lineshape estimation following the same assumptions proposed by Maudsley [106]. In [156] extended Monte Carlo simulation studies were used to analyze the automatic estimation of the unknown lineshape distortion. The signals used here contained eight metabolites and were inspired by typical short TE MRS signals from healthy human brain. In particular, the smoothing step for spike removal of the estimated lineshape function was addressed by comparing three smoothing methods based on the sum of complex damped exponentials, splines and wavelets. Altogether, unavoidable hyper-parameters of the smoothing methods need to be well chosen.

5.2 Materials and Methods

5.2.1 MRS signals

- **Simulated signals.** Generation of simulated signals was performed in Matlab[®] (The MathworksTM). A simulated MRS signal ($y_m(t)$) was created composed of 7 *in vitro* measured metabolites from the basis set described in chapter 2 section 2.1.3: Ala, Cr, Gln, Glu, Lac, NAA, and Tau. The MRS signal was generated by summing up the signals of all 7 metabolites, then a distortion was included to simulate a damping different from the basic Lorentzian (See Fig. 2.11 from chapter 2).

$y_m(t)$ was point-wise multiplied by a damping function:

$$D(t) = A(t) \cdot e^{j(c_1 e^{\lambda_1 t} + c_2 e^{\lambda_2 t})} \quad (5.1)$$

where $\lambda_1, \lambda_2 < 0$, $j = \sqrt{-1}$ and $A(t)$ is the Fourier Transform of an asymmetric triangular shape,

$$A(t) = \frac{1}{2(f_3 - f_1)} \cdot \frac{1}{2\pi j t} \left[\frac{e^{x_1} - e^{x_2}}{x_2 - x_1} + \frac{e^{x_3} - e^{x_2}}{x_3 - x_2} \right] \quad (5.2)$$

where $x_i = 2\pi j f_i t$ for $i = 1, 2, 3$ and f_i are the 3 frequencies defining the triangle. See [156] for further details. The second factor of $D(t)$ represents eddy currents in the metal walls of the magnet.

Then the distorted signal $y_d(t)$ becomes:

$$y_d(t) = y_m(t) \cdot D(t) + N(t) \quad (5.3)$$

where $N(t)$ is the added white Gaussian noise.

The white Gaussian noise corresponding to several SNRs is added in the time domain (see Fig. 5.1) and is related to the measured power of the signal in dB:

$$P_{sig} = 10 \log_{10} \frac{\|y_d(t)\|^2}{n} \quad (5.4)$$

i.e., the squared Euclidean norm of the signal ($\|y_d(t)\|^2$) divided by the length of the signal (n), transformed to dB. Then the added noise $N(t)$ has standard deviation of:

$$\sigma = \sqrt{10^{\frac{P_{sig} - SNR}{10}}} \quad (5.5)$$

The simulated signal with different damping and noise levels is shown in Fig. 5.4.

- ***In vitro* signals.** Single voxel spectra of an *in vitro* phantom solution containing 5 mM of the following metabolites was measured: Ala, Cr, Gln, Glu, Lac, NAA and Tau (see Fig. 5.5). The MR acquisition parameters are similar to those described in chapter 2 section 2.1.3. After acquiring an undistorted signal with default shimming settings, the shimming parameters were mis-set by changing the shim current of the X coil generating two distorted signals for analysis.
- ***In vivo* signal.** Single voxel spectra of rat brain were acquired with the VOI placed on the right hemisphere of the thalamus. The MR acquisition parameters are similar to those described in chapter 2 section 2.1.2. Then, two additional distorted signals were acquired (see Fig. 5.6) by mis-setting the shimming parameters, where the Z^2 second order shim coil and the first order X coil values were mis-set. The SNR of the *in vivo* signals is 12, calculated in the time domain according to Eq.(5.5).

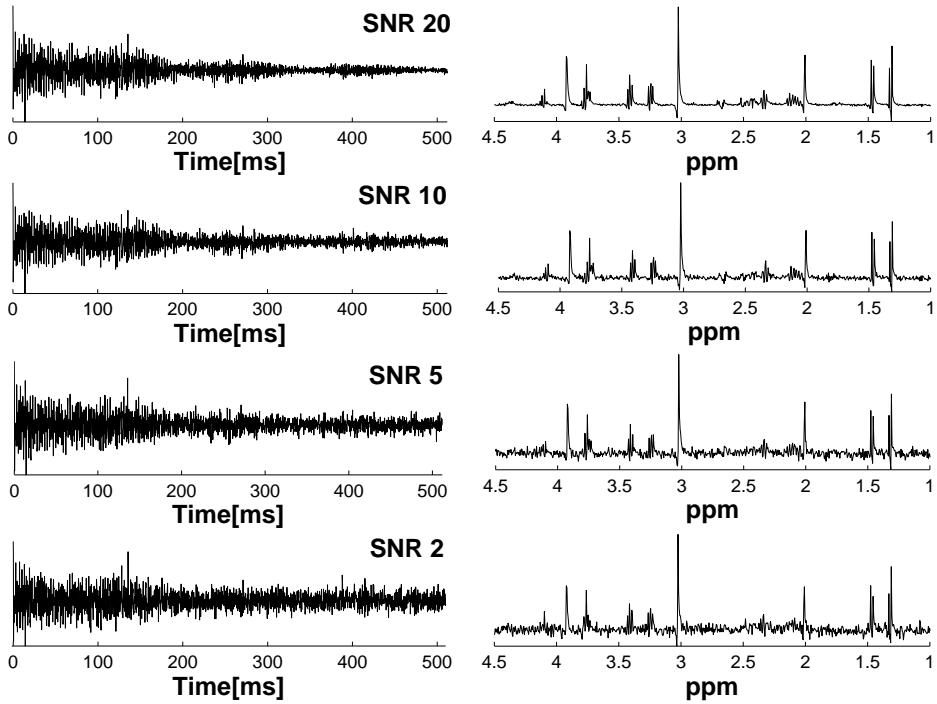


Figure 5.1: Simulated distorted MRS signal with different SNR levels (in dB). The white Gaussian noise is added in the time domain and is related to the measured power of the signal.

As explained in chapter 1, shimming is the procedure to optimize the homogeneity of the magnetic field, is aimed to counteract the effects of faster relaxation, lower spectral resolution and an overall lower signal to noise ratio, thus, optimal shimming of the magnet is essential. Nevertheless, when high shimming procedures do not optimize the homogeneity, additional post-acquisition methods are required.

5.2.2 Quantification with lineshape estimation

- **Signal processing.** All *in vitro* and *in vivo* MR signals were time circular shift corrected using the jMRUI software package [165]. Further processing consisted of filtering out the residual water and the components corresponding to reference peaks. To filter without affecting the metabolite resonances, we applied HLSVD-PRO [90] (see chapter also 4).

- **Basis set of reference metabolites.** A complete description of the acquisition protocol and a figure illustrating the basis set is presented in chapter 2 section 2.1.3.

The macromolecular contribution (MM) was measured using an inversion recovery sequence with a 1 ms Hermitian inversion pulse. The inversion time and repetition time were 800 ms and 3 s respectively and 1024 averages were acquired. The inversion time was fine-tuned experimentally for metabolite nulling. Remaining peaks of Cr and Tau were filtered with HLSVD-PRO [90]. Finally, the whole spectrum was apodized with a line broadening of 10 Hz.

- **AQSES.** The quantification method used for analyzing the signals was AQSES [137] (see chapter 3). A measured basis set of metabolites was used for quantification and an additional signal corresponding to macromolecules was added to the basis set.

AQSES uses the model described in chapter 2 section 2.1.2 Eq.(2.1). $B(t)$ is in this case measured *in vivo* and included in the basis set of metabolites as $v_{K+1}(t)$.

- **AQSES Lineshape.** Given the fact that the volume of interest is supposed to be sufficiently homogeneous for the metabolites to share the same inhomogeneity profile, and no motion or contamination are supposed to be present, the same lineshape distortion is assumed for all components. Thus, for correcting lineshape distortions during quantification, a common lineshape is considered for all spectral components in the model of AQSES, except the macromolecular signal measured *in vivo* [156]. The exponential dampings $e^{(-d_k t)}$ in Eq.(2.1) are then replaced by the common factor $g(t)$, of arbitrary shape, resulting in:

$$y(t) = g(t) \sum_{k=1}^K a_k e^{(j\phi_k)} e^{(2\pi j f_k t)} v_k(t) + B(t) + \epsilon(t) \quad (5.6)$$

The same AQSES optimization problem could be formulated following Eq.(3.1) described in chapter 3 section 3.2.1, which uses a nonlinear least squares criterion, in this case with additional constraints on the decay $g(t)$ to be smooth in the time domain. We avoid the arbitrary parametrization of the decay function $g(t)$, which may add a large number of variables to the optimization problem and require the selection of its degree of smoothness *a priori*. Therefore, we propose the following data-driven algorithm that estimates and smoothens the decay $g(t)$ iteratively.

Because MM has a shorter relaxation time, it was excluded when calculating the common lineshape $g(t)$, but it was included in the metabolite basis set for the quantification.

The present implementation of AQSES Lineshape contains the over-optimistic Cramér-Rao bounds computed under the assumption that the final $g(t)$ is the true lineshape of the model.

The algorithm for lineshape estimation is then:

Step 1 Fitting. First, with a preliminary spectral analysis we quantify the signal assuming the basic lineshape (*i.e.*, Lorentzian) to extract the spectral parameters calculated by AQSES: amplitudes, frequencies, phases and dampings. Then, the signal is reconstructed from the estimated spectral parameters not taking into account the damping part.

Step 2 Damping. The damping function is computed as the ratio formula for the common damping $g(t)$:

$$g(t) = \frac{y(t) - B(t)}{\sum_{k=1}^K a_k e^{(j\phi_k)} e^{(2\pi j f_k t)} v_k(t)} \quad (5.7)$$

where in the numerator $y(t)$ is the experimental signal and $B(t)$ is the current baseline estimate; and in the denominator K is the number of metabolites, $v_k(t)$ the metabolite signal k in the basis set, and the amplitudes a_k , frequency shifts f_k and phase shift ϕ_k are estimated from a previous AQSES iteration from **Step 1** or **Step 4**.

Step 3 Smoothing. Numerical instability caused by noise and division by small numbers in Eq.(5.7) creates big outliers which are tackled by smoothing $g(t)$. We employ a robust version of local regression using weighted linear least squares with a second degree polynomial (LOESS), which assigns lower weight to outliers in the regression [24, 131]. Thus, we make use of the robust smoothing implementation from Matlab[®] (*smooth (loess) and (rloess)*).

Initially, the tail of $g(t)$ is set to zero because in MRS signals the information about the damping is contained in the decaying part of the signal. The selection of the cut-off point is described in chapter 4 section 4.2.3.

At last, RLOESS and LOESS are applied, which require the selection of a smoothing parameter, being in this case a percentage of the number of data points. Thus, we allow values between 5 and 30 % and use cross-validation [94] to select the parameters that better fit the damping function. A two-fold cross-validation method was used, by partitioning the even and odd data points of the time domain signal in order to keep the time indexing, which is essential in MRS signals.

Step 4 Estimate. Spectral analysis is carried out again, point-wise multiplying the original metabolite basis set with the new smoothed function $g(t)$.

Steps 2-4 are repeated until a residual smaller than a chosen threshold is obtained or a convergence of the amplitude estimates is reached; additionally the norm of the current residual should be smaller than that of the previous iteration. The number of iterations is fixed to a maximum of 30. Finally, the amplitude estimates are calculated by a final quantification of the signal which allows small damping variations of metabolites additional to the common damping function.

5.2.3 Smoothing methods

In this section we discuss possible methods for smoothing the noisy damping estimate $g(t)$ obtained via the ratio formula from Eq.(5.7).

- **Based on the sum of complex damped exponentials.** The lineshape can be modelled by representing a non-Lorentzian lineshape as a sum of several complex damped exponentials. For instance, Maudsley [106] used a limited number of exponentials with the decay parameters fitted by a NLLS procedure using the Levenburg-Marquardt method. Additionally, the subspace-based method HSVD [129] has also been successfully used [124, 156]. With HSVD it is possible to accurately model non-Lorentzian signals depending on the signal quality (*e.g.*, the SNR). HSVD computes the truncated singular value decomposition (SVD) of a Hankel matrix H , containing the noisy signal in its first column and row. The rank of the matrix H is given by the number of K complex damped exponentials describing the signal, which should be high enough to model a distorted peak with several Lorentzians [156]. However, when a too large model order is selected, the spikes in the lineshape function and the noise are also modelled. Therefore, a selection of the adequate model order considering *prior* knowledge about the lineshape has been proposed in [156]. Thus, the lineshape distortion is centered at zero and therefore a frequency band can be set considering first a large number of components and sorting them according to the increasing absolute value of the frequency and finally reconstructing the lineshape by selecting components starting with the lowest-frequency component. For this, four model selection criteria are used: Bayesian information criterion, L-curve and Akaike's information criterion and its second-order correction. Finally, the median value of the number of components given by the four methods is taken [156].
- **Based on a polynomial function.** In [106], a polynomial function of at least sixth order was necessary to smooth the lineshape function. This method was found to provide adequate amplitude values for simple lineshape functions, but unsatisfactory for signals with eddy current or large lineshape distortions.

- **Based on wavelets.** Discrete wavelets have also been used for denoising (decomposing) the noisy damping estimate [156]. Some of the obtained wavelet coefficients correspond to noise components while others correspond to the actual features of the data. A wavelet thresholding is commonly used to set to zero all coefficients below a specified value and then use the inverse wavelet transform to reconstruct the denoised data [156]. A drawback of this smoothing method is the lack of appropriate and automated selection of several parameters such as the wavelet family, the number of vanishing moments, the level of wavelet decomposition and the threshold value itself.
- **Based on splines.** Splines are piecewise polynomial functions linearly combined in order to fit a noisy signal. The degree of smoothness is defined by: (a) tuning the number and shape of the spline components, or (b) considering a very dense spline basis and constraining the roughness of the fitted signal. In [156], penalized splines are considered and tuning the smoothing parameter is necessary. This parameter gives the weighting between the approximate error and the roughness measure.
- **Based on local regression.** The local regression method LOWESS or LOESS was proposed by Cleveland [24]. This is an approach of fitting curves to noisy data by a multivariate smoothing procedure, fitting a linear or quadratic function of the predictor variables in a moving fashion, only in a small range of data points similar to how a moving average is computed for a time series. This moving window is also called span. Compared to classical approaches like fitting global parametric functions, local regression substantially increases the type of functions that can be estimated. Another characteristic of local regression is that the methods for making inferences based on local regression fits are nearly the same as those used in parametric fitting. If the function has peaks and valleys, which is the case for the lineshape function, a local linear fit can partially eliminate them, whereas the curvature associated with peaks and valleys is better fit by local quadratic curves. Outliers may strongly influence regression results, but LOESS and RLOESS [131] can iteratively down-weight data points that have large residuals. Fig. 5.2 shows the schema of the local regression procedure.

Concerning the span used during the fitting, here we considered a percentage of the data points to be more adequate instead of using a fixed number because the length of the experimental signals may vary. The size of this span parameter has an important effect on the fitting, thus a span that is too small leads to a large number of windows, providing little smoothing and rather a function characterized by noise with a large variance. On the other hand, if the span is too large, the regression curve will be over-smoothed and the local polynomial may not fit well the data, resulting in loss of important information, and therefore the fit will have large bias. Fig. 5.3 shows examples of the resulting lineshape function for simulated, *in vitro*

and *in vivo* signals. Another parameter to be selected in LOESS is the degree of the polynomial, which can be set according to the data. Thus, for a simple function a zero degree polynomial (*i.e.*, a moving average) may be good enough, however, for the damping function $g(t)$ it is necessary to consider a higher degree. In [123] a quadratic degree appeared to be good enough to fit the lineshape function, however, higher degrees may also be adequate with high computational time, though.

5.3 Results with AQSES and AQSES Lineshape

The following results show the performance of the proposed AQSES Lineshape method [123] according to the type of signal studied. The residual was evaluated with the goodness of the fit using a linear polynomial computing the sum of square errors (SSE) and the root mean square errors (RMSE).

- **Simulated signals.** Fig. 5.4 shows the quantification results obtained for the simulated signals with triangular and eddy current distortions having small and big damping as well as high and low SNR. The top row shows the fits with AQSES and AQSES Lineshape considering a small damping in the simulations, while the bottom row shows the fits with AQSES and AQSES Lineshape considering a big damping. At the bottom of each plot, the residual for each method is also shown. The residual from AQSES may contain some patterns corresponding to metabolite contributions that were not correctly quantified due to the Lorentzian lineshape model; whereas the residuals corresponding to AQSES Lineshape show a nearly flat line that we attribute to the free lineshape model.

Table 5.1 shows the results of mean amplitude estimates and the corresponding standard deviation obtained for each metabolite when quantifying the original simulated and distorted signal over a set of 100 noise realizations at two SNR levels for small (*a*) and big damping (*b*). In the first place, the original simulated signals were quantified with AQSES (with true amplitude 1), then the distorted signals were quantified with AQSES and AQSES Lineshape.

The results obtained show small variations between both methods, however, results with AQSES Lineshape are closer to the original values, which suggests that the estimates with AQSES are biased from the original expected amplitude estimates.

- ***In vitro* signals.** Results of quantification of *in vitro* signals are shown in Fig. 5.5. The undistorted *in vitro* signal is fitted identically by AQSES and AQSES Lineshape, *i.e.*, AQSES Lineshape reports convergence after the

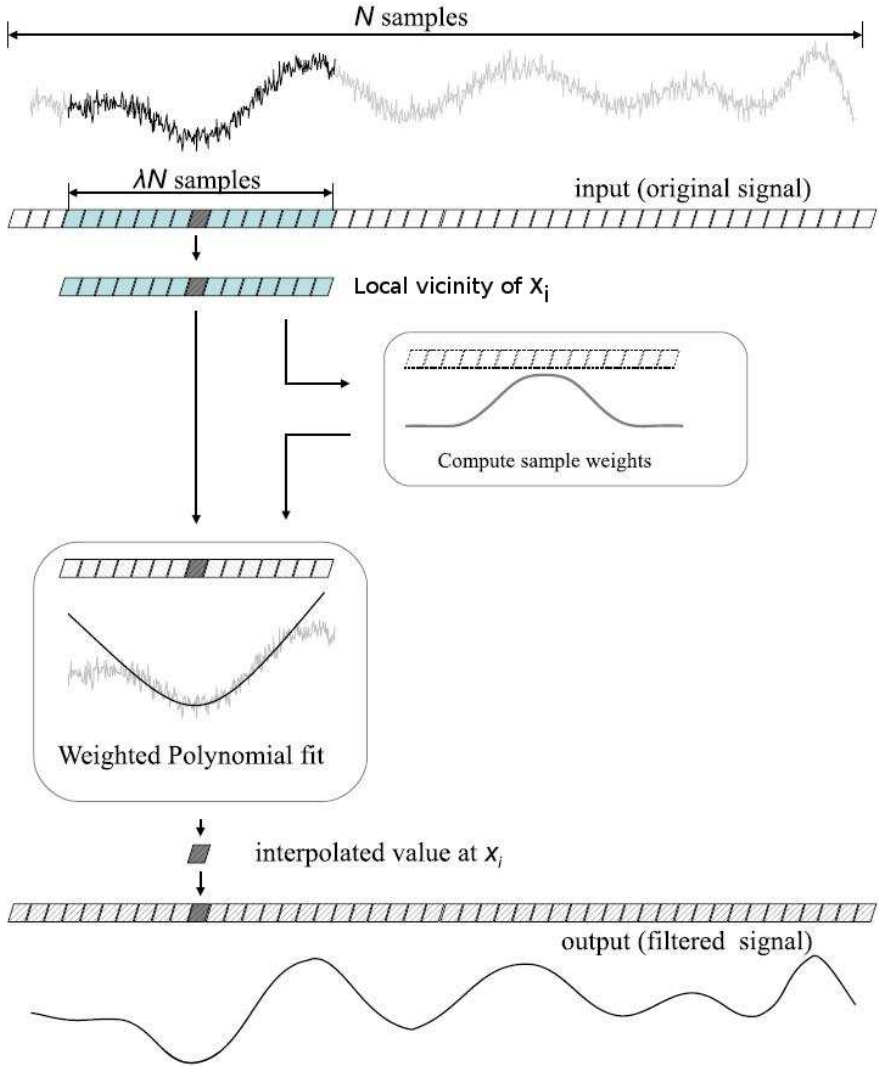


Figure 5.2: Illustration of the steps necessary to obtain the smooth function using local regression in a selected number of points from a given signal. LOESS gives weights to the selected points and uses a polynomial interpolation for the computed weights. Figure from [131].

Table 5.1: Mean amplitude estimates and standard deviations for the simulated signals containing 7 metabolites for a set of 100 noise realizations. (a) Estimates corresponding to simulated signals with SNR=30 and SNR=2 having small damping (to simulate in vitro signals); (b) estimates corresponding to simulated signals with SNR=20 and SNR=5 having big damping (to simulate in vivo signals). Results in column ‘Original’ show the amplitude estimates for the undistorted signals quantified with AQSES; while the results in columns ‘AQSES’ and ‘AQSES L’ correspond to those of the distorted signals quantified with AQSES and AQSES Lineshape, respectively. The true amplitudes are equal to 1 for all metabolites.

Metabolites	SNR 30			SNR 2		
	Original	AQSES	AQSES L	Original	AQSES	AQSES L
Ala	1.0000±0.0025	1.1291±0.0028	1.0124±0.0031	0.9949±0.0732	1.1433±0.0709	1.0353±0.0780
Cr	1.0000±0.001	1.1002±0.0028	1.0162±0.0014	0.9976±0.0274	1.1059±0.0277	1.0125±0.0584
Gln	1.0002±0.004	1.0084±0.0042	1.0058±0.0047	1.0142±0.0960	0.9990±0.1167	0.9968±0.1158
Glu	1.0006±0.0038	1.0555±0.0044	1.0028±0.0048	1.0054±0.1120	1.0733±0.1222	1.0305±0.1184
Lac	1.0000±0.0026	1.1512±0.0027	1.0120±0.0027	1.0001±0.0659	1.1556±0.0627	1.0325±0.0686
NAA	0.9999±0.0022	1.1295±0.0020	1.0171±0.0024	0.9992±0.0499	1.1172±0.0542	0.9987±0.0785
Tau	1.0004±0.0025	1.0678±0.0023	1.0111±0.0024	1.0046±0.0733	1.0670±0.0622	1.0112±0.0666

(a)

Metabolites	SNR 20			SNR 5		
	Original	AQSES	AQSES L	Original	AQSES	AQSES L
Ala	0.9998±0.0464	0.9177±0.0079	0.9536±0.0079	1.0001±0.0464	0.9222±0.0571	0.9663±0.0480
Cr	1.0009±0.0171	1.0111±0.0031	1.0023±0.0049	1.0008±0.0171	1.0129±0.0176	1.0059±0.0248
Gln	0.9933±0.0735	1.0529±0.0122	0.9476±0.0121	0.9946±0.0735	1.0076±0.1027	0.9477±0.0808
Glu	1.0009±0.0647	0.8501±0.0139	1.0098±0.0143	0.9999±0.0647	0.8776±0.0915	1.0185±0.0699
Lac	1.0050±0.0476	0.9191±0.0083	0.9654±0.0088	1.0052±0.0476	0.9257±0.0519	0.9847±0.0547
NAA	1.0048±0.0388	0.9686±0.0074	0.9919±0.0082	1.0048±0.0388	0.9758±0.0396	1.0065±0.0454
Tau	0.9983±0.0349	1.0796±0.0080	1.0202±0.0081	0.9980±0.0349	1.0738±0.0421	1.0140±0.0382

(b)

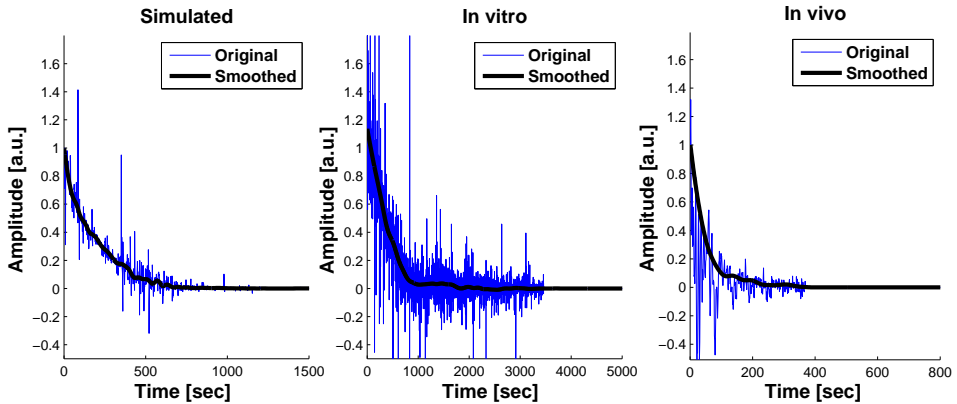


Figure 5.3: Time domain signal of the resulting lineshape for the simulated (left), *in vitro* (middle) and *in vivo* (right) signals. The original signal corresponds to the $g(t)$ function calculated with the ratio formula in Eq.(5.7) and the smoothed signal is its final denoised version after convergence.

first iteration. For the two distorted signals, the resonances of Cr at 3 ppm and 3.9 ppm and the one from NAA at 2 ppm are not very well fitted with AQSES, while AQSES Lineshape is able to fit these peaks. This could be due to the fact that the lineshape distortions have a shape different from the typical Lorentzian type considered by AQSES. For both signals in (b) and (c), exhibiting slightly different levels of distortions, we observe similar improvements in the quantification results.

- ***In vivo* signals.** The undistorted *in vivo* signal was fitted similarly by AQSES and AQSES Lineshape, *i.e.*, AQSES Lineshape reports convergence after the first iteration. Results of quantification are shown in Fig. 5.6. The small residuals obtained with AQSES Lineshape shown in Fig. 5.6 suggest good fitting results.

5.4 Discussion

5.4.1 General considerations about AQSES-Lineshape

MRS signals are ideally composed of Lorentzian lineshapes, however, when magnetic field perturbations, field inhomogeneities or tissue heterogeneities are present, these lineshapes are disturbed (in symmetry and linewidth) and make the fitting of the signal using an basic lineshape (*e.g.*, Lorentzian, Gaussian or

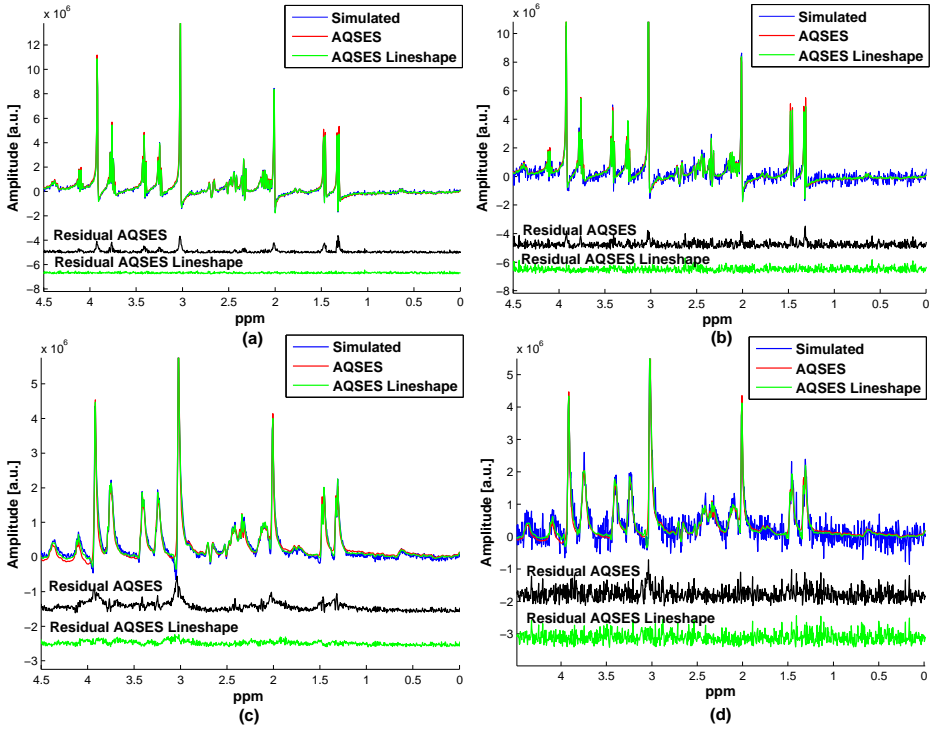


Figure 5.4: Simulated MRS signals with lineshape distortions and quantification results for different SNR levels and different dampings. These signals are composed of multiple resonances derived from 7 *in vitro* measured metabolites at 9.4 T: Ala, Cr, Gln, Glu, Lac, NAA, and Tau with acquisition parameters: PRESS sequence, $TR=8$ s, $TE=20$ ms, $SW=4$ KHz, $NDP=2048$ points and 64 averages. Top row with small dampings (to simulate *in vitro* signals): (a) $SNR=30$, the quantification with AQSES and AQSES-Lineshape resulted in fittings where residual analysis provided: $SSE=5.557e+013$, $RMSE=1.648e+005$ and $SSE=2.0348e+013$, $RMSE=9.962e+004$, respectively. (b) $SNR=2$, the quantification with AQSES and AQSES-Lineshape resulted in fittings where residual analysis provided: $SSE=2.217e+014$, $RMSE=3.291e+005$ and $SSE=1.863e+014$, $RMSE=3.018e+005$, respectively. Bottom row with big damping (to simulate *in vivo* signals): (c) $SNR=20$, the quantification with AQSES and AQSES-Lineshape resulted in fittings where residual analysis provided: $SSE=2.2437e+013$, $RMSE=1.0472e+005$ and $SSE=6.9799e+012$, $RMSE=5.8408e+004$, respectively. (d) $SNR=5$, the quantification with AQSES and AQSES-Lineshape resulted in fittings where residual analysis provided: $SSE=6.3189e+013$, $RMSE=1.7574e+005$ and $SSE=4.4352e+013$, $RMSE=1.4723e+005$, respectively.

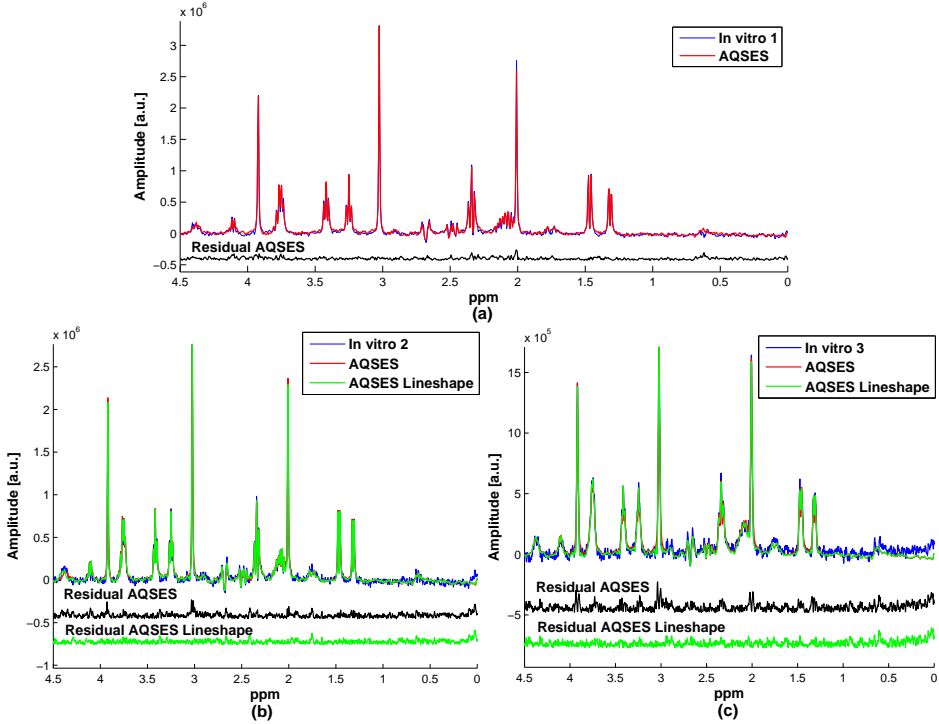


Figure 5.5: Spectra of in vitro MRS signals measured at 9.4 T containing 7 metabolites: Ala, Cr, Gln, Glu, Lac, NAA, and Tau. Acquisition parameters: PRESS sequence, $TR=8$ s, $TE=20$ ms, $SW=4$ KHz, $NDP=2048$ points and 128 averages. (a) ‘In vitro 1’ was acquired using the default shimming technique with linewidth=1.36 Hz and $SNR=22$; the quantification with AQSES resulted in a good fitting where residual analysis provided: $SSE=1.3461e+012$ and $RMSE=2.5650e+004$. (b) ‘In vitro 2’ is a distorted signal acquired by mis-setting the shim current of the X coil with linewidth=3.92 Hz and $SNR=20$; the quantification with AQSES and AQSES-Lineshape resulted in fittings where residual analysis provided: $SSE=5.9428e+012$, $RMSE=3.1279e+004$ and $SSE=5.2867e+012$, $RMSE=2.9502e+004$, respectively. (c) ‘In vitro 3’ is a distorted signal acquired by mis-setting the shim current of the X coil with linewidth=6.52 Hz and $SNR=18$; the quantification with AQSES and AQSES-Lineshape resulted in fittings where residual analysis provided: $SSE=8.6829e+012$, $RMSE=3.7809e+004$ and $SSE=6.5681e+012$, $RMSE=3.2884e+004$, respectively.

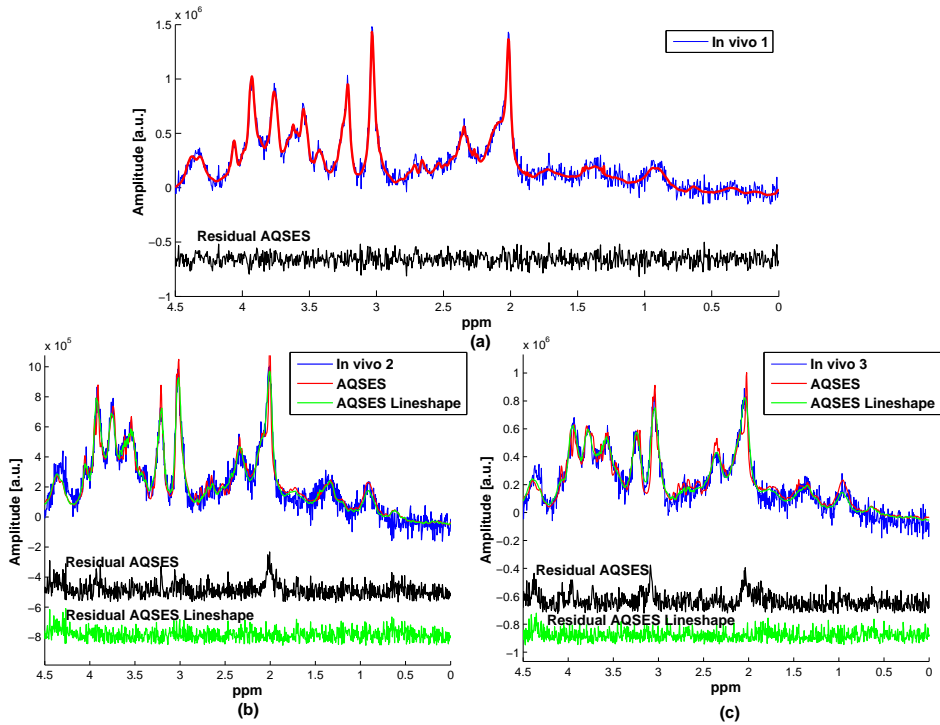


Figure 5.6: Rat brain in vivo spectra from the right hemisphere of the thalamus measured at 9.4 T with acquisition parameters: PRESS sequence, $TR=8$ s, $TE=20$ ms, $SW=4$ KHz, $NDP=2048$ points and 128 averages. (a) 'In vivo 1' was measured with the default shimming technique with linewidth=17.36 Hz, $SNR=20$; it was quantified using AQSES. Residual analysis provided: $SSE=7.087e+012$, $RMSE=5.986e+004$. (b) 'In vivo 2' acquired by mis-setting the shimming parameters of the first order shim coil X with linewidth=27.8 Hz, $SNR=20$; the quantification with AQSES and AQSES Lineshape provided residual analysis with: $SSE=6.631e+012$, $RMSE=5.79e+004$ and $SSE=6.257e+012$, $RMSE=5.624e+004$, respectively. (c) 'In vivo 3' was acquired by mis-setting the shimming parameters of the second order shim coil Z^2 with linewidth=39.69 Hz, $SNR=20$; the quantification with AQSES and AQSES Lineshape provided residual analysis with: $SSE=7.2e+012$, $RMSE=6.033e+004$ and $SSE=6.6e+012$, $RMSE=5.776e+004$, respectively.

Voigt) unreliable or thereby enlarging the errors on the metabolite estimates. As described in the literature [140, 106, 158, 156, 132, 123], one could also estimate the lineshape of MRS signals and include it inside the quantification algorithm.

Other methods require starting values for estimating the lineshape [158], however, the first iteration on AQSES Lineshape can also be considered as a way to initialize the $g(t)$ function by using the ratio formula followed by fully-automated denoising when cross-validation is employed for tuning the smoothing level. Since none of the current MRS quantification methods uses global optimization techniques, the problem of providing good enough initial values on the parameters is essential for the convergence of local NLLS methods. Thus, a quantification method that needs as few initial values as possible and implicitly adapts the initial values to the signal under analysis, has practical advantages.

When MRS signals are not heavily distorted it may occur that Lorentzian lineshape corrections are a good for the experimental data. Thus, AQSES Lineshape works iteratively and evaluates the performance of the quantification after each fit. So the first fit is performed assuming a Lorentzian lineshape, which is then estimated (*i.e.*, with a free model). Finally, in each iteration, residuals of the current and previous fits are compared and the best fit is selected. If the fit using the Lorentzian model is selected, the algorithm will stop after the first iteration.

Quantification of distorted signals with lineshape estimation showed good quantification results for simulated, *in vitro* and *in vivo* distorted signals. The performance of the method was evaluated by validation of amplitude estimates and visual assessment of the residual.

AQSES Lineshape is an automated quantification method and no user input is required for estimating the lineshape, which is essential for clinical use.

5.4.2 Residual and other imperfections

When a quantification method like AQSES is used and a significant residual is observed after the estimation, several factors can be attributed to this problem. One of them is the lineshape distortion. However, incomplete metabolite basis set and spectral differences between the *in vivo* signal and the metabolite basis set (*e.g.*, non-fitted peaks due to temperature effects or chemical shift displacement errors), may also cause an increase in the residual and thus an inaccurate quantification. To identify which of those factors is predominant in the estimation of metabolites is not obvious. However, it is recommended to choose the appropriate *prior* knowledge and consider the possible disturbances and external factors affecting the signals.

Potential imperfections could be due to phase distortions caused by J-modulation, however, with relatively short TEs only marginal phase errors may occur for

functional groups with relatively large J-coupling constants (for example GABA, Gln, Glu or m-Ins with J-coupling up to 15 Hz).

Additional ‘ghost’ echoes may be introduced in the signals caused by local gradients at tissue interferences. These echoes can be, for instance, eliminated in the time domain by truncation of the last points where the echo is present. The use of navigator scans can track patient movements and potentially compensate for it. In AQSES Lineshape these kind of echoes must be avoided when calculating the SNR for estimation of the cut-off point at which the decay function is set to zero.

5.5 Conclusion

Accurate quantification of MRS signals is essential when clinical data need to be analyzed, therefore the lineshape estimation is considered an important step towards the accurate quantification of *in vivo* MRS signals.

The quantification of MRS signals with lineshape estimation has been considered in three different scenarios of distorted MRS signals, namely on simulated, *in vitro* and *in vivo* signals [123]. Asymmetric lineshape distortions with eddy current effects were considered in simulations, while mis-shimming effects were used to broaden and distort the measured *in vitro* and *in vivo* signals.

Finally, it has been shown that the lineshape estimation by self-deconvolution is applicable to *in vivo* MRS signals [106, 132, 156, 123] and can be successfully imposed to the metabolite profiles in quantification methods such as AQSES [156, 123].

Chapter 6

Parametric method for baseline estimation of MRS signals

*In this chapter the macromolecular and lipids contribution are addressed via a parametric method presented in [121]. A brief introduction to the macromolecular baseline is given and a set of *in vivo* signals with their corresponding baseline measured via inversion recovery are used to assess a parametric modelling method. Comparison of results using different ways of taking the macromolecular baseline into account are presented. Finally, some conclusions about quantification with the studied baseline methods are described.*

6.1 Introduction

Besides the metabolites, an MR signal also contains other kind of components of potential interest, pertaining to macromolecules and lipids, denoted here as ‘MM’. In normal brain tissue a small contribution from MM in the frequency regions between 0.5 and 2 ppm can be observed, while in different brain tumours and metabolic diseases, lipid contributions increase in concentration providing useful diagnostic information. On the other hand, in measurements close to the skull and the scalp, MR spectra from healthy tissue contain unavoidable high lipid contamination.

In the frequency domain, MM contributions are observed as an underlying profile called baseline (see bottom curve in Fig. 6.1), which overlaps with the metabolite peaks and complicates quantification. Because there exist no exact chemical substances similar to MM (*i.e.*, to measure it *in vitro*), different studies focused on

the detection, suppression, evaluation and modeling of this baseline (see chapter 2 section 2.2.8 and chapter 3 section 3.2.4). In the literature, several advanced acquisition techniques using inversion recovery [71, 128, 33, 111, 88], parametric [5, 154] and non-parametric methods [155, 143] have been widely used.

The measurement time of MM via inversion recovery depends on the acquisition parameters (TI, TR, number of averages, etc.), but it requires a long acquisition time. Although this MM signal is known to provide a good approximation of the baseline, it is not reproducible when the conditions of the region of interest are affected by acquisition problems and various diseases. Moreover, it also contains some unsuppressed metabolite resonances possibly causing underestimation of metabolite estimates [88].

It would be advantageous to use an inversion recovery measurement for several *in vivo* MRS signals, however, the single MM contribution may vary from subject to subject. Seeger *et al.* [154] and Bartha *et al.* [5] made use of the *prior* knowledge from different MM signals obtained to determine the position of specific macromolecular resonances. These resonances were fixed and empirically determined values for the damping were used. Similarly, Behar *et al.* [7] used the spectrum of dialyzed cytosol to characterize individual contributions of MM. Finally, the physiological macromolecular components detected with any of the metabolite suppression methods mentioned above are added to the basis set for the quantification as additional model components.

In this chapter we focus on a similar way of extracting characteristic information from a database of inversion recovery MM signals. We then propose an extension of the AQSES Lineshape algorithm described in chapter 5, that is capable to deal with various ways of incorporating the baseline.

6.2 Materials and Methods

6.2.1 Animals

Alzheimer's disease has been studied using ^1H MRS in different brain regions, where metabolite changes have been observed [103]. Twelve control wild-type and APP.V717I transgenic mice [113] of age 16-18 months were used for this study. Mice were anesthetized by using 1.25% isoflurane and their heads were immobilized. Breathing was measured during the experiment for monitoring the physiological status of the animals. Respiration and body temperature were measured with the MR compatible small animal monitoring and gating device model 1025 from S.A. Instruments (Stony Brook, NY, USA). Hereby, respiration is measured using a small pneumatic pillow placed under the abdomen of the animal. Measured pressure changes are digitized and transmitted to the control/gating module using

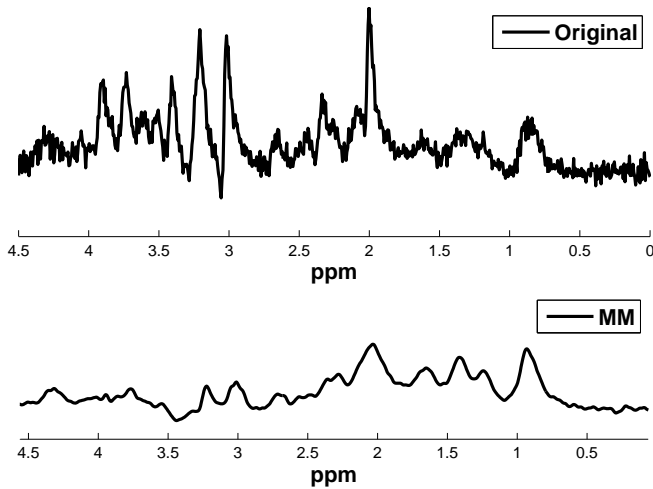


Figure 6.1: Real part of the spectrum of an *in vivo* MRS signal and an MM signal obtained from a mouse. MRS acquisition parameters: 9.4 T, PRESS sequence, $TR=4$ s, $TE=12$ ms, $SW=4$ KHz, $NDP=2048$ points and 256 averages. MM acquisition parameters: 9.4 T, PRESS sequence, $TI=800$ ms, $TR=3$ s, $NDP=2048$ points and 1024 averages.

optical fibres. Body temperature was measured using a rectal thermometer, the room temperature was maintained around 31°C.

6.2.2 *In vivo* ^1H MRS signals

In vivo single voxel MRS signals from mice were acquired on a 9.4 T Bruker Biospec small animal MR scanner (Bruker BioSpin MRI, Ettlingen, Germany). A complete description of the acquisition protocol is presented in chapter 2 section 2.1.2. Single voxel spectra and FASTMAP VOI was positioned on the mice hippocampus. The voxel size was $3 \times 1.75 \times 1.75$ mm³. The widths of unsuppressed water lines were between 20 and 25 Hz. All acquired *in vivo* and MM ^1H MRS signals are shown in Fig. 6.2 and 6.3.

Macromolecules are characterized by shorter T_1 and T_2 relaxation times than those of metabolites. Therefore, signals from macromolecules can be separated by introducing a T_1 selective encoding of the signal which can be achieved by a non-selective inversion pulse and an appropriate time delay *prior* to the measurement sequence (inversion time). For studying the MM estimation, individual metabolite-nulled signals were measured using inversion recovery with a 1 ms Hermitian

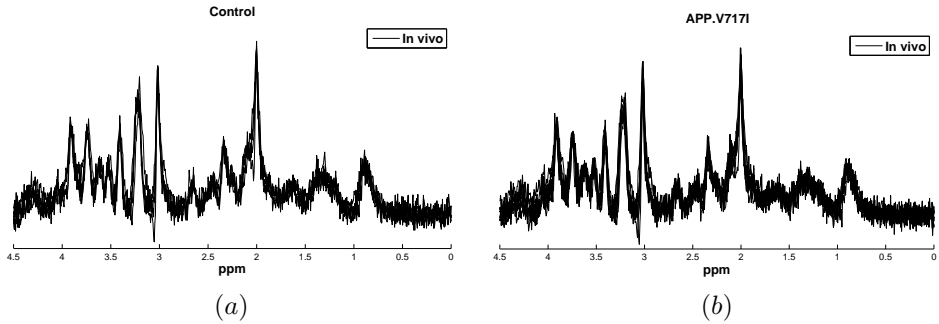


Figure 6.2: Real part of the spectra of all in vivo MRS signals from mice obtained from the frontal hippocampus. Acquisition parameters of in vivo signals: 9.4 T, PRESS sequence, TR=4 s, TE=12 ms, SW=4 KHz, NDP=2048 points and 256 averages in a VOI of size $3 \times 1.75 \times 1.75 \text{ mm}^3$. The measurement time for the MRS signal was approximately 15 minutes. (a) Control mice MR signals. (b) APP.V717I mice MR signals.

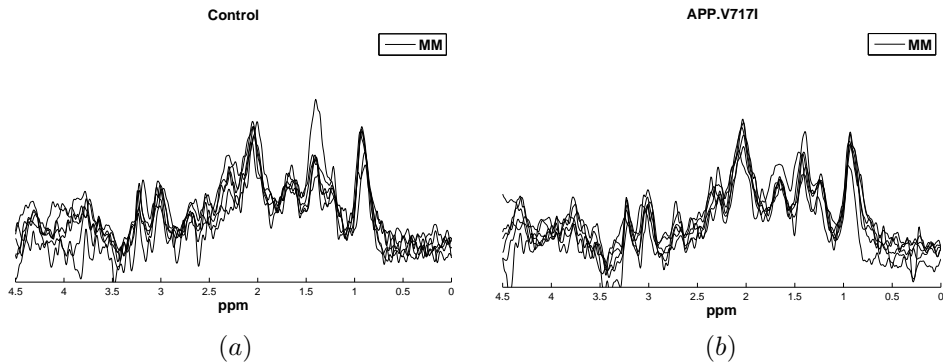


Figure 6.3: Real part of the spectra of all MM background signals from mice obtained from the frontal hippocampus. Acquisition parameters: 9.4 T, TI=800 ms, TR=3 s, NDP=2048 points and 1024 averages. The measurement time for the MM was approximately 50 minutes. (a) Control mice metabolite-nulled signals. (b) APP.V717I mice metabolite-nulled signals.

inversion pulse. TI can be adjusted to suppress signals from metabolites, however, a full suppression of metabolites is not possible due to their different T_1 s. The best metabolite suppression was achieved for the first animal with TI=800 ms, TR=3 s and 1024 averages (see Fig. 6.4). After fixing this TI, MMs were measured individually for each mouse.

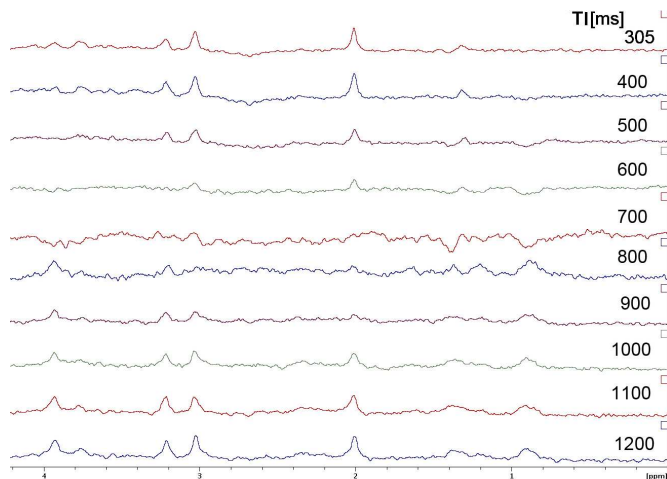


Figure 6.4: Set of metabolite-nulled acquisitions obtained at different TIs. The signal obtained at 800 ms was experimentally selected to be a good TI for metabolite nulling.

6.2.3 Metabolite basis set

The following metabolites were measured *in vitro* to be used as basis set for quantification: Ala, Asp, Cr, GABA, Glc, Gln, Glu, GPC, GSH, Lac, m-Ins, NAA, PCh, PCr, PE and Tau. A complete description of the acquisition protocol and a figure illustrating the basis set is presented in chapter 2 section 2.1.3.

6.2.4 Baseline estimation

All *in vivo* signals were preprocessed following the steps described in chapter 2 section 2.2. Furthermore, the quantification was performed using AQSES [137].

Characterization of the macromolecular contamination was addressed in two ways, where MM is either (a) measured or (b) modeled using m profiles:

- (a) *Measured via inversion recovery.* An MM signal was obtained from each of the 12 mice. An example of a measured macromolecular signal is shown

in Fig. 6.5 obtained with $TI=800$ ms and $TR=3$ s and preprocessed as described in chapter 2 section 2.2. In particular, the short T_1 of Cr [128] caused an incomplete suppression of the Cr/PCr peak located at 3.9 ppm at any TI tested. The top curve in Fig. 6.5 shows the unsuppressed methylene resonance of Cr, which was filtered out using the time domain method HLSVD-PRO. All spectra were further apodized by multiplication with an exponential function of Lorentzian type (e^{-xt}) of 15 Hz. Because the MM signal does not account for all baseline issues, the spline baseline from AQSES was used in combination with the MM signal to account for extra baseline contamination. In this case, the smoothing parameter λ from AQSES (see chapter 3 section 3.2.1 Eq.(3.1)) was set high, indicating a very smooth spline function, while in cases when the MM signal is not available, λ is then set low to allow a good modelling of lipid and macromolecular resonances.

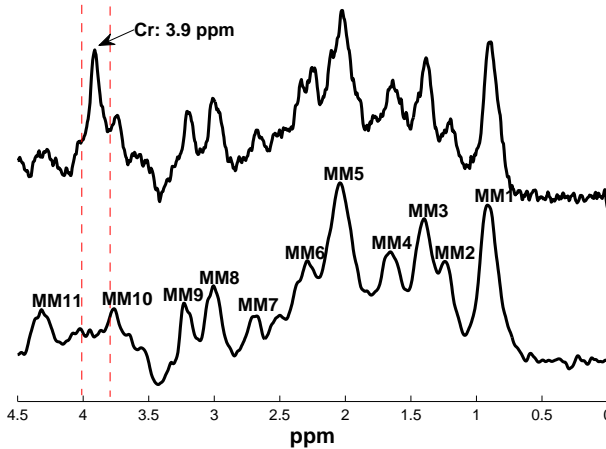


Figure 6.5: Real part of an *in vivo* metabolite-nulled MM spectra acquired at 9.4 T, $TE=12$ ms, $TI=800$ ms, $TR=3$ s, $NDP=2048$ points and 1024 averages. Spectra were post-processed with a 15 Hz Lorentzian linebroadening. Top: Due to a shorter T_1 , the marked (Cr + PCr) resonance at 3.9 ppm was not completely minimized, therefore this peak was filtered out using HLSVD-PRO. Macromolecular resonances are labeled by MM from 1 until 11 at the following central frequencies: 0.89, 1.20, 1.36, 1.63, 2.02, 2.29, 2.65, 3.03, 3.21, 3.75, 4.31 ppm. Bottom: Mean of filtered MM signals.

- (b) Computed using prior knowledge from a database of the inversion recovery signals. A second approach to estimate the baseline consisted of computing individual lipid and macromolecular peaks using a database of MM signals as *prior* knowledge. From these signals the major resonances were observed at frequency locations around: 0.89 (MM1), 1.20 (MM2), 1.36 (MM3),

1.63 (MM4), 2.02 (MM5), 2.29 (MM6), 2.65 (MM7), and 3.03 (MM8), 3.21 (MM9), 3.75 (MM10), and 4.31 ppm (MM11) (see Fig. 6.5). These resonances are in accordance to [7, 128, 67, 154] and extended with the MM7 which appeared to be also present in all individual MM signals. AMARES [176] in jMRUI [165] was used to compute individual spectral components. From the twelve available MM signals from different mice, the mean of amplitudes, frequency locations and linewidths were used to create the individual macromolecule and lipid resonances that were further included in the basis set of AQSES. It is important to notice that the model used in AQSES allows small parameter variations to better accommodate individual conditions of each signal under analysis. The simulated MM components are also subject to such corrections. Results of this estimation are shown in Fig. 6.6.

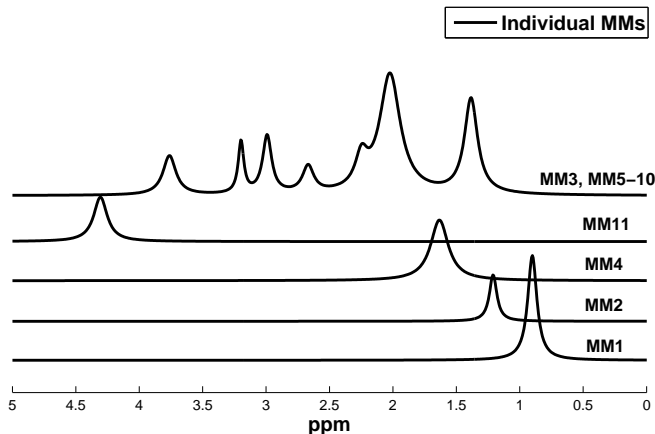


Figure 6.6: Real part of the MM spectrum obtained with AMARES using prior knowledge from the measured inversion recovery signals. This plot shows the individual MMs computed based on the mean of the AMARES estimates of all measured MMs. Small variations are expected for different signals which are then corrected by AQSES.

6.2.5 Combination of baseline and lineshape estimation

Due to unavoidable spectral distortions that can not always be corrected with advanced shimming techniques, lineshape corrections of ^1H MRS signals measured at high magnetic field are necessary. Within one measurement the same lineshape is assumed for all components; thus, for taking into account lineshape distortions in the quantification method, a common decay is considered for all spectral components in the model of AQSES, with the exception of the macromolecular

signal measured *in vivo*. Note that the contribution of local inhomogeneity on the already fast decay of $B(t)$ is only marginal. Moreover, the measured MM has the same properties as the signal when measured in the same location, thus lineshape corrects are unnecessary. As in chapter 5, the exponential decays $e^{-d_k t}$ of the model in AQSES are replaced by the common factor $g(t)$, of arbitrary shape, resulting in the following models and ratio formulas (to be compared in *Step 2* of the algorithm for lineshape estimation):

In (a) the model is (compare to Eq.(5.6) and Eq.(5.7)):

$$y(t) = g(t) \sum_{k=1}^K a_k e^{(j\phi_k)} e^{(2\pi j f_k t)} v_k(t) + \tilde{a} e^{(j\tilde{\phi})} e^{(2\pi j \tilde{f} t)} MM(t) + B(t) + \epsilon(t) \quad (6.1)$$

and $g(t)$ is estimated as:

$$g(t) = \frac{y(t) - \tilde{a} e^{(j\tilde{\phi})} e^{(2\pi j \tilde{f} t)} MM(t) - B(t)}{\sum_{k=1}^K a_k e^{(j\phi_k)} e^{(2\pi j f_k t)} v_k(t)} \quad (6.2)$$

In (b) the model is (compare to Eq.(5.6) and Eq.(5.7)):

$$y(t) = g(t) \left(\sum_{k=1}^K a_k e^{(j\phi_k)} e^{(2\pi j f_k t)} v_k(t) + \sum_{i=1}^m \tilde{a}_i e^{(j\tilde{\phi}_i)} e^{(2\pi j \tilde{f}_i t)} MM_i(t) \right) + B(t) + \epsilon(t) \quad (6.3)$$

and $g(t)$ is estimated as:

$$g(t) = \frac{y(t) - B(t)}{\sum_{k=1}^K a_k e^{(j\phi_k)} e^{(2\pi j f_k t)} v_k(t) + \sum_{i=1}^m \tilde{a}_i e^{(j\tilde{\phi}_i)} e^{(2\pi j \tilde{f}_i t)} MM_i(t)} \quad (6.4)$$

where $y(t)$ is the experimental signal, $B(t)$ is the non-parametric (spline) baseline from the previous iteration, $MM(t)$ is the measured baseline, $MM_i(t)$ is the set of modelled profiles, K is the number of metabolites, $v_k(t)$ the metabolite signal k in the basis set, and the amplitudes a_k , \tilde{a}_i , frequency shifts f_k , \tilde{f}_i and phase shift ϕ_k , $\tilde{\phi}_i$ are estimated from the previous iteration of the AQSES Lineshape algorithm. Thus, $g(t)$ can be estimated at the same time as the spectral parameters (a_k and f_k) using an iterative method similar to the methods described in chapter 5.

6.3 Results

6.3.1 Lineshape

Fig. 6.7 shows the fits with and without lineshape estimation for one of the mouse signals. Due to the fact that the model in AQSES assumes spectral components

with Lorentzian shape, the quantification with the conventional AQSES presents some problems which can be observed around 3 ppm. By allowing a free lineshape model in AQSES, $g(t)$ is adjusted to fit such non-ideal shapes. Furthermore, the residual was evaluated with the goodness of the fit using a linear polynomial computing the sum of square errors (SSE) and the root mean square errors (RMSE).

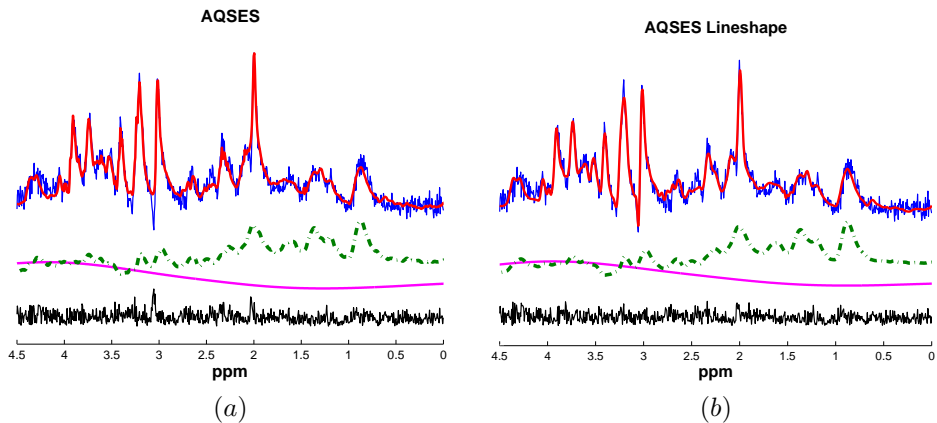


Figure 6.7: AQSES fit for one of the short TE 1H MRS *in vivo* signals from mouse brains with lineshape distortion. Real part of the *in vivo* spectrum (noisy signal) together with the fit using AQSES (bold line on top of the signal), MM measured signal (dotted curve below the signal), spline baseline (smooth curve below MM) and the residual (curve beneath). This quantification was made including the measured macromolecular signal in the basis set and a very smooth splines function to fit any additional baseline. Residual analysis provided: $SSE=1.8264e+013$, $RMSE=9.6091e+004$ and $SSE=1.6923e+013$, $RMSE=9.2497e+004$, for the fits with AQSES and AQSES Lineshape, respectively.

6.3.2 Baseline

Macromolecule estimation: inversion recovery vs splines

We evaluated quantification results comparing the spectra of each group (control and APP mice), and in particular the influence of the background estimation considering the measured MM signal and the splines estimation from AQSES. Thus, we use three approaches:

- (i) considering MM together with splines to estimate the macromolecular contribution,
- (ii) considering only the MM to estimate the macromolecular contribution, and
- (iii) considering only splines to estimate the macromolecular contribution.

Results shown in Fig. 6.8 suggest that the combination of MM and splines is

a good approach for estimating the baseline of *in vivo* MRS signals. Instead, using only the MM signal to estimate the baseline may produce an inaccurate fit that is reflected in the residual. On the other hand, using only splines for estimating the baseline produces a good approximation of the macromolecular contribution. However, the smoothing hyper-parameter must be carefully selected to avoid underestimation of metabolites (if the splines are too flexible) or a bad fit (if the splines are too smooth).

In Fig. 6.9 we present the results of amplitude estimates of all metabolites with the corresponding Cramér-Rao lower bounds for the mean spectra of the control and disease mice using the MM and splines to fit the baseline. As can be seen here, no significant differences can be observed between the control and APP metabolite estimates and therefore, no reliable separation between the groups is obtained. Small variations in metabolites such as NAA [103] of the APP group were expected, however, the age differences of APP mice may influence the variability of metabolites compared to control mice. Additionally, quantification using a simulated or *in vitro* basis set showed insignificant differences in the metabolite estimates (see chapter 2 section 2.1.3). Finally, the variability in quantification results shown here indicates that the detection of Alzheimer's disease using ^1H MRS in the hippocampus may not provide a reliable class separation.

Macromolecule estimation: with prior knowledge obtained from a database of inversion recovery signals using AMARES

Table 6.1 shows the results of macromolecule fitting using AMARES. Macromolecule resonances are simulated independently, however, to avoid mis-quantification as suggested in [154], MMs overlapping with metabolites were combined in a single spectrum to fix the ratio between those resonances. We have tested the case when the macromolecules are kept free, thus frequencies, amplitudes and dampings can vary independently. This resulted in MMs fitting metabolites peaks (*e.g.*, NAA) leading to mis-quantification. To avoid this problem, we combined MM3 with MM5-MM11 to obtain a single profile of seven resonances located in the region between 2 - 4.1 ppm where all important metabolites are resonating.

Fig. 6.10 shows the results of fitting the mean of spectra using both approaches: *a*) the mean of measured MMs signals (1 MM profile) and *b*) the mean of individual MMs obtained with AMARES (5 MM profiles). The corresponding fitting of the MMs is shown to demonstrate that both estimations reflect comparable MM contributions. Moreover, Fig. 6.11 shows the amplitude estimates for the corresponding fittings, which confirm that rather similar estimates can be obtained (by grouping metabolites, such as, NAA and NAAG) with either of the two approaches. Nevertheless, there is a trend that most of the metabolites that overlap with MM components are lower in case *a*) than in case *b*).

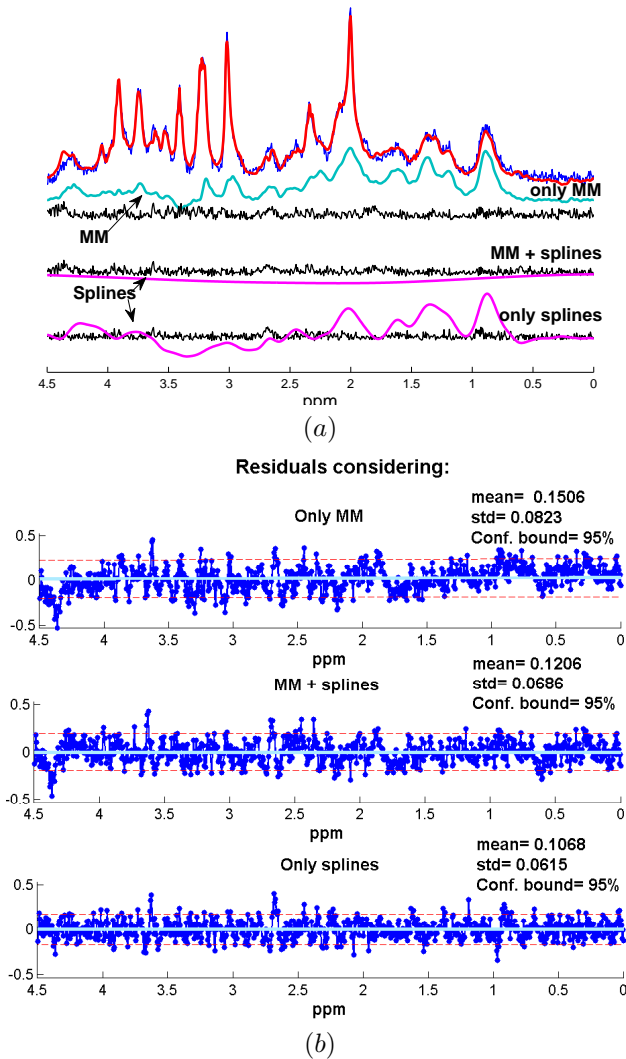


Figure 6.8: (a) Results of quantification with AQSES for a short TE ^1H MRS in vivo signal from mouse brain. This quantification was made including or not the mean of the measured macromolecular signal (MM) in the basis set and the splines function to account for any additional baseline problems. (i) only MM, (ii) MM and splines and (iii) only splines. Real part of the in vivo spectrum (noisy signal) together with the fit using AQSES (line on top of the signal), residual (noisy signals below), MM estimated signal (bold curve below), spline estimated baseline (smooth curves below). (b) Residual analysis of the quantification provided: $SSE = 24.08$ and $RMSE = 0.1103$, $SSE = 19.06$ and $RMSE = 0.09816$, $SSE = 15.18$ and $RMSE = 0.0876$, for the plots from top to bottom, respectively.

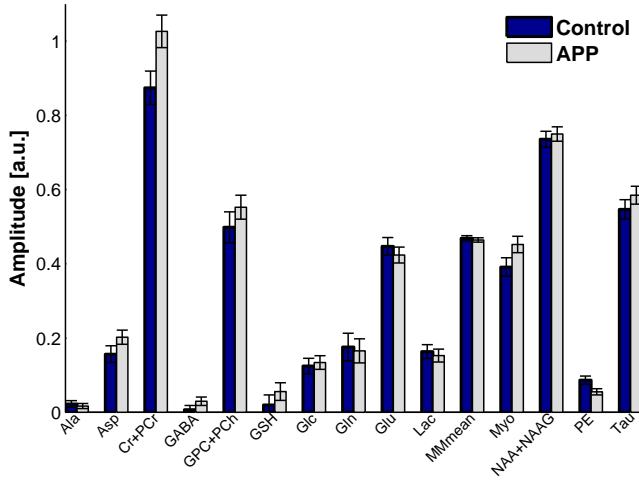


Figure 6.9: Metabolite estimates with the corresponding Cramér-Rao lower bounds for the mean spectra of the control and disease mice using the MM and splines to fit the background. In this study, no significant differences were observed in the metabolite concentrations between the controls and disease mice.

Table 6.1: Results from AMARES for the mean of amplitudes, frequencies and linewidths obtained from the fit of all macromolecular signals

Components	Position (ppm) \pm SD	Linewidth (Hz) \pm SD	Amplitude/MM1 \pm SD
MM1	0.901 \pm 0.007	109.377 \pm 26.529	1.000
MM2	1.210 \pm 0.000	89.681 \pm 26.959	0.363 \pm 0.123
MM3	1.384 \pm 0.010	156.800 \pm 36.492	1.301 \pm 0.799
MM4	1.633 \pm 0.022	211.219 \pm 37.678	1.119 \pm 0.722
MM5	2.023 \pm 0.008	248.888 \pm 27.485	2.601 \pm 0.892
MM6	2.247 \pm 0.012	145.477 \pm 107.953	0.394 \pm 0.333
MM7	2.668 \pm 0.013	132.942 \pm 70.944	0.309 \pm 0.301
MM8	2.992 \pm 0.020	107.262 \pm 34.717	0.543 \pm 0.369
MM9	3.198 \pm 0.017	66.016 \pm 41.417	0.299 \pm 0.286
MM10	3.762 \pm 0.032	154.517 \pm 84.011	0.530 \pm 0.475
MM11	4.306 \pm 0.028	161.256 \pm 102.208	0.625 \pm 0.737

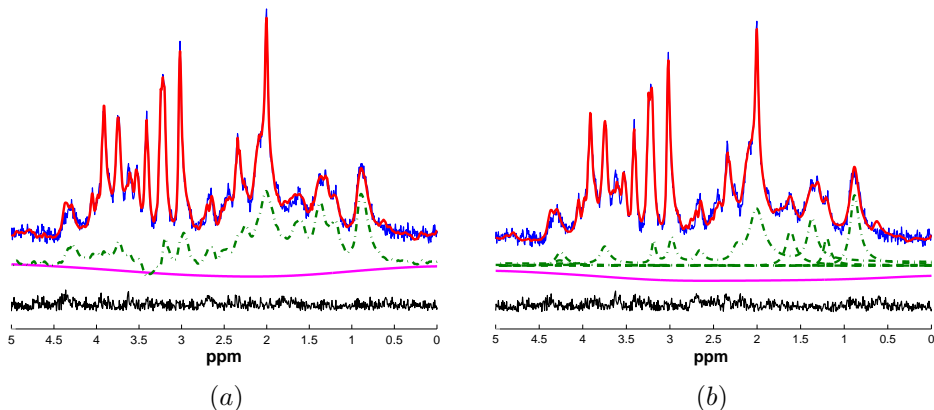


Figure 6.10: AQSES fit for the mean spectra of short TE ^1H MRS *in vivo* from mouse brains. Real part of the *in vivo* spectrum (noisy signal) together with the fit using AQSES (bold line on top of signal), MM (dash-dotted curve below the signal), spline baseline (smooth curve below the MM signal) and the residual (curve beneath). This quantification was made including the MM signal (measured (a) and simulated (b)) in the basis set and a very smooth splines function to fit any additional baseline. The residual analysis provided: $SSE=19.0580$, $RMSE=0.0982$ and $SSE=25.5416$, $RMSE=0.1136$ for the fit with the measured and the simulated MM, respectively.

6.4 Discussion

In vivo MRS signals of 12 mouse brains measured in the hippocampus were quantified to study the baseline estimation. The hippocampus is a rather problematic region for achieving good homogeneity of the magnetic field in animals as well as in human brain [82]. This implies that lineshape distortions are likely to occur in such signals, justifying the development of lineshape estimation methods, such as those proposed in [158, 6, 141, 42, 156, 132].

In particular, the self-deconvolution method proposed in [156, 123] and detailed in chapter 5 has been successfully used. This method can be combined with a measured baseline or a set of simulated macromolecular components. In the first case, the MM signal is measured in the same location as the *in vivo* signal and therefore, influenced by the same tissue heterogeneities. This MM signal has been included in the model (5.6) without multiplying it with the common decay $g(t)$. In the second case, the modeled MM components have an ideal shape, and should be corrected with the common decay $g(t)$.

Although the MM signal acquired by inversion recovery is known to provide a good approximation of the macromolecular contamination, it also requires a long acquisition time and is not reproducible when the conditions of the region of

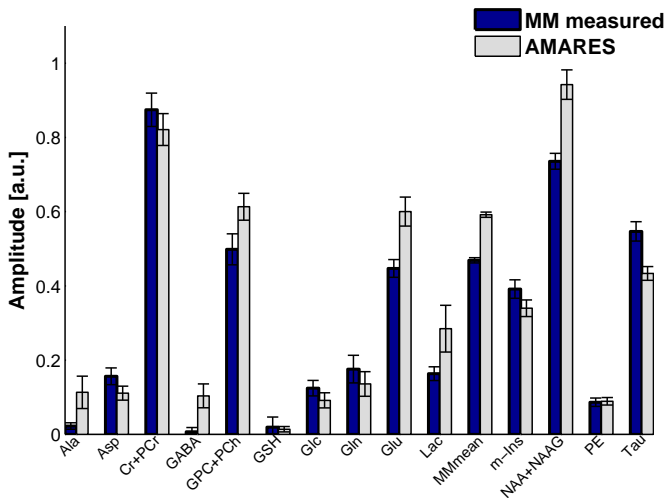


Figure 6.11: Amplitude estimates of metabolites with corresponding Cramér-Rao lower bound quantified using AQSES with: a) the measured and b) simulated set of MMs (obtained from AMARES) to fit the macromolecular baseline.

interest are affected by acquisition problems and various diseases. Moreover, it also contains some unsuppressed metabolites. A promising new acquisition technique based on diffusion weighted spectroscopy has recently been proposed [88], and was shown to be less contaminated by unsuppressed metabolites.

In order to build up *prior* knowledge about the MM contributions in mouse hippocampus, we extracted eleven peaks from the inversion recovery spectra containing resonances of macromolecules and lipids. For this purpose, the quantification method AMARES was used and the MM parameters (amplitudes, frequencies and linewidths) from all available inversion recovery signals were computed. The mean of those estimates shown in Table 6.1 was then used to create individual MMs to be included in the basis set. This *prior* knowledge contains essential information about the MM of healthy mice which provides spectral parameters close to the MM of *in vivo* signals. Quantification of the MM spectra in AMARES using both Gaussian and Lorentzian shapes has been evaluated. Only small differences were found using both lineshapes to fit the MM peaks. However, for the resonance located at 0.89 ppm a better fit was obtained using a Gaussian lineshape, while most of the peaks between 2 ppm and 4.3 ppm were better fitted with a Lorentzian lineshapes. Moreover, because we also include a method to estimate the lineshape, the shape of all individual metabolites and MM profiles will also be corrected according to the shape of the *in vivo* signal (*i.e.*, $g(t)$ will also correct MM profiles). Using this approach, the shape of the

individual MMs will not play an important role, but good *prior* knowledge about approximate values for frequency locations, amplitudes and linewidths will be beneficial for AQSES Lineshape.

Due to low SNR of the individual MM signals, all MM components could not always be clearly localized and therefore some variability has been observed. In *in vivo* MRS signals, this variability in the data is also expected, therefore the quantification method AQSES allows small variations in damping and frequency.

Several papers have focused on comparing inversion recovery macromolecular baselines with mathematical models for background accommodation. At lower magnetic fields (human MR scanner at 3 T) it has been shown that using Subtract-QUEST [143] similar quantification results in terms of metabolite concentrations can be obtained, but had lower precision than using measured macromolecular signals [55]. In [33], the spline fitting of LCModel [141] resulted in a smooth approximation of the *in vivo* macromolecules, and could not reproduce completely all features of the *in vivo* spectrum of macromolecules at 14.1 T. However, when the knot spacing is reduced beyond the default value, the LCModel spline model is more flexible to follow closely the measured MM at 9.4 T, as illustrated in [128].

At high magnetic field the macromolecular contamination plays an important role; however, even at 1.5 T the resonances of lipids and macromolecules affect the reliable estimation of the relevant metabolites. Therefore, this macromolecular estimation is essential in the quantification of metabolites in *in vivo* ^1H MRS spectra. The location and characterization of all individual MMs and lipids in mice and human brain has been studied previously at various magnetic field strengths, *e.g.*, at 8.4 T [7] and 1.5 T [154]. Consequently, resonances similar to those observed in the mouse brains have been observed in the *in vivo* ^1H MRS spectra of human brain [154, 67, 55]. However, we decisively had to include 11 instead of 8-10 macromolecular components [154, 128], due to a pronounced peak at 2.66 ppm.

6.5 Conclusion

An extension of the quantification method AQSES Lineshape has been proposed by optimally exploiting *prior* knowledge to handle both lineshape and baseline perturbations. One important aspect to consider when estimating the baseline is the fact that metabolite amplitudes may be underestimated. This issue depends on *a)* the measurement conditions for the case when MM is obtained *in vivo* or *b)* setting the AMARES parameters for the case when the MM components are computed via modelling. Moreover, the lipid contamination becomes more important at high magnetic field and therefore, adequate *prior* knowledge on lipids is beneficial for improving quantification.

To our knowledge, the use of an individually measured macromolecular background signal has not been presented using a series of inversion recovery signals measured at 9.4 T. We observed that good fits are obtained when the MMs are used in combination with splines, which compensates for the extra background contributions. Moreover, in the absence of measured MM signals, we proved that allowing a flexible spline model in AQSES can compensate for the missing macromolecular components.

Finally, we addressed the fact that good starting values and *prior* knowledge are advantageous for the quantification methods, providing a strong motivation for using simulated macromolecular and lipid components that should be appropriate for specific measurement and experimental conditions and reduce the introduction of systematic errors.

Concerning the MR signals studied, the hippocampus has a small size and is located near to air cavities and the skull, affecting spectral quality and challenging the metabolite estimation.

Chapter 7

Residual analysis

In this chapter, preliminary achievements of the residual analysis based on quantification results from ^1H in vivo MRS signals are illustrated. Firstly, an introduction to the residual and its characteristics is presented. Then, the data used for analysis and the statistical tools used are described. Finally, results and further perspectives in this direction are presented.

7.1 Introduction

Quantification of MRS signals is commonly evaluated visually by checking the residual and numerically by checking the Cramér-Rao lower bounds of the fitted metabolites. A fit can be considered unsuccessful when the residual contains small spikes which can be attributed to metabolite contributions or the error estimation is large (*i.e.*, Cramér-Rao bounds $> 30\%$). A well-fitted signal contains no metabolites in its residual and therefore, the residual should contain only white complex Gaussian noise. A thorough investigation of the MRS noise and the conditions for this noise being white complex Gaussian are presented by Grage and Akke [57].

A joint analysis of graphical statistical measures and numerical measures is useful for a direct assessment of the residual. Indeed, they are related to visual inspection of the entire data set at once and can easily point out a range of relationships between the model and the data. On the other hand, numerical measures are more focused on a particular property of the data and information is often compressed into a single number. Depending on the data and analysis requirements, one might need to use both types of measures to evaluate the quality of the fit.

We focus on two aspects that have strong influence on the quantification method's performance. First, we show that mis-specification of the damping factor constraint (*i.e.*, the upper and lower bounds allowed variation of the damping factor d_k of each metabolite) in the quantification method AQSES is systematically reflected in the residual of the fit. Second, we examine the influence of the number and importance of the reference metabolites used in the basis set and how residual analysis can help in identifying incomplete metabolite basis sets. To evaluate the goodness of the fit, we compute a quality factor proposed by Slotboom *et al.* [159] and extend it to estimate problematic frequency regions in the residual by using a moving window strategy. Furthermore, we employ the normal probability plot, the cumulative probability and the Rayleigh distribution to study the behavior of the complex residual. In particular, we assess whether it contains only Gaussian noise (whiteness test) or whether systematic patterns from the metabolites are still present.

7.2 Materials and methods

7.2.1 MRS signals.

In order to illustrate the residual analysis methods, two types of signals have been analyzed:

- ^1H MRS signal from human brain acquired at 1.5 T on a Philips NT Gyroscan scanner.
- ^1H MRS signal from rat brain acquired at 9.4 T on a Bruker Biospec small animal MR scanner (Bruker BioSpin MRI, Ettlingen, Germany).

A complete description of the acquisition protocol of both signals is presented in chapter 2 section 2.1.2 and a plot illustrating the spectra is presented in Fig. 7.1.

An *in vitro* basis set of reference metabolites was measured at both magnetic fields. The following metabolites were used at 1.5 T: Ala, Asp, Cr, GABA, Glc, Gln, Glu, GPC, Lac, m-Ins, NAA and Tau; and the following additional metabolites were used at 9.4 T: GSH, PCh, PCr and PE. Moreover, an *in vivo* spectrum of macromolecules and lipids (MM) was measured using inversion recovery and added to the basis set of metabolites (see dotted line at the bottom of Fig. 7.1). A complete description of the acquisition protocols and figures illustrating the basis sets is presented in chapter 2 section 2.1.3.

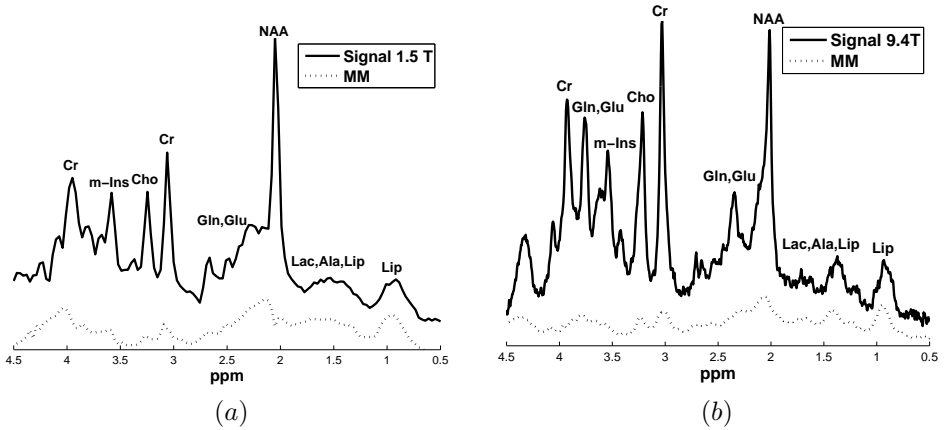


Figure 7.1: Real part of the *in vivo* spectra. The dotted curve below corresponds to the metabolite-nulled signal of measured macromolecule and lipids (MM). (a) Human brain signal acquired at 1.5 T. (b) Rat brain signal acquired at 9.4 T.

7.2.2 Quantification

In vivo MRS signals were preprocessed according to the steps described in chapter 2, section 2.2. and the quantification method used for analyzing the spectra was AQSES. The *upper bound* for the damping used as a constraint is essential when setting the quantification parameters. This so-called soft constraint is needed in order to avoid metabolite profiles to become too broad and fit the baseline or too narrow and not being able to correctly fit all resonances. Thus, when a too low upper bound is used, metabolites having a smaller damping compared to that of the *in vivo* signal will have a damping correction factor that leads to inaccurate quantification. Until now this damping bound was chosen in the in-house graphical user interface for MRS preprocessing and quantification [135] as a fixed value based on the sampling interval (*i.e.*, $\frac{Dwell_{time}}{10}$) and set by default to 40 Hz in jMRUI. Here, we propose to estimate this bound as an adaptive method that takes into account information from the signal and the metabolite basis set. To this end, we make use of the fact that the damping of a complex damped exponential is equal to the linewidth divided by π (*i.e.*, $\frac{FWHM}{\pi}$) of the corresponding Lorentzian peak. Thus, we approximate the upper bound for the damping factor constraint as the difference between the FWHM of the unsuppressed water signal and a singlet from the *in vitro* metabolites (*e.g.*, NAA). This implementation was included in SPID. Finally, the measured macromolecular background signal was included in the basis set of metabolites and used to compute the baseline together with the penalized splines computed in AQSES, in order to account for additional baseline distortions.

7.2.3 Statistical residual analysis

The residual is the difference between the measured signal and the fit of this signal as obtained by AQSES. We use the residual in the frequency domain either for graphical assessment of the goodness of the fit, or as an indication of possible fitting problems. If the fit is correct, the residual should not contain metabolites and should be white noise, under the assumption that only white noise is affecting the measured signal. To assess the goodness of the fit, we use a quality factor proposed by Slotboom *et al.* [159]: $Q_{fit}(N) = \frac{R^2}{N \cdot \sigma^2}$, where σ^2 is the variance of the signal noise calculated in the metabolite-free region, R is the norm of the residual and N is the number of points of the least-squares fit. This value of Q_{fit} is close to 1 when the fit is perfect, bigger than 1 when the model is probably incomplete (lack of metabolites) and smaller than 1 when parts of the noise are fitted (overfitting) which means that the model has too many degrees of freedom.

7.3 Results and discussion

7.3.1 Effect of damping factor constraint

We study the effect of the damping factor constraint, which allows each metabolite in the basis set to be as narrow or wide as the *in vivo* signal. Figure 7.2 shows the results of quantification for 3 different damping factor constraint values. Quantification can be firstly evaluated by visual inspection of the residual, which already provides information about the regions that are not well-fitted. Setting the upper bound on the damping factors too low is clearly reflected in the pattern of the residual, having peaks with similar shape in the region of the metabolites. Subsequently, when a bigger damping is allowed, improvements in the fitting are reflected in the residual (see Fig. 7.2, *e.g.*, around 2 ppm, 3 ppm and 3.9 ppm). Although large increases of the damping with regards to an approximate good bound do not improve or worsen the residual, a more detailed look into the results illustrates that when a too large damping factor constraint is allowed, some metabolites may wrongly fit other metabolites or the baseline (see especially the bottom profile of Glc in Fig. 7.3). Moreover, this effect is not obvious from the fitting results and it may affect the stability of the method, thereby miscalculating the amplitude estimates. The residual of the fitting was also evaluated with the goodness of the fit using a linear polynomial computing the sum of square errors (SSE) and the root mean square errors (RMSE).

Correlation is also used to evaluate the goodness of the fit by correlating the original signal with the fitting. Values close to 1 reflect a good correlation and thus a good fit. The correlations of the original and the fitted signal for the three damping values at 1.5 T were 0.9234, 0.9770 and 0.9786 respectively. The

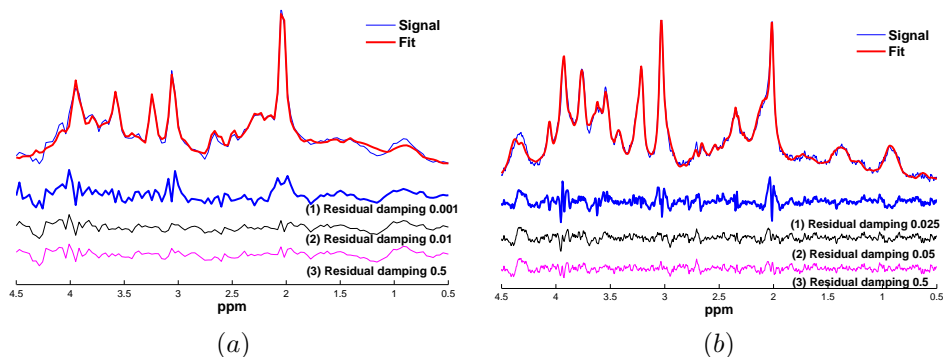


Figure 7.2: Quantification results using different damping factor constraints which reflect the over- or underestimation of amplitude estimates and the importance of its careful selection. The best fitted signal is the overlapped thick line and the residuals are the curves beneath. (a) 1.5 T signal and (b) 9.4 T signal. (1) Residual with small damping factor constraint (small bound), $SSE=0.0105$, $RMSE=0.0045$ and $SSE=72.22$, $RMSE=0.1911$, for the 1.5 T and 9.4 T signals, respectively. (2) Residual with good damping factor constraint (adequate bound), $SSE=0.0045$, $RMSE=0.0030$ and $SSE=40.43$, $RMSE=0.143$, for the 1.5 T and 9.4 T signals, respectively. (3) Residual with big damping factor constraint (big bound), $SSE=0.004354$, $RMSE=0.002922$ and $SSE=39.34$, $RMSE=0.141$, for the 1.5 T and 9.4 T signals, respectively.

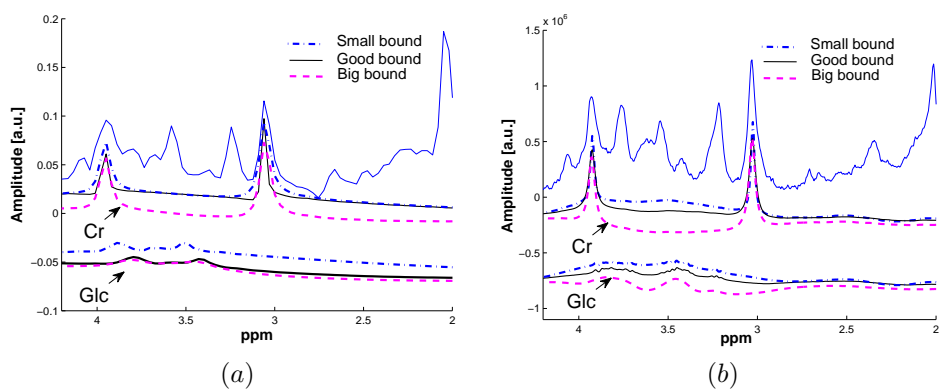


Figure 7.3: Effect of damping factor constraint in metabolites shows a higher impact in small metabolites. The curves beneath the signal correspond to metabolite estimates of Creatine and Glucose using small, good and big damping factor constraints. (a) 1.5 T signal and (b) 9.4 T signal.

correlations for the 9.4 T signal were 0.9241, 0.9808 and 0.9861 respectively. These numbers indicate that the original and the estimated signal are well correlated, however, a complementary analysis is recommended. Moreover, this parameter only gives a rough estimate about the overall fitting, but a more detailed analysis reflecting information about individual metabolite fitting is more advantageous. In a study performed by Grage and Akke [57], NMR noise from a scanner was analyzed by assessing whether the real and imaginary parts of the residual are independent and identically distributed. Here, a zero mean bivariate normal variable $Z = (X, Y)$ with X and Y uncorrelated with equal variances, $\sigma_X^2 = \sigma_Y^2 = \sigma$ can be expressed in polar coordinates as $Z = (R \cos(\theta), R \sin(\theta))$ where the radius R has a Rayleigh distribution with scale parameter σ and the angle θ is uniformly distributed on the interval $[-\pi, \pi]$. For testing the assumption that the residual estimated after a good fit represents random noise (*i.e.*, white Gaussian noise), we evaluated the normality and distribution of real and imaginary parts of the residuals (see Fig. 7.4).

If the residual contains only noise, the probability plots should show a normal distribution. The cumulative distribution function also shows the probability that the residuals follow the normal distribution as long as they fall into the critical bounds (in this case with 95% confidence). Comparison of the normal and Weibull distribution when some residual is left, may give an indication that it does not follow the assumption of uniformity.

7.3.2 Lack of metabolites in the basis set

We study the effect of the number of metabolites used for quantification as this may also cause over- or underestimation. Fig. 7.5 shows the results for the 1.5 T and 9.4 T signals when using a complete and incomplete basis set of metabolites. For the 1.5 T signal we considered 3 groups of metabolite profiles:

- (a) all 13 metabolites (Ala, Asp, Cho, Cr, GABA, Glc, Gln, Glu, Lac, m-Ins, NAA, Tau),
- (b) the 6 most relevant metabolites having a high concentration in normal brain (Cho, Cr, Gln, Glu, m-Ins, NAA),
- (c) the 4 most relevant metabolites having the highest concentration (Cho, Cr, Glu, NAA).

For the 9.4 T signal we also considered 3 groups of metabolite profiles:

- (a) all 14 metabolites (Ala, Asp, Cr, GABA, GPC, GSH, Glc, Gln, Glu, Lac, m-Ins, NAA, PE, Tau),

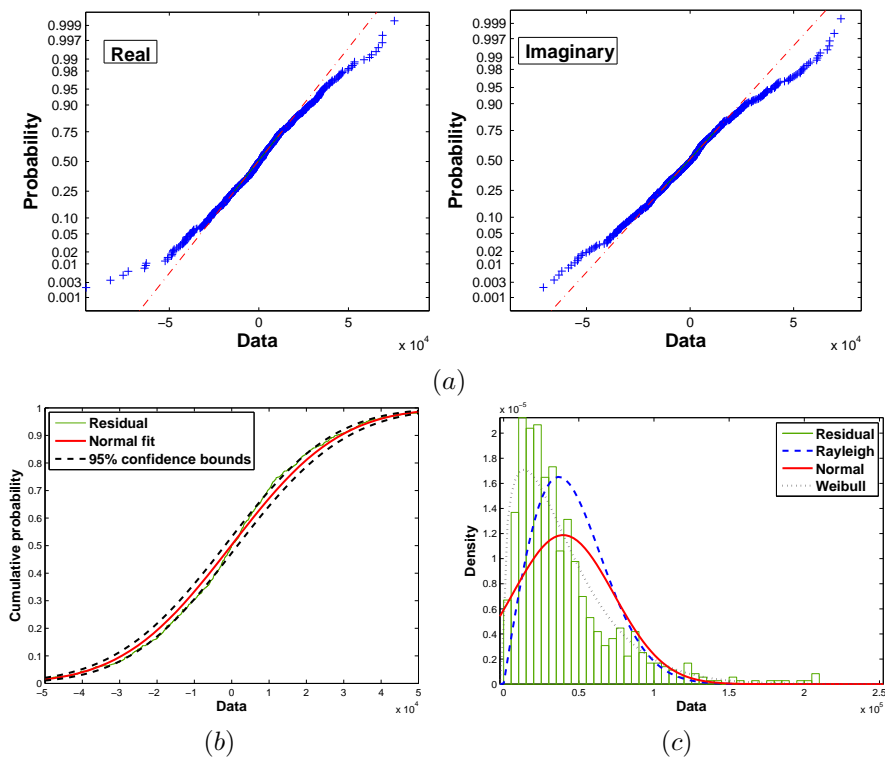


Figure 7.4: Normality plots of residual for the signal at 9.4 T. (a) Normal probability plot shows the distribution of the residual related to the normal distribution (left: real part, right: imaginary part) and (b) Cumulative distribution function plot with 95% confidence bounds, both using a damping factor constraint of 0.05 (good bound). (c) Distribution plots of the absolute value of the complex residual using a small bound of 0.025.

- (b) the 8 more relevant metabolites having a high concentration (Cr, GPC, GSH, Gln, Glu, m-Ins, NAA, PE),
- (c) the 4 most relevant metabolites having the highest concentration (Cr, GPC, Glu, NAA).

Each basis set is extended with the corresponding MM signal. The lack of some metabolites in the basis set leads to a slight under- or overestimation of some other metabolites, which is also reflected in the residual. Amplitude estimates in Fig. 7.5 show the variability of results obtained using different number of metabolites. A direct comparison with the literature is complicated because estimated amplitudes are highly affected by individual conditions of the tissues, small differences in the

measurement parameters, size of the voxel measured, etc., and therefore, diverse concentration ranges are found in similar studies, leading to a high variability of the amplitude estimates.

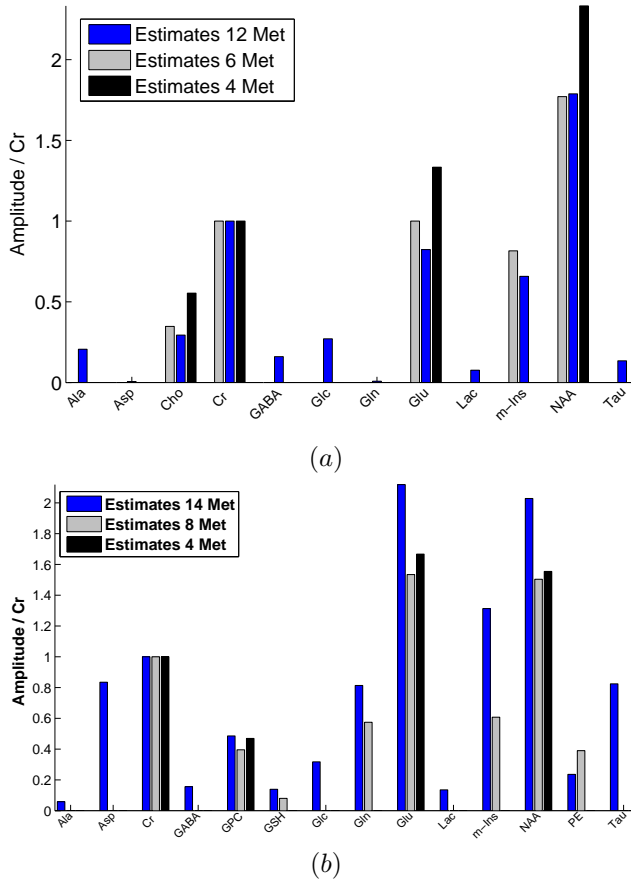


Figure 7.5: Amplitude estimates and comparison using a complete and incomplete basis set. (a) Comparison of amplitude estimates relative to Cr for the 1.5 T signal using 12, 6 and 4 metabolites. (b) Comparison of amplitude estimates relative to Cr for the 9.4 T signal using 14, 8 and 4 metabolites.

Identifying whether a metabolite is missing in the basis set is a difficult assessment. However, considering the main metabolites (not too many) known to be observable at specific magnetic fields is a good approach; consequently, if specific patterns are observed in the residual, the inclusion of additional metabolites is recommended. In general, there are difficulties when fitting metabolites whenever they have low concentrations or are highly overlapping with the baseline. This is the case for

Ala, Asp, Lac, GABA and Tau. Furthermore, the resonances of Glu and Gln are very similar to each other, and especially at low magnetic fields they can hardly be estimated separately. Therefore, during quantification one of them may fit the region that corresponds to both of them. In this case, the inclusion of *prior* knowledge to separate their contributions may be beneficial. If the disease studied is not influenced by their individual contributions, a common strategy is to sum their amplitude estimates, also known as the contribution of Glx (Glu+Gln). In Fig. 7.6 (a) and 7.7 (a) we observe that the fits with an incomplete basis set are not good and the corresponding Q_{fit} of 7.4472 (for the 1.5 T signal) and 5.1740 (for the 9.4 T signal) also confirm the imperfect quantification. In order to further evaluate the quantification, we selected a span or window of 0.1 ppm to evaluate the quality factor in a moving approach. In Fig. 7.6 (b) and 7.7 (b) we present the results of this quality measure where the plotted curves represent the Q_{fit} values obtained for all the selected frequency intervals and the dashed line represents the confidence bound calculated as three times the standard deviation ($\frac{R^2}{N} > (3\sigma)^2$). A missing metabolite is considered when the Q_{fit} value is higher than the selected threshold.

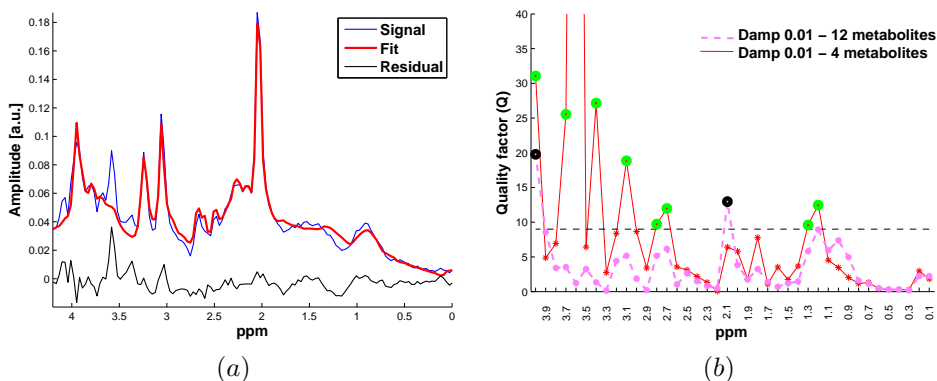


Figure 7.6: Quantification results together with the Quality factor (Q) for the signal acquired at 1.5 T using an incomplete basis set of metabolites. (a) Fit using a basis set with 4 metabolites (the fit using 12 metabolites is shown in Fig. 7.3 (a)). (b) Quality factor plot for the signal using a complete and incomplete basis set (12 and 4 metabolites). The quality factor computed for the signals was 2.1207 and 7.4472 respectively.

In spite of the good fits using the full basis set of metabolites, Q factor results shown in Fig. 7.6 (b) and 7.7 (b) suggest that particularly the peaks of Cr near 3.9 ppm are not well fitted which may be explained by a strong influence of the suppressed water. On the other hand, results considering the incomplete basis set of metabolites show that metabolites in the region between 3.5 and 3.7 ppm are missing which correspond mainly to resonances of m-Ins and Gln. Particularly for the signal at 1.5 T, there is an imperfect match between the MM signal and the *in*

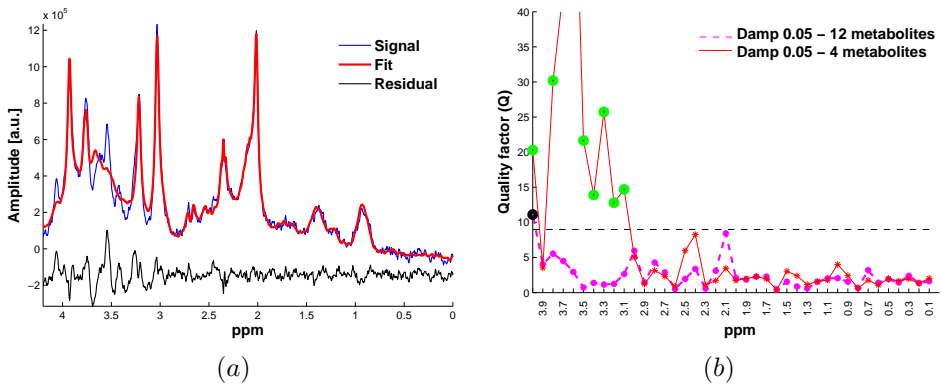


Figure 7.7: Quantification results together with the Quality factor (Q) for the signal at 9.4 T using an incomplete basis set of metabolites. (a) Fit using a basis set with 4 metabolites (the fit using 12 metabolites is shown in Fig. 7.3 (b)). (b) Quality factor plot for the signal using a complete and incomplete basis set (14 and 4 metabolites). The quality factor computed for the signals was 1.4033 and 5.1740 respectively.

in vivo signal at 0.9 ppm which can be seen in Fig.7.6 (b) where the quality measure is close or higher than 9.

7.4 Conclusions

Reliable metabolite estimation of *in vivo* MRS signals for determination of metabolite concentrations is of paramount importance for obtaining additional information in the diagnostics of cancer and metabolic diseases. Therefore, quantification of MRS signals was performed evaluating the influence of the damping factor constraint and the number of components used in the metabolite basis set. We observed in particular, that the damping factor in the quantification method AQSES plays an important role for the amplitude estimates.

From the quantification results, we examined the residual and analyzed the fit of the individual components which are sensible to quantification constraints. Moreover, the selection of the metabolites for the basis set is important for quantification, thus an incomplete basis set will provide fits where one metabolite fits the region that corresponds to its neighbour. Finally, the residual is used to determine the goodness of the estimates and it is assumed that a good estimate leads to residuals resembling pure white noise.

Chapter 8

Summary and further research

This final chapter presents a short summary and contributions of this thesis. Additionally, further perspectives towards the improvement of quantification of MRS(I) signals are also outlined.

8.1 Summary

- Chapter 1 outlines the main acquisition parameters for MRS(I) data and the biochemical features involved in the diagnosis of different cancer and metabolite diseases. In order to reliably obtain these metabolites, it is essential to preprocess and quantify MRS(I) signals and apply different correction/estimation methods. Some of these methods, which are partially improved in this thesis, are presented in the subsequent chapters.
- In chapter 2 we describe the main preprocessing methods used in this thesis and the major problems faced before quantification.
- The quantification methods presented in chapter 3 are meant to introduce the main parameters to be considered before quantification, such as filtering of unwanted peaks, setting the damping and frequency constraints, defining the baseline estimation method, estimating the lineshape and finally including *prior* knowledge for improving the metabolite estimates. Special attention is given to the metabolite basis set and its acquisition *in vitro* or its quantum mechanical simulation. Finally, it is emphasized that it is essential to consider all quantification parameters in order to avoid mis-quantification.
- The importance of filtering unwanted peaks was outlined in chapter 4. Here, we focused on the water and reference peaks filtering, based on HSVD

methods and illustrated with several examples the variation of filtering performance when using different available methods. In particular, HLSVD-PRO is used for filtering these unwanted peaks and special attention is drawn to the selection of the model order to be used in this method.

- Chapter 5 describes AQSES Lineshape, a lineshape estimation method to determine the actual lineshape of distorted MRS signals. This method is evaluated in simulated, *in vitro* and *in vivo* signals. The advantage of this method is that it does not require the use of a reference signal and can be used for signals originated from other nuclei than ^1H .
- In chapter 6 we propose a method to estimate the macromolecular baseline making use of a series of *in vivo* inversion recovery acquisitions to obtain *prior* knowledge of single macromolecule and lipid components. Here, a basis set of macromolecule and lipid resonances is created, and further included in the basis set of metabolites used for quantification. This method allows the inclusion of *prior* knowledge between individual peaks and allows the possibility to adjust the frequency, damping and phase of individual components. Experiments based on *in vivo* MRS signals showed satisfactory results in the sense that the mathematical modelling of the baseline could replace the time consuming inversion recovery acquisition of the macromolecules and lipids.
- Finally, chapter 7 focused on the analysis of the quantification results, more specifically, the residual obtained after quantification. Quantification results need to be analyzed, and basically the residual provides some indication of how well the fitting was done. Although quantification results are usually analyzed considering the Cramér-Rao Lower bounds, a further residual analysis may provide an indication of the quality of the fit. Therefore, some statistical tools together with a quality factor are used to evaluate the results considering different metabolites in the basis set and varying the damping factor constraint of the quantification method.

8.2 Future work and open problems

Additional work on the improvement, evaluation and automation of quantification of MRS signals is necessary in order to increase the use of MRS as a diagnosis technique.

- Lineshape. Different lineshape estimation methods have been described in chapter 5 and it has been proved that for ^1H a more realistic lineshape can be obtained. Additionally, the lineshape estimation method presented in this thesis has been implemented in the quantification method AQSES, which

quantifies short TE ^1H MRS signals. Moreover, the lineshape estimation may be beneficial for other quantification methods, such as AMARES, where spectra from other nuclei can be quantified.

Further evaluation of the lineshape estimation algorithm is being performed in ^1H MRS of lipid voxels (adipous tissue), using a set of individual simulated lipids for quantification. Until now HLSVD, AQSES, QUEST and LCModel have been used to quantify these lineshape distorted data, nevertheless, successful results have been only obtained with the latest version of the LCModel quantification package. However, initial AQSES Lineshape results are satisfactory, thus a deeper quantification analysis will be performed.

- It would be very interesting to perform a comparison of different lineshape estimation methods (*i.e.*, LCModel [141], the frequency domain fitting method using time domain models and *prior* knowledge proposed by Slotboom *et al.* [158], the semi-parametric estimation method without searching in function space proposed by Popa *et al.* [133], QUALITY [34], QUECC [6] and the proposed AQSES Lineshape algorithm presented in chapter 5) on a large benchmark of simulated, *in vitro* and *in vivo* signals of different nuclei, measured at different magnetic fields and acquisition conditions.
- Baseline. Chapter 6 described an alternative method to estimate the baseline based on *prior* knowledge from *in vivo* signals of healthy mice, however, although the presented method is capable to handle any kind of MR signals, a complementary study based on the validation of the method considering different kind of baseline distorted signals (*e.g.*, from different pathologies) is also interesting.

Additional quantification of ^1H MRS signals obtained from Parkinson's disease mice will be performed to evaluate first the metabolic differences between the control and disease mice and secondly, to further evaluate the baseline approach presented in chapter 6.

- *Prior* knowledge. In order to improve the accuracy of metabolite estimates, it will be beneficial to include more *prior* knowledge in the quantification method. This *prior* knowledge could, for instance, proceed from typical relations between individual metabolites obtained from different kinds of tissues.
- An interesting extension of the lineshape and baseline estimation methods is to incorporate spatial information to 2D (as published in [28]) and 3D MRSI data. This will be beneficial for the automation of spectral analysis in the MR unit. Here, it is important to consider *prior* information from the region analyzed and to impose additional constraints in the quantification method, such as similarities between the lineshape and baseline of neighboring voxels.

Such constraints are expected to lead to more robust quantification results in the case of very noisy MRSI data sets.

- Implementation of the lineshape and baseline estimation methods in the jMRUI software package is foreseen and may bring advantages in the quantification of MRS data, especially with lineshape distortions.

Finally, the automation of these techniques is essential for the acceptance of MRS in the clinical practice. Therefore, numerous evaluations of the presented approaches on MRS measurements from different diseases is required.

Bibliography

- [1] A. Abragam. *Principles of nuclear magnetism*. Oxford University Press Inc., 1961.
- [2] J-P. Antoine, A. Coron, and J-M. Dereppe. Water peak suppression: Time-frequency vs time-scale approach. *Journal of Magnetic Resonance*, 144(2):189 – 194, 2000.
- [3] R. Badeau, B. David, and G. Richard. Selecting the modeling order for the esprit high resolution method: an alternative approach. In *Acoustics, Speech, and Signal Processing, 2004. Proceedings. (ICASSP '04). IEEE International Conference on*, volume 2, pages ii – 1025–8 vol.2, May 2004.
- [4] H. Barkhuijsen, R. de Beer, and D. van Ormondt. Improved algorithm for noniterative time-domain model fitting to exponentially damped magnetic resonance signals. *Journal of Magnetic Resonance*, 73(3):553 – 557, 1987.
- [5] R. Bartha, D. J. Drost, and P. C. Williamson. Factors affecting the quantification of short echo *in vivo* ^1H MR spectra: prior knowledge, peak elimination, and filtering. *NMR in Biomedicine*, 12(4):205–216, 1999.
- [6] R. Bartha, D.J. Drost, R.S. Menon, and P.C. Williamson. Spectroscopic lineshape correction by QUECC: Combined QUALITY deconvolution and eddy current correction. *Magnetic Resonance in Medicine*, 44(4):641–645, 2000.
- [7] K. L. Behar and T. Ogino. Characterization of macromolecule resonances in the ^1H NMR spectrum of rat brain. *Magnetic Resonance in Medicine*, 30(1):38–44, 1993.
- [8] D. Belkić. Exact quantification of time signals in padé-based Magnetic Resonance Spectroscopy. *Physics in Medicine and Biology*, 51(10):2633, 2006.
- [9] D. Belkić and K. Belkić. *In vivo* Magnetic Resonance Spectroscopy by the fast Padé transform. *Physics in Medicine and Biology*, 51(5):1049, 2006.

- [10] H. Bhat, B. R. Sajja, and P. A. Narayana. Fast quantification of proton Magnetic Resonance Spectroscopic Imaging with artificial neural networks. *Journal of Magnetic Resonance*, 183(1):110 – 122, 2006.
- [11] A. M. Blamire, D. L. Rothman, and T. Nixon. Dynamic shim updating: A new approach towards optimized whole brain shimming. *Magnetic Resonance in Medicine*, 36(1):159–165, 1996.
- [12] P. A. Bottomley. Selective volume method for performing localized NMR spectroscopy. in *U.S patent*, (4 480 228), 1984.
- [13] T. R. Brown and R. Stoyanova. NMR Spectral Quantitation by Principal Component Analysis. II.Determination of frequency and phase shifts. *Journal of Magnetic Resonance, Series B*, 112(1):32 – 43, 1996.
- [14] E. Cabanes, S. Confort-Gouny, Y. Le Fur, G. Simond, and P. J. Cozzone. Optimization of residual water signal removal by HLSVD on simulated short echo time proton MR spectra of the human brain. *Journal of Magnetic Resonance*, 150(2):116 – 125, 2001.
- [15] V. Callot, D. Galanaud, Y. Le Fur, S. Confort-Gouny, J-P Ranjeva, and P. J. Cozzone. ^1H MR Spectroscopy of human brain tumours: a practical approach. *European Journal of Radiology*, 67(2):268 – 274, 2008. Clinical ^1H MR Spectroscopy.
- [16] S. Cavassila, S. Deval, C. Huegen, D. van Ormondt, and D. Graveron-Demilly. The beneficial influence of *Prior Knowledge* on the quantitation of *In vivo* Magnetic Resonance Spectroscopy signals. *Investigative Radiology*, 34:242–246, 1999.
- [17] S. Cavassila, S. Deval, C. Huegen, D. van Ormondt, and D. Graveron-Demilly. Cramér-Rao bound expressions for parametric estimation of overlapping peaks: Influence of *Prior Knowledge*. *Journal of Magnetic Resonance*, 143(2):311 – 320, 2000.
- [18] S. Cavassila, S. Deval, C. Huegen, D. van Ormondt, and D. Graveron-Demilly. Cramér-Rao bounds: an evaluation tool for quantitation. *NMR in Biomedicine*, 14(4):278–283, 2001.
- [19] D. Chang, C. D. Banack, and S. L. Shah. Robust baseline correction algorithm for signal dense NMR spectra. *Journal of Magnetic Resonance*, 187(2):288 – 292, 2007.
- [20] H. Chen, S. Van Huffel, D. van Ormondt, and R. de Beer. Parameter estimation with *Prior Knowledge* of known signal poles for the quantification of NMR spectroscopy data in the time domain. *Journal of Magnetic Resonance, Series A*, 119(2):225 – 234, 1996.

- [21] J-H. Chen, E. B. Sambol, P. T. Kennealey, R. B. O'Connor, P. L. DeCarolis, D. G. Cory, and S. Singer. Water suppression without signal loss in HR-MAS ^1H NMR of cells and tissues. *Journal of Magnetic Resonance*, 171(1):143 – 150, 2004.
- [22] L. Chen, Z. Weng, L. Goh, and M. Garland. An efficient algorithm for automatic phase correction of NMR spectra based on entropy minimization -ACME. *Journal of Magnetic Resonance*, 158(1-2):164 – 168, 2002.
- [23] Y. Chen, F. Zhang, and R. Brüschweiler. Residual water suppression by indirect covariance NMR. *Magnetic Resonance in Chemistry*, 45(11):925–928, 2007.
- [24] W. S. Cleveland. Robust locally weighted regression and smoothing scatterplots. *Journal of the American Statistical Association*, 74(368):pp. 829–836, 1979.
- [25] J. C. Cobas, M. A. Bernstein, M. Martín-Pastor, and P. García Tahoces. A new general-purpose fully automatic baseline-correction procedure for 1D and 2D NMR data. *Journal of Magnetic Resonance*, 183(1):145 – 151, 2006.
- [26] J. C. Cobas and F. J. Sardina. Nuclear Magnetic Resonance data processing. MestRe-C: A software package for desktop computers. *Concepts in Magnetic Resonance Part A*, 19A(2):80–96, 2003.
- [27] A. Coron, L. Vanhamme, J-P. Antoine, P. Van Hecke, and S. Van Huffel. The filtering approach to solvent peak suppression in MRS: A critical review. *Journal of Magnetic Resonance*, 152(1):26 – 40, 2001.
- [28] Anca R. Croitor Sava, Diana M. Sima, Jean-Baptiste Poulet, Alan J. Wright, Arend Heerschap, and Sabine Van Huffel. Exploiting spatial information to estimate metabolite levels in two-dimensional mrsi of heterogeneous brain lesions. *NMR in Biomedicine*, 24(7):824–835, 2011.
- [29] C. Cudalbu, O. Beuf, and S. Cavassila. *In vivo* short echo time localized ^1H MRS of the rat brain at 7 T: Influence of two strategies of background-accommodation on the metabolite concentration estimation using QUEST. *Journal of Signal Processing Systems*, 55:25–34, 2009. 10.1007/s11265-008-0187-5.
- [30] C. Cudalbu, A. Bucur, D. Graveron-Demilly, O. Beuf, and S. Cavassila. Comparison of two strategies of background-accommodation: Influence on the metabolite concentration estimation from *in vivo* magnetic resonance spectroscopy data. In *Engineering in Medicine and Biology Society, 2007. EMBS 2007. 29th Annual International Conference of the IEEE*, pages 2077–2080, 2007.

- [31] C. Cudalbu, S. Cavassila, H. Rabeson, D. van Ormondt, and D. Graveron-Demilly. Influence of measured and simulated basis sets on metabolite concentration estimates. *NMR in Biomedicine*, 21(6):627–636, 2008.
- [32] C. Cudalbu, B. Lanz, J. M. Duarte, N. Kunz, and R. Gruetter. Impact of the *prior knowledge* on the quantification of *in vivo* ^{13}C spectra using two different algorithms: LCMoDel and AMARES. In *Proc. of the 19th International Society of Magnetic Resonance in Medicine - ISMRM 2011*, May 2011.
- [33] C. Cudalbu, V. Mlynárik, L. Xin, and R. Gruetter. Quantification of *in vivo* short echo-time proton magnetic resonance spectra at 14.1 T using two different approaches of modelling the macromolecule spectrum. *Measurement Science and Technology*, 20(10):104034 (7pp), 2009.
- [34] A. A. de Graaf, J. E. van Dijk, and W. M. Bovée. Quality: quantification improvement by converting lineshapes to the lorentzian type. *Magnetic Resonance in Medicine*, 13(3):343–357, 1990.
- [35] R. de Graaf. *In vivo NMR Spectroscopy Principles and Techniques*. Wiley: Chichester, 1998.
- [36] B. De Neuter, J. Luts, Vanhamme L., P. Lemmerling, and S. Van Huffel. Java-based framework for processing and displaying short-echo-time Magnetic Resonance Spectroscopy signals. *Computer Methods and Programs in Biomedicine*, 85:129–137, February 2007.
- [37] S. De Sanctis, W. M. Malloni, W. Kremer, A. M. Tomé, E. W. Lang, K-P. Neidig, and H. R. Kalbitzer. Singular spectrum analysis for an automated solvent artifact removal and baseline correction of 1D NMR spectra. *Journal of Magnetic Resonance*, 210(2):177 – 183, 2011.
- [38] D. K. Deelchand, P-F. Van de Moortele, G. Adriany, I. Iltis, P. Andersen, J. P. Strupp, J. T. Vaughan, K. Uğurbil, and P-G. Henry. *In vivo* ^1H NMR spectroscopy of the human brain at 9.4 T: Initial results. *Journal of Magnetic Resonance*, 206(1):74 – 80, 2010.
- [39] M. Dezortova and M. Hajek. ^1H MR Spectroscopy in pediatrics. *European Journal of Radiology*, 67(2):240 – 249, 2008. Clinical ^1H MR Spectroscopy.
- [40] I. Dologlou, S. Van Huffel, and D. Van Ormondt. Frequency-selective MRS data quantification with frequency *Prior Knowledge*. *Journal of Magnetic Resonance*, 130(2):238 – 243, 1998.
- [41] Z. Dong, W. Dreher, and D. Leibfritz. Toward quantitative short-echo-time *in vivo* proton MR spectroscopy without water suppression. *Magnetic Resonance in Medicine*, 55(6):1441–1446, 2006.

- [42] Z. Dong and B. S. Peterson. Spectral resolution amelioration by deconvolution (SPREAD) in MR Spectroscopic Imaging. *Journal of Magnetic Resonance Imaging*, 29(6):1395–1405, 2009.
- [43] A. J. Dwyer, J. A. Frank, V. J. Sank, J. W. Reinig, A. M. Hickey, and J. L. Doppman. Short-TI inversion-recovery pulse sequence: analysis and initial experience in cancer imaging. *Radiology*, 168(3):827–836, 1988.
- [44] P. H. C. Eilers, D. M. Rijnmond, and B. D. Marx. Flexible smoothing with b-splines and penalties. *Statistical Science*, 11:89–121, 1996.
- [45] C. Elster, F. Schubert, A. Link, M. Walzel, F. Seifert, and H. Rinneberg. Quantitative Magnetic Resonance Spectroscopy: Semi-parametric modeling and determination of uncertainties. *Magnetic Resonance in Medicine*, 53(6):1288–1296, 2005.
- [46] T. Ernst and L. Chang. Elimination of artifacts in short echo time ^1H MR Spectroscopy of the frontal lobe. *Magnetic Resonance in Medicine*, 36(3):462–468, 1996.
- [47] T. Ernst and J. Hennig. Improved water suppression for localized *in vivo* ^1H Spectroscopy. *Journal of Magnetic Resonance, Series B*, 106(2):181 – 186, 1995.
- [48] J. Frahm, K-D. Merboldt, and W. Hänicke. Localized proton spectroscopy using stimulated echoes. *Journal of Magnetic Resonance (1969)*, 72(3):502 – 508, 1987.
- [49] B. D. Frederick, I. K. Lyoo, A. Satlin, K. H. Ahn, M. J. Kim, D. A. Yurgelun-Todd, B. M. Cohen, and P. F. Renshaw. *In vivo* proton Magnetic Resonance Spectroscopy of the temporal lobe in Alzheimer’s disease. *Progress in Neuro-Psychopharmacology and Biological Psychiatry*, 28(8):1313 – 1322, 2004.
- [50] E. Fuster-Garcia, C. Navarro, J. Vicente, S. Tortajada, J. García-Gómez, C. Sáez, J. Calvar, J. Griffiths, M. Julià-Sapé, F. Howe, J. Pujol, A. Peet, A. Heerschap, A. Moreno-Torres, M. Martínez-Bisbal, B. Martínez-Granados, P. Wesseling, W. Semmler, J. Capellades, C. Majós, A. Alberich-Bayarri, A. Capdevila, D. Monleón, L. MartíBonmatí, C. Arús, B. Celda, and M. Robles. Compatibility between 3 T ^1H SV-MRS data and automatic brain tumour diagnosis support systems based on databases of 1.5 T ^1H SV-MRS spectra. *Magnetic Resonance Materials in Physics, Biology and Medicine*, 24:35–42, 2011. 10.1007/s10334-010-0241-8.
- [51] R. E. Gabr, R.d Ouwkerk, and P. A. Bottomley. Quantifying *in vivo* MR spectra with circles. *Journal of Magnetic Resonance*, 179(1):152 – 163, 2006.

- [52] G. F. Giskeødegård, T. G. Bloemberg, G. Postma, B. Sitter, M-B. Tessem, I. S. Gribbestad, T. F. Bathen, and L. M.C. Buydens. Alignment of high resolution magic angle spinning magnetic resonance spectra using warping methods. *Analytica Chimica Acta*, 683(1):1 – 11, 2010.
- [53] J. M. Gledhill and A. J. Wand. Phasing arbitrarily sampled multidimensional NMR data. *Journal of Magnetic Resonance*, 187(2):363 – 370, 2007.
- [54] S. Golotvin and A. Williams. Improved baseline recognition and modeling of FT NMR spectra. *Journal of Magnetic Resonance*, 146(1):122 – 125, 2000.
- [55] M. Gottschalk, L. Lamalle, and C. Segebarth. Short-TE localised ^1H MRS of the human brain at 3 T: quantification of the metabolite signals using two approaches to account for macromolecular signal contributions. *NMR in Biomedicine*, 21(5):507–517, 2008.
- [56] V. Govindaraju, K. Young, and A. A. Maudsley. Proton NMR chemical shifts and coupling constants for brain metabolites. *NMR in Biomedicine*, 13(3):129–153, 2000.
- [57] H. Grage and M. Akke. A statistical analysis of NMR spectrometer noise. *Journal of Magnetic Resonance*, 162(1):176 – 188, 2003.
- [58] D. Graveron-Demilly, A. Diop, A. Briguet, and B. Fenet. Product-operator algebra for strongly coupled spin systems. *J. Magn. Reson.*, A101(3):233–239, 1993.
- [59] R. Gruetter. Automatic localized *in vivo* adjustment of all first- and second-order shim coils. *Magnetic Resonance in Medicine*, 29(6):804–811, 1993.
- [60] R. Gruetter, S. A. Weisdorf, V. Rajanayagan, M. Terpstra, H. Merkle, C. L. Truwit, M. Garwood, S. L. Nyberg, and K. Uğurbil. Resolution improvements in *in vivo* ^1H NMR spectra with increased magnetic field strength. *Journal of Magnetic Resonance*, 135(1):260 – 264, 1998.
- [61] P. Güntert and K. Wüthrich. FLATT-a new procedure for high-quality baseline correction of multidimensional NMR spectra. *Journal of Magnetic Resonance*, 96(2):403 – 407, 1992.
- [62] U. L. Günther, C. Ludwig, and H. Rüterjans. WAVEWAT–improved solvent suppression in NMR spectra employing wavelet transforms. *Journal of Magnetic Resonance*, 156(1):19 – 25, 2002.
- [63] Y. Guo, S. Ruan, J. Landré, and J. M. Constans. A sparse representation method for Magnetic Resonance Spectroscopy quantification. *Biomedical Engineering, IEEE Transactions on*, 57(7):1620 –1627, 2010.

- [64] M. Hajek, M. Dezortova, and P. Krsek. ^1H MR spectroscopy in epilepsy. *European Journal of Radiology*, 67(2):258 – 267, 2008. Clinical ^1H MR Spectroscopy.
- [65] G. Helms. The principles of quantification applied to *in vivo* proton MR Spectroscopy. *European Journal of Radiology*, 67(2):218 – 229, 2008. Clinical ^1H MR Spectroscopy.
- [66] Y. Hiltunen, J. Kaartinen, J. Pulkkinen, A-M. Häkkinen, N. Lundbom, and R. A. Kauppinen. Quantification of human brain metabolites from *in vivo* ^1H NMR magnitude spectra using automated artificial neural network analysis. *Journal of Magnetic Resonance*, 154(1):1 – 5, 2002.
- [67] L. Hofmann, J. Slotboom, C. Boesch, and R. Kreis. Characterization of the macromolecule baseline in localized ^1H -MR spectra of human brain. *Magnetic Resonance in Medicine*, 46(5):855–863, 2001.
- [68] J. P. Hornak. *The basics of NMR*. Online textbook, 2002. <http://www.cis.rit.edu/htbooks/nmr/>.
- [69] S.-L. J. Hu, X. Bao, and H. Li. Model order determination and noise removal for modal parameter estimation. *Mechanical Systems and Signal Processing*, 24(6):1605 – 1620, 2010.
- [70] W. Huang, G. E. Alexander, E. M. Daly, H. U. Shetty, J. S. Krasuski, S. I. Rapoport, and M. B. Schapiro. High brain myo-inositol levels in the predementia phase of Alzheimer’s disease in adults with Down’s syndrome: A ^1H MRS study. *Am J. Psychiatry*, 156(12):1879–1886, 1999.
- [71] J-H. Hwang, G. D. Graham, K. L. Behar, J. R. Alger, J. W. Prichard, and D. L. Rothman. Short echo time proton Magnetic Resonance Spectroscopic Imaging of macromolecule and metabolite signal intensities in the human brain. *Magnetic Resonance in Medicine*, 35(5):633–639, 1996.
- [72] J. F. A. Jansen, W. H. Backes, K. Nicolay, and M. E. Kooi. ^1H MR spectroscopy of the brain: Absolute quantification of metabolites. *Radiology*, 240(2):318–332, August 2006.
- [73] F. Jiru. Introduction to post-processing techniques. *European journal of radiology*, 67(2):202–217, 2008.
- [74] C. Juchem, B. Muller-Bierl, F. Schick, N. K. Logothetis, and J. Pfeuffer. Combined passive and active shimming for *in vivo* MR spectroscopy at high magnetic fields. *J. Magn. Reson.*, 183(2):278 – 289, 2006.
- [75] C. Juchem, T. W. Nixon, S. McIntyre, D. L. Rothman, and R. A. de Graaf. Magnetic field homogenization of the human prefrontal cortex with a set of localized electrical coils. *Magn. Reson. Med.*, 63(1):171–180, 2010.

- [76] M. Kanowski, J. Kaufmann, J. Braun, J. Bernarding, and C. Tempelmann. Quantitation of simulated short echo time ^1H human brain spectra by LCModel and AMARES. *Magnetic Resonance in Medicine*, 51(5):904–912, 2004.
- [77] K. Kazimierczuk, A. Zawadzka, W. Koźmiński, and I. Zhukov. Lineshapes and artifacts in multidimensional Fourier transform of arbitrary sampled NMR data sets. *Journal of Magnetic Resonance*, 188(2):344 – 356, 2007.
- [78] B. M. Kelm, F. O. Kaster, A. Henning, M-A. Weber, P. Bachert, P. Boesiger, F. A. Hamprecht, and B. H. Menze. Using spatial *prior knowledge* in the spectral fitting of MRS images. *NMR in Biomedicine*, 2011.
- [79] U. Klose. *In vivo* proton spectroscopy in presence of eddy currents. *Magnetic Resonance in Medicine*, 14(1):26 – 30, 1990.
- [80] U. Klose. Measurement sequences for single voxel proton MR Spectroscopy. *European Journal of Radiology*, 67(2):194 – 201, 2008. Clinical ^1H MR Spectroscopy.
- [81] J. Knight-Scott. Application of multiple inversion recovery for suppression of macromolecule resonances in short echo time ^1H NMR spectroscopy of human brain. *Journal of Magnetic Resonance*, 140(1):228 – 234, 1999.
- [82] K. M. Koch, L. I. Sacolick, T. W. Nixon, S. McIntyre, D. L. Rothman, and R. A. de Graaf. Dynamically shimmed multivoxel ^1H Magnetic Resonance Spectroscopy and multislice magnetic resonance spectroscopic imaging of the human brain. *Magnetic Resonance in Medicine*, 57(3):587–591, 2007.
- [83] R. Kreis. Issues of spectral quality in clinical ^1H -Magnetic Resonance Spectroscopy and a gallery of artifacts. *NMR in Biomedicine*, 17(6):361–381, 2004.
- [84] R. Kreis, T. Ernst, and B. D. Ross. Absolute quantitation of water and metabolites in the human brain. II. Metabolite concentrations. *Journal of Magnetic Resonance, Series B*, 102(1):9 – 19, 1993.
- [85] R. Kreis, J. Slotboom, L. Hofmann, and C. Boesch. Integrated data acquisition and processing to determine metabolite contents, relaxation times, and macromolecule baseline in single examinations of individual subjects. *Magnetic Resonance in Medicine*, 54(4):761–768, 2005.
- [86] R. Kumaresan and D. Tufts. Estimating the parameters of exponentially damped sinusoids and pole-zero modeling in noise. *Acoustics, Speech and Signal Processing, IEEE Transactions on*, 30(6):833 – 840, December 1982.
- [87] S. Y. Kung, K. S. Arun, and D. V. Bhaskar Rao. State-space and singular-value decomposition-based approximation methods for the harmonic retrieval problem. *J. Opt. Soc. Am.*, 73(12):1799–1811, Dec 1983.

- [88] N. Kunz, C. Cudalbu, V. Mlynárik, P. S. Hüppi, S. V. Sizonenko, and R. Gruetter. Diffusion-weighted spectroscopy: A novel approach to determine macromolecule resonances in short-echo time ^1H -MRS. *Magnetic Resonance in Medicine*, 64(4):939–946, 2010.
- [89] M. Ladisa, A. Lamura, T. Laudadio, and G. Nico. Application of the HLSVD technique to the filtering of X-ray diffraction data. *EURASIP Journal on Advances in Signal Processing*, 2007:65–65, January 2007.
- [90] T. Laudadio, N. Mastronardi, L. Vanhamme, P. Van Hecke, and S. Van Huffel. Improved Lanczos algorithms for blackbox MRS data quantitation. *Journal of Magnetic Resonance*, 157(2):292 – 297, 2002.
- [91] T. Laudadio, Y. Selén, L. Vanhamme, P. Stoica, P. Van Hecke, and S. Van Huffel. Subspace-based MRS data quantitation of multiplets using *prior knowledge*. *Journal of Magnetic Resonance*, 168(1):53 – 65, 2004.
- [92] A. Lazarev, A-R. Allouche, M. Aubert-Frécon, F. Fauvelle, K. Elbayed, M. Piotto, I. J. Namer, D. van Ormondt, and D. Graveron-Demilly. Optimization of metabolite basis-sets prior to quantitation: a quantum mechanics approach. In *Proc. of the 19th International Society of Magnetic Resonance in Medicine - ISMRM 2011*, May 2011.
- [93] G-C. Lee and D. L. Woodruff. Beam search for peak alignment of NMR signals. *Analytica Chimica Acta*, 513(2):413 – 416, 2004.
- [94] J. S. Lee and D. D. Cox. Robust smoothing: Smoothing parameter selection and applications to fluorescence spectroscopy. *Computational Statistics & Data Analysis*, 54(12):3131 – 3143, 2010.
- [95] B. S. Li, H. Wang, and O. Gonen. Metabolite ratios to assumed stable creatine level may confound the quantification of proton brain MR Spectroscopy. *Magnetic Resonance Imaging*, 21(8):923 – 928, 2003.
- [96] Y-Y. Lin, P. Hodgkinson, M. Ernst, and A. Pines. A novel detection-estimation scheme for noisy NMR signals: Applications to delayed acquisition data. *Journal of Magnetic Resonance*, 128(1):30 – 41, 1997.
- [97] L. Ljung. *System Identification: Theory for the User*. Prentice-Hall, 1987.
- [98] J. Luts, A. Heerschap, J. Suykens, and S. Van Huffel. A combined MRI and MRSI based multiclass system for brain tumour recognition using LS-SVMs with class probabilities and feature selection. *Artificial Intelligence in Medicine*, 40(2):87 – 102, 2007.
- [99] J. Machann, N. Stefan, and F. Schick. ^1H MR spectroscopy of skeletal muscle, liver and bone marrow. *European Journal of Radiology*, 67(2):275 – 284, 2008. Clinical ^1H MR Spectroscopy.

- [100] I. Mader, S. Rauer, P. Gall, and U. Klose. ^1H MR spectroscopy of inflammation, infection and ischemia of the brain. *European Journal of Radiology*, 67(2):250 – 257, 2008. Clinical ^1H MR Spectroscopy.
- [101] A. M. Mans, M. R. DeJoseph, and R. A. Hawkins. Metabolic abnormalities and grade of encephalopathy in acute hepatic failure. *Journal of Neurochemistry*, 63(5):1829–1838, 1994.
- [102] D. Marion, M. Ikura, and A. Bax. Improved solvent suppression in one and two-dimensional NMR spectra by convolution of time-domain data. *Journal of Magnetic Resonance*, (84):425 – 430, 1989.
- [103] M. Marjanska, G. L. Curran, T. M. Wengenack, P-G Henry, R. L. Bliss, J. F. Poduslo, C. R. Jack, Kamil Uğurbil, and Michael Garwood. Monitoring disease progression in transgenic mouse models of Alzheimer’s disease with proton Magnetic Resonance Spectroscopy. *Proceedings of the National Academy of Sciences of the United States of America (PNAS)*, 102(33):11906–11910, August 2005.
- [104] Ian Marshall, John Higinbotham, Stephen Bruce, and Andreas Freise. Use of voigt lineshape for quantification of in vivo ^1H spectra. *Magn. Reson. Med.*, 37(5):651–657, 1997.
- [105] E. Martin, A. Capone, J. Schneider, J. Hennig, and T. Thiel. Absence of n-acetylaspartate in the human brain: Impact on neurospectroscopy? *Annals of Neurology*, 49(4):518–521, 2001.
- [106] A. A. Maudsley. Spectral lineshape determination by self-deconvolution. *Journal of Magnetic Resonance, series B*, 106(1):47 – 57, 1995.
- [107] K. R. Metz, M. M. Lam, and A. G. Webb. Reference deconvolution: A simple and effective method for resolution enhancement in Nuclear Magnetic Resonance Spectroscopy. *Concepts in Magnetic Resonance*, 12(1):21–42, 2000.
- [108] G. J. Metzger, M. Patel, and X. Hu. Application of genetic algorithms to spectral quantification. *Journal of Magnetic Resonance, Series B*, 110(3):316 – 320, 1996.
- [109] S. Mierisová and M. Ala-Korpela. MR Spectroscopy quantitation: a review of frequency domain methods. *NMR in Biomedicine*, 14(4):247–259, 2001.
- [110] M. Miyake, Y. Kakimoto, and M. Sorimachi. A gas chromatographic method for the determination of N-Acetyl-L-Aspartic Acid, N-Acetyl- α -Aspartylglutamic Acid and β -Citryl-L-Glutamic Acid and their distributions in the brain and other organs of various species of animals. *Journal of Neurochemistry*, 36(3):804–819, 1981.

- [111] V. Mlynárik, C. Cudalbu, L. Xin, and R. Gruetter. ^1H NMR Spectroscopy of rat brain *in vivo* at 14.1 Tesla: Improvements in quantification of the neurochemical profile. *Journal of Magnetic Resonance*, 194(2):163 – 168, 2008.
- [112] H. Mo and D. Raftery. Pre-SAT180, a simple and effective method for residual water suppression. *Journal of Magnetic Resonance*, 190(1):1 – 6, 2008.
- [113] D. Moechars, I. Dewachter, K. Lorent, D. Reversé, V. Baekelandt, A. Naidu, I. Tesseur, K. Spittaels, C. Van den Haute, F. Checler, E. Godaux, B. Cordell, and F. Van Leuven. Early phenotypic changes in transgenic mice that overexpress different mutants of amyloid precursor protein in brain. *Journal of Biological Chemistry*, 274(10):6483–6492, 1999.
- [114] J. Moré. The Levenberg-Marquardt algorithm: Implementation and theory. In G. Watson, editor, *Numerical Analysis*, volume 630 of *Lecture Notes in Mathematics*, pages 105–116. Springer Berlin / Heidelberg, 1978. 10.1007/BFb0067700.
- [115] G. A. Morris, H. Barjat, and T. J. Horne. Reference deconvolution methods. *Journal of progress in Nuclear Magnetic Resonance Spectroscopy*, 31:197–257, 1997.
- [116] U. G. Mueller-Lisse and M. K. Scherr. Proton MR Spectroscopy of the prostate. *European Journal of Radiology*, 63(3):351 – 360, 2007. Prostate.
- [117] B. D. Nguyen, X. Meng, K. J. Donovan., and A. J. Shaka. SOGGY: Solvent-optimized double gradient spectroscopy for water suppression. A comparison with some existing techniques. *Journal of Magnetic Resonance*, 184(2):263 – 274, 2007.
- [118] K. S. Opstad, J. R. Griffiths, B. A. Bell, and F. A. Howe. Apparent T_2 relaxation times of lipid and macromolecules: A study of high-grade tumor spectra. *Journal of Magnetic Resonance Imaging*, 27(1):178–184, 2008.
- [119] M. I. Osorio-Garcia, D. M. Sima, Caicedo-Dorado A., Van Cauter S., F. U. Nielsen, T. Dresselaers, F. Van Leuven, U. Himmelreich, and S. Van Huffel. Model order selection of Hankel Lanczos Singular Value Decomposition (HLSVD) for peak removal of *in vitro* and *in vivo* ^1H Magnetic Resonance Spectroscopy signals. Technical report, 2011.
- [120] M. I. Osorio-Garcia, D. M. Sima, F. U. Nielsen, T. Dresselaers, U. Himmelreich, F. Van Leuven, and S. Van Huffel. *In vivo* ^1H MRS quantification of Alzheimer’s disease in frontal hippocampus of mice with and without inversion recovery to assess the macromolecular contribution. In *Proc. of the 19th International Society of Magnetic Resonance in Medicine - ISMRM 2011*, May 2011.

- [121] M. I. Osorio-Garcia, D. M. Sima, F. U. Nielsen, T. Dresselaers, F. Van Leuven, U. Himmelreich, and S. Van Huffel. Quantification of *in vivo* ^1H Magnetic Resonance Spectroscopy (MRS) signals with baseline and lineshape estimation. *Measurement Science and Technology*, 22(11):114011, 2011.
- [122] M. I. Osorio-Garcia, D. M. Sima, F. U. Nielsen, U. Himmelreich, and S. Van Huffel. Damping factor constraints and metabolite profile selection influence Magnetic Resonance Spectroscopy data quantification. In *Proceedings of the International Conference on Bioinspired Systems and Biosignals 2011 (BIOSTEC)*, pages 176–181, January 2011.
- [123] M. I. Osorio-Garcia, D. M. Sima, F. U. Nielsen, U. Himmelreich, and S. Van Huffel. Quantification of Magnetic Resonance Spectroscopy signals with lineshape estimation. *Journal of Chemometrics*, 25(4):183–192, 2011.
- [124] M. I. Osorio-Garcia, D. M. Sima, J-B Poulet, D. van Ormondt, and S. Van Huffel. Improvement of lineshape estimation. In *Proceedings of 4th European Congress of the International Federation for Medical and Biomedical Engineering (ECIFMBE)*, pages 138–141, Antwerp, Belgium, November 2008.
- [125] J-M Papy, L. De Lathauwer, and S. Van Huffel. A shift invariance-based order-selection technique for exponential data modelling. *IEEE Signal Processing Letters*, 14(7), July 2007.
- [126] E. K. Paulson and K. W. Zilm. Linear phase correction of folded multidimensional NMR data by zero inter-filling. *Journal of Magnetic Resonance*, 168(2):217 – 219, 2004.
- [127] Leonidas Petrakis. Spectral line shapes - gaussian and lorentzian functions in magnetic resonance. *Journal of Chemical Education*, 44(8), 1967.
- [128] J. Pfeuffer, I. Tkáč, S.W. Provencher, and R. Gruetter. Toward an *in vivo* neurochemical profile: Quantification of 18 metabolites in short-echo-time ^1H NMR spectra of the rat brain. *Journal of Magnetic Resonance*, 141(1):104 – 120, 1999.
- [129] W. W. F. Pijnappel, A. van den Boogaart, R. de Beer, and D. van Ormondt. SVD-based quantification of Magnetic Resonance signals. *Journal of Magnetic Resonance (1969)*, 97(1):122 – 134, 1992.
- [130] R. Pintelon and J. Schoukens. *System Identification - A Frequency Domain Approach*. IEEE Press, 2001.
- [131] E. Popa. *Algorithms for handling arbitrary lineshape distortions in Magnetic Resonance Spectroscopy and Spectroscopy Imaging*. PhD thesis, 2010.

- [132] E. Popa, E. Capobianco, R. de Beer, D. van Ormondt, and D. Graveron-Demilly. *In vivo* quantitation of metabolites with an incomplete model function. *Measurement Science and Technology*, 20(10):104032, 2009.
- [133] E. Popa, D.A. Karras, B.G. Mertzios, D.M. Sima, R. de Beer, D. van Ormondt, and D. Graveron-Demilly. Semi-parametric estimation without searching in function space. Application to *in vivo* metabolite quantitation. *Measurement Science and Technology*, 22(11):114014, 2011.
- [134] J-B. Poulet. *Quantification and classification of Magnetic Resonance Spectroscopic data for brain tumor diagnosis*. PhD thesis, 2008.
- [135] J-B. Poulet. Spid: Simulation Package based on *in vitro* databases, 2008.
- [136] J-B. Poulet, D. M. Sima, S. Van Huffel, and P. Van Hecke. Frequency-selective quantitation of short-echo time ^1H magnetic resonance spectra. *Journal of Magnetic Resonance*, 186(2):293 – 304, 2007.
- [137] J-B. Poulet, D. M. Sima, A. W. Simonetti, B. De Neuter, L. Vanhamme, P. Lemmerling, and S. Van Huffel. An automated quantitation of short echo time MRS spectra in an open source software environment: AQSES. *NMR in Biomedicine*, 20(5):493–504, 2007.
- [138] J-B. Poulet, D. M. Sima, and S. Van Huffel. MRS signal quantitation: A review of time- and frequency-domain methods. *Journal of Magnetic Resonance*, 195(2):134 – 144, 2008.
- [139] P. J. W. Pouwels and J. Frahm. Differential distribution of NAA and NAAG in human brain as determined by quantitative localized proton MRS. *NMR in Biomedicine*, 10(2):73–78, 1997.
- [140] S. W. Provencher. Estimation of metabolite concentrations from localized *in vivo* proton NMR spectra. *Magnetic Resonance in Medicine*, 30(6):672–679, 1993.
- [141] S. W. Provencher. Automatic quantitation of localized *in vivo* ^1H spectra with LCModel. *NMR Biomed.*, 14(4):260–264, 2001.
- [142] S. W. Provencher. *LCModel & LCMgui Users Manual*, May 2010.
- [143] H. Ratiney, Y. Coenradie, S. Cavassila, D. van Ormondt, and D. Graveron-Demilly. Time-domain quantitation of ^1H short echo-time signals: background accommodation. *Magnetic Resonance Materials in Physics, Biology and Medicine*, 16:284–296, 2004. 10.1007/s10334-004-0037-9.
- [144] H. Ratiney, M. Sdika, Y. Coenradie, S. Cavassila, D. van Ormondt, and D. Graveron-Demilly. Time-domain semi-parametric estimation based on a metabolite basis set. *NMR in Biomedicine*, 18(1):1–13, 2005.

- [145] G. Reynolds, M. Wilson, A. Peet, and T. N. Arvanitis. An algorithm for the automated quantitation of metabolites in *in vitro* NMR signals. *Magnetic Resonance in Medicine*, 56(6):1211–1219, 2006.
- [146] J. Rissanen. Modeling by shortest data description. *Automatica*, 14(5):465 – 471, 1978.
- [147] R. Romano, A. Motta, S. Camassa, C. Pagano, M. T. Santini, and P. L. Indovina. A new time-domain frequency-selective quantification algorithm. *Journal of Magnetic Resonance*, 155(2):226 – 235, 2002.
- [148] B. D. Ross. Biochemical considerations in ^1H Spectroscopy. Glutamate and glutamine; myo-inositol and related metabolites. *NMR in Biomedicine*, 4(2):59–63, 1991.
- [149] B. D. Ross. Real or imaginary? human metabolism through nuclear magnetism. *IUBMB Life*, 50(3):177–187, 2000.
- [150] B. D. Ross, T. Ernst, R. Kreis, L. J. Haseler, S. Bayer, E. Danielsen, S. Blüml, T. Shonk, J. C. Mandigo, W. Caton, C. Clark, S. W. Jensen, N. L. Lehman, E. Arcinue, R. Pudenz, and C. H. Shelden. ^1H MRS in acute traumatic brain injury. *Journal of Magnetic Resonance Imaging*, 8(4):829–840, 1998.
- [151] R. P. Saneto, S. D. Friedman, and D. W. Shaw. Neuroimaging of mitochondrial disease. *Mitochondrion*, 8(5-6):396 – 413, 2008.
- [152] G. Schwarz. Estimating the dimension of a model. *Annals of Statistics*, 6(2):461–464, 1978.
- [153] U. Seeger, U. Klose, O. Lutz, and W. Grodd. Elimination of residual lipid contamination in single volume proton MR spectra of human brain. *Magnetic Resonance Imaging*, 17(8):1219 – 1226, 1999.
- [154] U. Seeger, U. Klose, I. Mader, W. Grodd, and T. Nägele. Parameterized evaluation of macromolecules and lipids in proton MR Spectroscopy of brain diseases. *Magnetic Resonance in Medicine*, 49(1):19–28, 2003.
- [155] U. Seeger, I. Mader, T. Nägele, W. Grodd, O. Lutz, and U. Klose. Reliable detection of macromolecules in single-volume ^1H NMR spectra of the human brain. *Magnetic Resonance in Medicine*, 45(6):948–954, 2001.
- [156] D. M. Sima, M. I. Osorio-Garcia, J-B. Pouillet, A. Suvichakorn, J-P. Antoine, S. Van Huffel, and D. van Ormondt. Lineshape estimation for Magnetic Resonance Spectroscopy (MRS) signals: self-deconvolution revisited. *Measurement Science and Technology*, 20(10):104031, 2009.

- [157] D. M. Sima and S. Van Huffel. Regularized semiparametric model identification with application to nuclear magnetic resonance signal quantification with unknown macromolecular base-line. *Journal of the Royal Statistical Society. Series B (Statistical Methodology)*, 68(3):pp. 383–409, 2006.
- [158] J. Slotboom, C. Boesch, and R. Kreis. Versatile frequency domain fitting using time domain models and *prior knowledge*. *Magnetic Resonance in Medicine*, 39(6):899–911, 1998.
- [159] J. Slotboom, A. Nirikko, C. Brekenfeld, and D. van Ormondt. Reliability testing of *in vivo* magnetic resonance spectroscopy (MRS) signals and signal artifact reduction by order statistic filtering. *Measurement Science and Technology*, 20(10):104030, 2009.
- [160] S. A. Smith, T. O. Levante, B. H. Meier, and R. R. Ernst. Computer simulations in Magnetic Resonance. An object-oriented programming approach. *Journal of Magnetic Resonance, Series A*, 106(1):75 – 105, 1994.
- [161] B. J. Soher, K. Young, and A. A. Maudsley. Representation of strong baseline contributions in ^1H MR spectra. *Magnetic Resonance in Medicine*, 45(6):966–972, 2001.
- [162] Z. Starčuk, Z. Starčuk Jr., and J. Halánek. Correction of baseline and lineshape distortions in Fourier transform NMR spectroscopy by estimation of missing signals. *Journal of Magnetic Resonance*, 86(1):30 – 38, 1990.
- [163] Z. Starčuk, J. Starčukova, and D. Graveron-Demilly. A multi-purpose simulator of coupled spin systems for MR localized Spectroscopy and Spectroscopic Imaging. In *Proc. of the 19th International Society of Magnetic Resonance in Medicine - ISMRM 2011*, May 2011.
- [164] D. Stefan, A. Andrasecu, E. Popa, H. Rabeson, O. Strbak, Z. Starčuk, M. Cabanas, D. van Ormondt, and D. Graveron-Demilly. jMRUI version 4: A plug-in platform. In *Imaging Systems and Techniques, 2008. IST 2008. IEEE International Workshop on*, pages 346 –348, 2008.
- [165] D. Stefan, F. Di Cesare, A. Andrasescu, E. Popa, A. Lazariiev, E. Vescovo, O. Strbak, S. Williams, Z. Starčuk, M. Cabanas, D. van Ormondt, and D. Graveron-Demilly. Quantitation of Magnetic Resonance Spectroscopy signals: the jMRUI software package. *Measurement Science and Technology*, 20(10):104035, 2009.
- [166] R. Stoyanova and T. R. Brown. NMR spectral quantitation by Principal Component Analysis. *NMR in Biomedicine*, 14(4):271–277, 2001.

- [167] T. Sundin, L. Vanhamme, P. Van Hecke, I. Dologlou, and S. Van Huffel. Accurate quantification of ^1H spectra: From finite impulse response filter design for solvent suppression to parameter estimation. *Journal of Magnetic Resonance*, 139(2):189 – 204, 1999.
- [168] C. G. Tang. An analysis of baseline distortion and offset in NMR spectra. *Journal of Magnetic Resonance, Series A*, 109(2):232 – 240, 1994.
- [169] I. Tkáč, G. Öz, G. Adriany, K. Uğurbil, and R. Gruetter. *In vivo* ^1H NMR spectroscopy of the human brain at high magnetic fields: Metabolite quantification at 4 T vs. 7 T. *Magnetic Resonance in Medicine*, 62(4):868–879, 2009.
- [170] I. Tkáč, Z. Starčuk, I-Y. Choi, and R. Gruetter. *In vivo* ^1H NMR spectroscopy of rat brain at 1 ms echo time. *Magnetic Resonance in Medicine*, 41(4):649–656, 1999.
- [171] A. van den Boogaart. Quantitative data analysis of *in vivo* MRS data sets. *Magnetic Resonance in Chemistry*, 35(13):146–152, 1997.
- [172] J. W. van der Veen, R. de Beer, P. R. Luyten, and D. van Ormondt. Accurate quantification of *in vivo* ^{31}P NMR signals using the variable projection method and *prior knowledge*. *Magnetic Resonance in Medicine*, 6(1):92–98, 1988.
- [173] S. Van Huffel and J. Vandewalle. *The Total Least Squares Problem: Computational Aspects and Analysis*. SIAM, 1991.
- [174] L. Vanhamme, T. Sundin, P. Van Hecke, and S. Van Huffel. MR spectroscopy quantitation: a review of time-domain methods. *NMR in Biomedicine*, 14(4):233–246, 2001.
- [175] L. Vanhamme, T. Sundin, P. Van Hecke, S. Van Huffel, and R. Pintelon. Frequency-selective quantification of biomedical Magnetic Resonance Spectroscopy data. *Journal of Magnetic Resonance*, 143(1):1 – 16, 2000.
- [176] L. Vanhamme, A. van den Boogaart, and S. Van Huffel. Improved method for accurate and efficient quantification of MRS data with use of *Prior Knowledge*. *Journal of Magnetic Resonance*, 129(1):35 – 43, 1997.
- [177] M. Wax and T. Kailath. Detection of signals by information theoretic criteria. *Acoustics, Speech and Signal Processing, IEEE Transactions on*, 33(2):387 – 392, April 1985.
- [178] P. Webb, D. Spielman, and A. Macovski. Inhomogeneity correction for *in vivo* spectroscopy by high-resolution water referencing. *Magn. Reson. Med.*, 23(1):1 – 11, 1992.

- [179] E. Westman, L-O. Wahlund, C. Foy, M. Poppe, A. Cooper, D. Murphy, C. Spenger, S. Lovestone, and A. Simmons. ^1H -MRS a valuable complement to MRI in the early diagnosis of Alzheimer's disease. *Alzheimer's and Dementia*, 6(4, Supplement 1):283 – 283, 2010. Alzheimer's Association - International Conference on Alzheimer's Disease 2010.
- [180] D. C. Williamson, H. Hawesa, N. A. Thacker, and S. R. Williams. Robust quantification of short echo time ^1H Magnetic Resonance spectra using the Padé approximant. *Magnetic Resonance in Medicine*, 55(4):762–771, 2006.
- [181] M. Wilson, N. P. Davies, Y. Sun, K. Natarajan, T. N. Arvanitis, R. A. Kauppinen, and A. C. Peet. A comparison between simulated and experimental basis sets for assessing short-TE *in vivo* ^1H MRS data at 1.5 T. *NMR in Biomedicine*, 23(10):1117–1126, 2010.
- [182] M. Wilson, G. Reynolds, R. A. Kauppinen, T. N. Arvanitis, and A. C. Peet. A constrained least-squares approach to the automated quantitation of *in vivo* ^1H Magnetic Resonance Spectroscopy data. *Magnetic Resonance in Medicine*, 65(1):1–12, 2011.
- [183] A. J. Wright, C. Arús, J. P. Wijnen, A. Moreno-Torres, J. R. Griffiths, B. Celda, and F. A. Howe. Automated quality control protocol for MR spectra of brain tumors. *Magnetic Resonance in Medicine*, 59(6):1274–1281, 2008.
- [184] W. Wu, M. Daszykowski, B. Walczak, B. C. Sweatman, S. C. Connor, J. N. Haselden, D. J. Crowther, R. W. Gill, and M. W. Lutz. Peak alignment of urine NMR spectra using fuzzy warping. *Journal of Chemical Information and Modeling*, 46(2):863–875, 2006.
- [185] Y. Xi and D. Rocke. Baseline correction for NMR spectroscopic metabolomics data analysis. *BMC Bioinformatics*, 9(1):324, 2008.
- [186] H. Yan and J. C. Gore. The relation of HSVD to LPSVD for fitting time-domain signals. *Journal of Magnetic Resonance*, 80(2):324 – 327, 1988.
- [187] H. Yin, Z. Zhu, and F. Ding. Model order determination using the Hankel matrix of impulse responses. *Applied Mathematics Letters*, 24(5):797 – 802, 2011.
- [188] O. Zerbe. Lecture course: NMR Spectroscopy. Website. www.oci.uzh.ch/group.pages/zerbe/NMR.pdf.
- [189] J. Zhang, A.K. Swain, and S.K. Nguang. Parameter estimation of exponentially damped sinusoids using HSVD based extended complex kalman filter. In *TENCON 2008 - 2008 IEEE Region 10 Conference*, pages 1 –6, 2008.

- [190] G. Zhu, D. Smith, and Y. Hua. Post-acquisition solvent suppression by singular-value decomposition. *Journal of Magnetic Resonance*, 124(1):286 – 289, 1997.
- [191] X. Zhu, N. Schuff, J. Kornak, B. Soher, K. Yaffe, J. H. Kramer, F. Ezekiel, B. L. Miller, W. J. Jagust, and M. W. Weiner. Effects of Alzheimer’s disease on fronto-parietal brain N-acetyl aspartate and myo-inositol using Magnetic Resonance Spectroscopic Imaging. *Alzheimer Disease & Associated Disorders*, 20:7785, 2006.

Publication List

Papers in international journals

1. D.M. Sima, **M.I. Osorio-Garcia**, J-B Pouillet, A. Suvichakorn, J-P Antoine, S. Van Huffel, and D. van Ormondt. Lineshape estimation for MRS signals: self-deconvolution revisited. *Meas. Sci. Technol.*, 20(10):104031 (12pp), 2009.
2. **M.I Osorio-Garcia**, D.M Sima, F.U Nielsen, T. Dresselaers, F. Van Leuven, U. Himmelreich and S. Van Huffel. Quantification of magnetic resonance spectroscopy signals with lineshape estimation. *J. Chemom.*, 25(4):183–192, 2011.
3. **M.I Osorio-Garcia**, D.M Sima, F.U Nielsen, U. Himmelreich and S. Van Huffel. Quantification of *in vivo* ^1H Magnetic Resonance Spectroscopy (MRS) signals with baseline and lineshape estimation. *Meas. Sci. Technol.*, 22(11):114011 (10pp), 2011.

Internal reports

4. **M.I Osorio-Garcia**, D.M Sima, A. Caicedo-Dorado, S. Van Cauter, F.U Nielsen, T. Dresselaers, F. Van Leuven, U. Himmelreich and S. Van Huffel. Model order selection of Hankel Lanczos Singular Value Decomposition (HLSVD) for peak removal of *in vitro* and *in vivo* ^1H Magnetic Resonance Spectroscopy signals.

Chapters in books

5. **M.I Osorio-Garcia**, A. Croitor Sava, D.M Sima, F.U Nielsen, U. Himmelreich and S. Van Huffel. Quantification Improvements of ^1H MRS Signals

Accepted for publication as book chapter in the book: "Magnetic Resonance Spectroscopy", ISBN 978-953-307-771-0.

Papers in proceedings of international conferences

6. **M.I. Osorio-Garcia**, D.M. Sima, J-B Pouillet, D. van Ormondt and S. Van Huffel. Improvement of lineshape estimation for MRS signals. Proc. IEEE workshop on Imaging Systems and Techniques (IST 2008), Chania, Crete, Greece, Sep. 2008, pp.326-329.
7. **M.I. Osorio-Garcia**, D.M. Sima, J-B Pouillet, D. van Ormondt and S. Van Huffel. Improvement of lineshape estimation. Proceedings of 4th European Congress of the International Federation for Medical and Biomedical Engineering (ECIFMBE), Antwerp, Belgium, Nov. 2008, pp.138-141.
8. **M.I. Osorio-Garcia**, D.M. Sima, F.U Nielsen, U. Himmelreich and S. Van Huffel. Quantification of *in vivo* Magnetic Resonance Spectroscopy signals with baseline and lineshape corrections. Proc. IEEE workshop on Imaging Systems and Techniques (IST 2010), Thessaloniki, Greece, Jul. 2010, pp.349-352.
9. A.R. Croitor-Sava, T. Laudadio, D.M. Sima, **M.I. Osorio-Garcia**, S. Van Huffel, M.C. Martinez-Bisbal, B. Celda, A. Heerschap. Incorporating *in vivo* and *ex vivo* NMR sources of information for modeling robust brain tumor classifiers. Proc. IEEE workshop on Imaging Systems and Techniques (IST 2010), Thessaloniki, Greece, Jul. 2010, pp.353 - 356.
10. C. Lemke, A. Schuck, J-P. Antoine, D.M. Sima, **M.I. Osorio-Garcia**. Metabolite-based wavelets for analyzing Magnetic Resonance Spectroscopic signals. Proc. IEEE workshop on Imaging Systems and Techniques (IST 2010), Thessaloniki, Greece, Jul. 2010, pp.357 - 360.
11. **M.I. Osorio-Garcia**, D.M. Sima, F.U Nielsen, U. Himmelreich and S. Van Huffel. Damping factor constraints and metabolite profile selection influence Magnetic Resonance Spectroscopy data quantification. Proceedings of the International conference on Bioinspired systems and Biosignals 2011 (BIOSTEC), Rome, Italy, Jan. 2011, pp.176-181.

Abstracts in proceedings of (inter)national conferences

12. **M.I. Osorio-Garcia**, D.M. Sima, J-B Pouillet, D. van Ormondt and S. Van Huffel. Iterative improvement of lineshape estimation. 25th Annual Meeting

- of the European Society for Magnetic Resonance in Medicine and Biology 2008 (ESMRMB), Valencia, Spain, Oct. 2008.
13. **M.I. Osorio-Garcia**, D.M. Sima, F.U Nielsen, U. Himmelreich and S. Van Huffel. Quantification of *in vitro* MRS signals with lineshape correction. 26th Annual Meeting of the European Society for Magnetic Resonance in Medicine and Biology 2008 (ESMRMB), Antalya, Turkey, Oct. 2009.
 14. **M.I. Osorio-Garcia**, D.M. Sima, E. Mosconi, M. Pellitteri, F. Schio, R. Lodico, L. Zanetti, G. Van Luijtelaar, S. Fiorini, E. Nicolato, P.F. Fabene, P. Marzola, S. Van Huffel. The influence of lineshape and baseline on quantification of *in vivo* Magnetic Resonance Spectroscopy (MRS) signals. 2nd Annual meeting of the Benelux ISMRM chapter, Utrecht, Netherlands, Jan. 2010.
 15. C. Lemke, A. Schuck Jr., D.M. Sima, **M.I. Osorio-Garcia**, S. Van Huffel J-P. Antoine. MRS signal analysis by metabolite-based wavelets. 2nd Annual meeting of the Benelux International Society for Magnetic Resonance in Medicine ISMRM chapter, Utrecht, Netherlands, Jan. 2010.
 16. **M.I. Osorio-Garcia**, D.M. Sima, F.U Nielsen, U. Himmelreich and S. Van Huffel. Residual analysis of quantification of Magnetic Resonance Spectroscopy signals. Leuven Statistical day 2010, Leuven, Belgium, May. 2010.
 17. **M.I. Osorio-Garcia**, D.M. Sima, U. Himmelreich and S. Van Huffel. Assessing the validity of Magnetic Resonance Spectroscopy metabolite quantification via residual analysis. XII International Conference on Chemometrics in Analytical Chemistry (CAC) 2010, Antwerp, Belgium, Oct. 2010.
 18. D.M. Sima, **M.I. Osorio-Garcia**, U. Himmelreich and S. Van Huffel. Baseline estimation for *in vivo* magnetic resonance spectroscopy: *prior* to or simultaneous with metabolite quantification. XII International Conference on Chemometrics in Analytical Chemistry (CAC) 2010, Antwerp, Belgium, Oct. 2010.
 19. **M.I. Osorio-Garcia**, D.M. Sima, F.U Nielsen, U. Himmelreich and S. Van Huffel. Evaluation of residual on quantified Magnetic Resonance Spectroscopy (MRS) signals. 9th Belgian day on Biomedical Engineering "Bridging the gap between medicine and engineering", Brussels, Belgium, Nov. 2010.
 20. **M.I. Osorio-Garcia**, D.M. Sima, F.U Nielsen, T. Dresselaers, F. Van Leuven, U. Himmelreich and S. Van Huffel. *In vivo* ¹H MRS quantification of early stage Alzheimer's disease in frontal hippocampus of mice with and without inversion recovery to assess the macromolecular contribution. 3th Annual

- meeting of the Benelux International Society for Magnetic Resonance in Medicine (ISMRM) chapter, Hoeven, The Netherlands, Jan. 2011.
21. S. Van Cauter, D.M Sima, L. ter Beek, J. Luts, Y. Li, **M.I Osorio-Garcia**, S. Van Huffel and U. Himmelreich. Reproducibility and variance of serial short echo time proton Magnetic Resonance Spectroscopic Imaging of the human brain at 3 T with automated planning software. 3th Annual meeting of the Benelux International Society for Magnetic Resonance in Medicine (ISMRM) chapter, Hoeven, The Netherlands, Jan. 2011.
 22. A.R. Croitor-Sava, S. Van Cauter, D.M Sima, **M.I Osorio-Garcia**, Y. Li, U. Himmelreich, S. Van Huffel. Non-negative blind source separation techniques for describing intratumoral histopathological tissue properties within MRSI measurements. 3th Annual meeting of the Benelux International Society for Magnetic Resonance in Medicine (ISMRM) chapter, Hoeven, The Netherlands, Jan. 2011.
 23. **M.I Osorio-Garcia**, D.M Sima, F.U Nielsen, T. Dresselaers, F. Van Leuven, U. Himmelreich and S. Van Huffel. *In vivo* ¹H MRS quantification of Alzheimer's disease in frontal hippocampus of mice with and without inversion recovery to assess the macromolecular contribution. 19th Annual meeting & Exhibition of the International Society for Magnetic Resonance in Medicine (ISMRM) 2011, Montreal, Quebec, Canada, May. 2011.
 24. S. Van Cauter, D.M Sima, L. ter Beek, J. Luts, Y. Li, **M.I Osorio-Garcia**, S. Sunaert, S. Van Huffel and U. Himmelreich. Reproducibility and variance of serial short echo time ¹H Magnetic Resonance Spectroscopic Imaging of the human brain at 3 T with automated planning software. 19th Annual meeting & Exhibition of the International Society for Magnetic Resonance in Medicine (ISMRM) 2011, Montreal, Quebec, Canada, May. 2011.
 25. A. Croitor Sava, S. Van Cauter, D.M Sima, **M.I Osorio-Garcia**, U. Himmelreich and S. Van Huffel. Non-negative blind source separation techniques for describing intratumoral histopathological tissue properties within MRSI measurements. 19th Annual meeting & Exhibition of the International Society for Magnetic Resonance in Medicine (ISMRM) 2011, Montreal, Quebec, Canada, May. 2011.

Curriculum vitae

Maria Isabel Osorio Garcia was born in Salgar-Antioquia, Colombia on June 17, 1981. In July 2005 she received the degree of biomedical engineer from the Antioquia School of Engineering (EIA) Joined with the Health Sciences Institute (CES), in Medellin Colombia.

In summer 2004, she participated in an exchange program as an IAESTE trainee in the Georg-August Universität Göttingen at the Universitätsklinikum in Germany. In this three months internship she worked in the Institute for Medical informatics where she was involved in the project INBED, which consisted in the development of a Graphical User Interface for data processing of embedded sensors in a bed for monitoring epileptic patients.

From July 2006 to June 2007, she was a researcher at the Otto-von-Guericke Universität Magdeburg, Germany in the Department of Electrical Engineering - IMOS, where she was involved in the European project ALFA PETRA-II (ALFA II-0343-FA-FCD-FI) - (www.apit.upv.es/petra): Piezoelectric Transducers and Applications II. During this year, she investigated about the behavior of quartz Crystal Resonators in presence of electrolytic and non-electrolytic solutions.

In July 2007, she joined the BIOMED research group at the Department Electrical Engineering (ESAT-SCD) of the Katholieke Universiteit Leuven, where she first was a pre-doctoral candidate and since January 2008, she is a PhD student under the supervision of Prof. Dr. Ir. Sabine Van Huffel, Prof. Dr. Ir. Uwe Himmelreich and Dr. Diana Sima. From 2008 till 2010 she was a Marie Curie fellow involved in the Research and Training Network (RTN) granted by Marie Curie Actions in the 6th Framework Program (2007-2010) FAST (MRTN-CT-2006-035801) - (www.fast-mrs.eu): FAST, Advanced Signal Processing for Ultra Fast Magnetic Resonance. Her research work was focused on signal processing and quantification of Magnetic Resonance Spectroscopy (MRS) signals.

Arenberg Doctoral School of Science, Engineering & Technology

Faculty of Engineering

Department of Electrical Engineering

Research group SISTA-BIOMED

Kasteelpark Arenberg 10, B - 3001 Leuven